MNRAS **000**, 1–35 (2015) Preprint 2 November 2016 Compiled using MNRAS LATEX style file v3.0

Absorption at 11 μm in the interstellar medium and embedded sources: evidence for crystalline silicates

Christopher M. Wright,[1⋆] Tho Do Duy,[1,2] and Warrick Lawson[1]
[1] *School of Physical, Environmental and Mathematical Sciences, UNSW Canberra, PO Box 7916, Canberra BC 2610, Australia*
[2] *Department of Physics, International University - Vietnam National University HCM, Block 6, Linh Trung, Thu Duc, Ho Chi Minh City, Viet Nam*

arXiv:1601.02329v1 [astro-ph.SR] 11 Jan 2016

Accepted XXX. Received YYY; in original form ZZZ

ABSTRACT

An absorption feature is occasionally reported around 11 μm in astronomical spectra, including those of forming stars. Candidate carriers include water ice, polycyclic aromatic hydrocarbons (PAHs), silicon carbide, crystalline silicates or even carbonates. All are known constituents of cosmic dust in one or more types of environments, though not necessarily together. In this paper we present new ground-based 8–13 μm spectra of one evolved star, several embedded young stellar objects (YSOs) and a background source lying behind a large column of the interstellar medium (ISM) toward the Galactic Centre. Our observations, obtained at a spectral resolution of $\sim$ 100, are compared with previous lower resolution data, as well as data obtained with the Infrared Space Observatory (ISO) on these and other targets. By presenting a subset of a larger sample our aim is to establish the reality of the feature and subsequently speculate on its carrier. All evidence points toward crystalline silicate. For instance, the 11 μm band profile is well matched with the emissivity of crystalline olivine. Furthermore, the apparent association of the absorption feature with a sharp polarisation signature in the spectrum of two previously reported cases suggests a carrier with a relatively high band strength compared to amorphous silicates. If true, this would either set back the evolutionary stage in which silicates are crystallised, either to the embedded phase or even before within the ISM, or else the silicates ejected from the outflows of evolved stars retain some of their crystalline identity during their long residence in the ISM.

Key words: young stellar objects – interstellar medium – cosmic dust – infrared

1 INTRODUCTION

The composition and evolution of cosmic dust is of great astrophysical interest as it from these tiny, sub-micron sized seeds that planets grow. With their enhanced wavelength coverage over the ground-based atmospheric windows at 2.9-3.4, 8-13 and 16-23 μm, the Infrared Astronomical Satellite (IRAS), Infrared Space Observatory (ISO) and Spitzer space telescope provided great impetus and progressively larger strides in the study and understanding of cosmic dust. This has been inclusive of ices and refractory species like silicates, amongst other less abundant components (e.g. Molster et al. (2010), Henning (2010), Gibb et al. (2004)). Of particular note has been the 'crystalline revolution', beginning with ISO, in which routine detection of crystalline silicates and even the study of their specific mineralogies has occurred.

Before the space-based spectrometers the existence of such crystalline silicates had been proposed in only a few sources. For the massive embedded YSO AFGL 2591 it was based on the presence of a 'shoulder' or 'inflection' around 11 μm in its conventional absorption spectrum, along with an accompanying polarisation signature (Aitken et al. (1988); Wright et al. (1999)). For other sources it was based on a similarly placed emission feature in the spectra of several comets, e.g. Comet Halley (Bregman et al. (1987); Campins & Ryan (1989)), and the debris disk around β Pictoris (Aitken et al. (1993); Knacke et al. (1993)).

Through necessity these earlier identifications were typically based on the presence of only a single spectroscopic feature, whilst ISO and Spitzer covered the location of several other cosmic dust bands in the mid- and far-IR which could obviously strengthen identification of a candidate carrier. In so doing it was discovered that crystalline silicates exist around many different types of astrophysical sources, including dust factories (i.e. winds of evolved stars wherein dust condenses) and repositories (i.e. circumstellar disks around T Tauri and Herbig stars). The 11 μm and accompanying spectral features were predominantly in emission –

⋆ E-mail: c.wright@adfa.edu.au (CMW)

© 2015 The Authors

indicating a temperature of several hundred Kelvin – such that the dust was obviously located in close proximity to the central star, perhaps the inner regions of the disk and/or above it within a disk 'atmosphere' (Chiang & Goldreich (1997); Calvet et al. (1992)).

Few examples of 11 μm absorption were found, where the dust would be much colder, less than $\sim$ 100 K, and located in the outer disk or envelope. For instance, Demyk et al. (1999) concluded that crystalline silicates comprised no more than 1-2% of the silicates in the envelopes of two massive embedded YSOs, AFGL7009S and IRAS19110+1045. Further, no feature was found in the ISM, where according to some models of cosmic dust evolution (e.g. Jones & Nuth (2011)) it resides during the interval between its ejection from evolved stars and eventual deposition into a star forming region. For instance, based on the lack of an 11 μm absorption feature Kemper et al. (2005) and Kemper et al. (2004) placed an upper limit mass fraction of 2.2% on crystalline silicates, with a most likely value of around 1%, along the $\sim$ 8 kpc path to the Galactic Centre, which intersects both diffuse (atomic) and dense (molecular) clouds. See also Li et al. (2007), who – using the same spectrum – raise the upper limit to 3–5% by assuming that the component in molecular clouds grows a water ice mantle, the broad 11–13 μm librational band of which effectively masks (or washes out) the narrower 11 μm crystalline silicate band. [Curiously, Min et al. (2007) also used the very same spectrum to infer the presence of SiC, which has a feature around 11.3 μm.]

Several scenarios have been put forward to explain the lack of a crystalline component in cold silicate dust. In one model the silicates condense as partially crystalline in the outflows of evolved stars, but are completely amorphised in the ISM by such processes as cosmic ray irradiation on a timescale as short as 70 Myr (e.g. Bringa et al. (2007)). Another instead proposes that the lifetime of dust – against destructive processes like sputtering and shattering in interstellar shocks – is only about 4×10^8 years, less than the $\sim 2 \times 10^9$ year cycling time between ejection and deposition (Draine (2009)). In this model the dust in the ISM is not stardust, but is predominantly made in the ISM, having re-condensed as entirely amorphous behind shock fronts. Obviously in both scenarios the ISM silicate dust population is amorphous, and thus so are the silicates eventually deposited into a molecular cloud, the gravitational collapse of which forms a new generation of stars. Consequently, the crystalline silicates seen around newly formed stars must have been annealed, probably within their inner disks when exposed to temperatures of $\sim$ 1000 K (van Boekel et al. (2004)). They are then seen in emission.

In those cases where 11 μm absorption has been detected, either from ground- or space-based facilities, its identification has in many instances been ambiguous. See for example Boogert et al. (2004) and Kessler-Silacci et al. (2005). For instance, a potential carrier is water ice, which has a relatively strong and broad libration band centred between $\sim$ 12 and 13 μm for its crystalline and amorphous end members respectively (Maldoni et al. (1998)). On the basis of accompanying strong 3.1 μm water ice absorption, such an identification was made by Soifer et al. (1981) and Roche & Aitken (1984b) for the OH/IR stars OH 231.8+4.2 and OH 32.8-0.3 respectively. For similar reasons de Muizon et al. (1986) also ascribed water ice to the feature in the IRAS spectra of two additional OH/IR stars, as well as the embedded YSO AFGL 4176. On the other hand, Smith & Herman (1990) found no corresponding feature of water ice at 3.1 μm in the spectrum of the OH/IR star OH 138.0+7.3, and suggested instead that the 11 μm absorption could be explained by annealed (i.e. crystalline) silicate.

Another potential carrier could be hydrocarbons, known to have a strong emission feature at 11.25 μm in the presence of ultraviolet radiation. In this context, Bregman et al. (2000) identified absorption centred at 11.25 μm in the embedded YSO MonR2 IRS3 with a C-H out-of-plane vibrational mode of PAH molecules, based on an accompanying PAH absorption at 3.25 μm.

More recently, with the aid of the longer wavelength coverage of ISO and/or Spitzer, Demyk et al. (2000) and de Vries et al. (2014) found that the dominant contributor of 11 μm absorption in their respective samples of OH/IR stars is crystalline forsterite. For a sample of protostars Riaz et al. (2009) instead suggest that water ice is the dominant component. On the other hand, Spoon et al. (2006) and Poteet et al. (2011) were able to firmly identify 11.1 μm absorption with crystalline silicate – notably the Mg end member forsterite – in the Ultraluminous Infrared Galaxy (ULIRG) IRAS08572+3915 and the envelope of the Class 0 YSO HOPS-68 respectively. Even more recently, Fujiyoshi et al. (2015) detected absorption bands of both crystalline olivine and pyroxene, as well as SiC, in the Subaru/COMICS 8–13 μm spectrum of the Class I YSO SVS13.

The review of literature described above suggests that a discrete feature around 11 μm is much rarer in absorption than it is in emission, especially in the spectra of young stars. And where such a band is inferred its identification is problematic, especially if only seen in isolation within the 8–13 μm atmospheric window. But is this really the case, or is its rarity instead due to insufficient signal-to-noise and/or an inappropriate observational approach? We have attempted to answer this question by conducting a mid-IR spectroscopic survey of a select sample of targets, motivated principally by the existence of an inflection at 11 μm in low resolution (R $\sim$ 40) spectra of many objects in the mid-IR polarisation atlas of Smith et al. (2000).

In this paper we present selected ground-based results of a much larger body of work, which is still being worked upon. Here we include 8–13 μm spectra of the cold silicate dust in the envelopes or disks of several massive embedded YSOs as well as the path to the Galactic Centre. As a 'control', or 'template', we include the OH/IR star and dust factory AFGL 2403, confirmed to have crystalline silicates by de Vries et al. (2014). These data are supported and complemented by ISO observations of the same and other targets from 10 to 45 μm, taken with the Short Wavelength Spectrometer (SWS). Our study is the first dedicated and systematic search for, plus statistical investigation of, the 11 μm absorption feature in these source types. For this paper we concentrate on the main phenomenological findings with some modelling of specific cases. We will present a full description of the sample and a complete discussion of the results and associated modelling in a forthcoming paper (Do Duy et al., in preparation).

2 OBSERVATIONS

The 8–13 μm spectra were obtained from 21/08/2005 to 27/01/2007 using the facility T-ReCS (Telesco et al. (1998)) and Michelle (Glasse et al. (1997)) mid-infrared long-slit spectrometers at the Gemini-S and -N telescopes respectively, under Gemini programmes GS-2006B-Q-81 and GN-2005B-Q-83. The slit width was 0.7 arcsec with T-ReCS and 0.4 arcsec with Michelle, providing a spectral resolving power of ~ 100. Standard chopping and nodding was implemented, with the throw chosen on the basis of the source extension. The data was reduced using in-house IDL codes, with the spectrum extracted by summing the pixels across the spatial profile. Whilst not an ideal technique, for these bright sources there is little loss in S/N compared to optimised extraction methods, or Gaussian and Moffat function fits which were also tested. A standard star well-matched in airmass was used to correct for telluric features and provide the absolute flux calibration. Wavelength calibration was performed using telluric features in both the target and standard star spectra, and/or features in the filter transmission profiles.

Complementary ISO and low resolution data was taken from the ISO Highly Processed Data Product archive and Smith et al. (2000) respectively. Table 1 provides some specific observational details. The number in brackets after the SWS01 designation refers to the speed with which the 2.4–45.2 μm spectrum was taken, which in turn determines the spectral resolution and signal-to-noise. Speed 1 is fastest and least sensitive and speed 4 is the slowest and most sensitive (Leech et al. (2003)). To produce the ISO spectra we have taken the Frieswijk de-fringed highly processed data products for the SWS01 Astronomical Observing Template (AOT), sigma-clipped them about a chosen S/N ratio, and then binned or smoothed them in wavelength bins appropriate for the respective SWS01 speeds. For SWS06 AOTs we have used the latest pipeline Auto-Analysis Result (AAR) product, sigma-clipped and then binned at a resolution more coarse than the fringe period.

3 RESULTS

3.1 Spectra

Figure 1 shows the reduced Gemini 8–13 μm spectra of our targets, including the control source AFGL 2403, three YSOs and SgrA IRS3. Along with the well known deep amorphous silicate absorption centred around 9.7 μm there is also a shallow feature around 11 μm, which is relatively deeper in AFGL 2403. The inflection seen at R $\simeq$ 40 in the UCLS spectra presented in Smith et al. (2000), shown also in Figure 1 as solid circles, is resolved here into a bona fide absorption band. For comparison we also show the ISO spectra of each object, noting however that they may contain relatively narrow artefacts around 9.35, 10.1 and 11.05 μm (with FWHM of 0.3, 0.1 and 0.1 μm respectively) introduced by imperfect correction for the Relative Spectral Response Function (RSRF) of the ISO–SWS. See Leech et al. (2003).

The Gemini spectrum of AFGL 2789 (V645 Cyg) is consistent with those previously published by Hanner et al. (1998) and Bowey et al. (2003) at lower spectral resolution, inclusive of the abrupt 'jump' in flux around 11 μm. Also, the Gemini spectrum of AFGL 2136 is consistent with the similar resolution 8.2–11.0 μm segment presented by Skinner et al. (1992), inclusive of the rather sharp minimum around 9.7 μm.

For the relatively isolated and point-like YSOs AFGL 2136 and AFGL 2789 (Monnier et al. (2009)) all three of their spectra are in reasonable agreement in both level and shape. For the OH/IR star AFGL 2403 the shapes are consistent but the flux levels are notably different for all three spectra, which is possibly due to intrinsic variability for this type of source (Jiménez-Esteban et al. (2006), Smith (2003), Glass et al. (2001), Herman & Habing (1985)). W3 IRS5 is a mid-IR double source (van der Tak et al. (2005)), separated by about 1.1 arcsec along a position angle of $\sim 37^\circ$ and embedded within more diffuse emission. The Gemini-Michelle spectrum presented here is of the slightly brighter NE component, which van der Tak et al. (2005) call MIR1, whilst the UCLS and ISO observations included both sources as well as the extended emission. This probably explains the slightly different fluxes, increasing from the Gemini to UCLS to ISO spectra in accordance with the increasing beam size of the respective observations. It probably also at least partly accounts for the apparent difference in the silicate depth between the Gemini and other spectra.

Perhaps the best demonstration of the advantages of 8–13 μm narrow slit absorption spectroscopy over broad beam observations is the Galactic Centre data set. Clearly there is a very large difference in the depth of the silicate feature between the Gemini and ISO data sets. There were two observations available in the ISO archive, one centred on IRS7 and the other on Sgr A*, which are very consistent with each other (see Appendix A). They have been coadded for Figure 1. The Sgr A* spectrum was first presented by Lutz et al. (1996) and subsequently by Kemper et al. (2004), who – along with Min et al. (2007) and Li et al. (2007) – concluded from its seemingly smooth and featureless profile was entirely due to amorphous silicate, and thereby placed limits on other possible constituents.

As well as varying amounts of extinction across the centre of the Galaxy (e.g. Schödel et al. (2010); Scoville et al. (2003)), even on spatial scales smaller than the $14'' \times 20''$ ISO beam, within that beam there are multiple mid-IR sources as well as extended emission comprising the N-S arm and E-W bar of the mini-spiral. Obviously such a complicated source structure will impact on the observed spectrum, e.g. partially 'filling in' the silicate absorption feature. Our Gemini observations are instead much closer to the ideal 'pencil beam' absorption experiment, and thus well suited to revealing trace mineralogical structure.

Another contributor to the aforementioned silicate depth difference, and the probably related narrowness of the minimum of W3 IRS5 as well as AFGL 2136, is the presence of NH_3 and/or CH_3OH ices at 9.0 and 9.7 μm respectively. This is almost certainly the case for methanol for AFGL 2136, based on the work of Skinner et al. (1992) and Gibb et al. (2004). Neither ice material has been identified in 3–10 μm ISO spectroscopy of W3 IRS5, e.g. Dartois & d'Hendecourt (2001), Gibb et al. (2004) and Gibb et al. (2001), or 3 μm ground-based spectroscopy of Brooke et al. (1996). But our Gemini spectra of both the NE and especially SW components (to be presented in Do Duy et al., in preparation) have a very similar shape between 9 and

Table 1. Table of new Gemini observations, plus supporting ground-based and ISO data

Object	Date	Instrument	Chop/Nod throw	Standard star	Airmass Src/Std	ISO ID
AFGL 2403	28 Sep 2006	T-ReCS	8″ N-S	γ Aql	1.62/1.42	
		SWS01(1)				32000603
		SWS01(1)				50200604
AFGL 2789	05 Sep 2005	Michelle	8″ N-S	η Peg	1.30/1.22	
		SWS01(2)				26301850
AFGL 2136	15 Oct 2006	T-ReCS	15″ 31.0°	λ Sgr	1.42/1.49	
		SWS01(3)				33000222
		SWS06				31101023
W3 IRS5 NE	24 Sep 2005	Michelle	8″ 36.4°	BS168	1.35/1.28	
		SWS01(3)				42701302
SgrA IRS3	21 Aug 2005	Michelle	15″ N-S	λ Sgr	1.52/1.42	
		Other supporting ground-based and ISO data				
AFGL 2591[a]	26 Jun 1986	UCLS-lo	25″ N-S	β Peg		
AFGL 2591[b]	29-30 Sep 1987	UCLS-hi	24″ E-W	β Peg		
		SWS01(1)				02800433
		SWS01(3)				35700734
AFGL 4176[b]	21 Jan 1989	UCLS-hi	24″	α Cen		
AFGL 4176[b]	18 May 1992	UCLS-hi	20″ N-S	α Cen		
		SWS01(1)				11701311
		SWS06				30601344
IRAS13481[c]	19 Jan 2006	TIMMI2	10″ N-S	λ Vel	1.35/1.04	
		Other supporting ISO data				
IRAS19110		SWS01(2)				49900902
W28 A2		SWS01(1)				09901027
Sgr A*		SWS01(4)				09401801
		SWS01(3)				13600935
Sgr A SW		SWS01(4)				09401905
Sgr A NE		SWS01(4)				09500203
GC Pistol		SWS01(4)				84101302
Orion IRc2		SWS01(1)				68901006
Orion Pk1		SWS01(4)				68701515
Orion Pk2		SWS01(4)				83301701
Orion Bar		SWS01(2)				69501409
OH26.5+0.6		SWS01(2)				33000525
OH32.8-0.3		SWS01(2)				32001560
AFGL 230		SWS01(2)				78800604
HD100546		SWS01(4)				27601036
HD45677		SWS01(4)				71101992
HD44179		SWS01(4)				70201801
IRAS02575		SWS01(2)				86300968
IRAS10589		SWS01(2)				26800760
S106		SWS01(2)				33504295

[a] Previously published in Aitken et al. (1988); [b] Previously presented in Wright (1994); [c] Previously published in Wright et al. (2008)

10 μm to those of W33A and NGC7538 IRS9, two ice-rich deeply embedded YSOs with confirmed detections of NH_3 and CH_3OH (Gibb et al. (2000), Lacy et al. (1998)).

Such ices would be unlikely in the case of AFGL 2403, whilst for SgrA IRS3 their contribution would be very small, if at all existent (based on the relatively small optical depth of the 3 μm water ice feature toward the Galactic Centre, compared to YSOs, to be discussed in a following section). But we note that their spectra in Figure 1 also show evidence for either a discrete feature at 9.7–9.8 μm (AFGL 2403), or again a narrow minimum of the 8–13 μm absorption band (SgrA IRS3). The feature in AFGL 2403, as well as another around 9.3 μm (probably from crystalline enstatite), are more or less replicated in the ISO spectrum so are likely to at least be partially real. For SgrA IRS3 the silicate depth is in good agreement with that of Pott et al. (2008), obtained at lower spectral resolution (R $\sim$ 30) but higher spatial resolution (mid-IR interferometry).

Unfortunately there are also potential artefacts that could produce a very deep and/or narrow minimum of the silicate band. One is that telluric ozone at 9.6 μm can make interpretation in this part of the spectrum problematic, such that some authors choose not to even show this segment of their data. But as seen in Table 1 our target and standard star airmasses are well matched. For example, there is no residual water vapour features at 11.7 μm or 12.5 μm in Figure 1, and the division of the standard spectrum into the source spectrum has not produced large 'up-down'-type

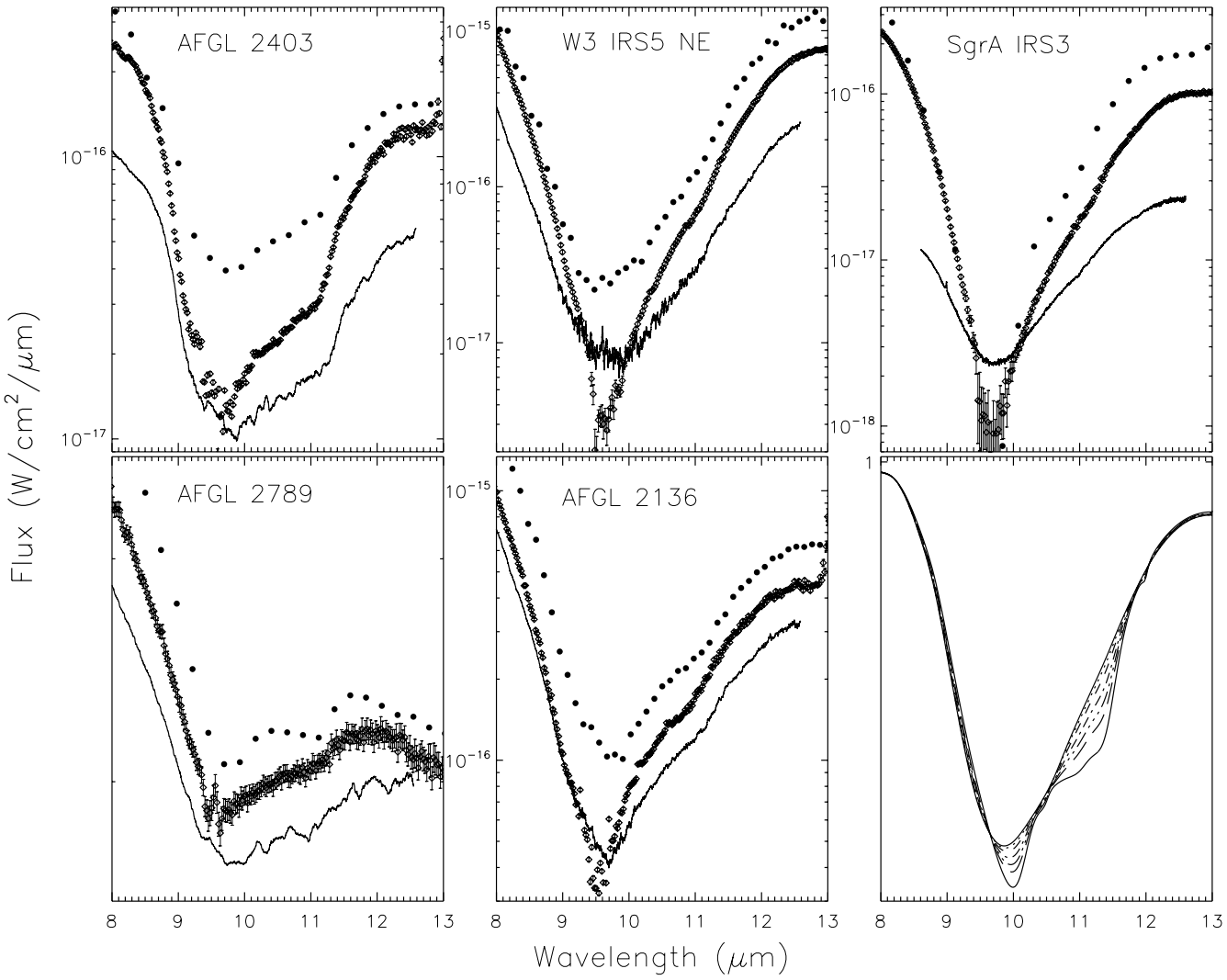

Figure 1. Gemini 8–13 μm spectra of the five targets listed in Table 1. The W3 IRS5 spectrum is of the slightly brighter NE component of this close double, also called MIR1 in van der Tak et al. (2005). For comparison lower spectral resolution data (solid circles) are also provided, obtained with the UCL Spectrometer (UCLS) and previously presented in the spectral atlas of Smith et al. (2000), scaled by factors of 0.4, 1.3, 1.0, 0.9 and 1.5 for AFGL 2403, W3 IRS5, SgrA IRS3, AFGL 2789 and AFGL 2136 respectively. Also shown is the higher spectral resolution data (solid lines) from ISO, being the Highly Processed Data Products from the ISO data archive, scaled by 0.20, 0.20, 0.01, 0.9, 0.8 respectively for AFGL 2403, W3 IRS5, SgrA IRS3, AFGL 2789 and AFGL 2136. The final panel instead shows a series of EMT models for amorphous olivine with increasing crystalline olivine content, using a CDE. See text for details.

artefacts that could occur if the two spectra were not well aligned. Thus we do not expect a significant contribution from poor ozone correction to the apparent depth of the silicate feature in our spectra. As some evidence of this the spectrum of a second position – which we call IRSX and will discuss in a following section – obtained from the same Gemini-Michelle observation as SgrA IRS3 shows no anomalous structure around the ozone wavelength. This strongly suggests that a reliable correction has been achieved (see also Appendix A).

The other artefact is difficult to quantify. As noted by Roche et al. (2015) and Roche et al. (2006) the T-ReCS and Michelle detectors suffer crosstalk between their different readout channels, especially prominent for bright sources (Sako et al. (2003)). Whilst obvious in imaging observations it is less so for spectroscopy, but can potentially diminish the signal along the spectral direction, and so perturb the level and shape of the silicate minimum. This will be discussed in more detail in our following paper with a larger sample (Do Duy et al., in preparation).

3.1.1 *Models*

Pre-empting the discussion to follow later, the final panel in Figure 1 shows a series of models containing an increasing quantity of crystalline olivine inclusions within an amorphous silicate matrix. Effective Medium Theory (EMT) has been used, wherein an 'average' or effective dielectic function – equivalently and otherwise referred to here as refractive indices or optical constants – can be derived from the optical

constants of two or more constituent materials. See Bohren & Huffman (1983) for general details.

For Figure 1 we have used the Maxwell-Garnett (MG) mixing rule, which requires defining so-called matrix (or host) and inclusion materials, here being amorphous and crystalline silicates respectively, as well as the volume fraction occupied by the inclusions. Although the generalised MG formula can accommodate spheroidally shaped inclusions this introduces an extra free parameter which is unconstrained by any observations of which we know. Thus the version we use assumes spherical inclusions.

Different optical constants for the amorphous silicate have been tested, including 'astronomical silicate' of Draine (2003b) and olivine from Dorschner et al. (1995). The olivine species with equal iron and magnesium content, i.e. $MgFeSiO_4$, from Dorschner et al. is used for the models in Figures 1, 2 and 3. This has also been used by different authors in their own studies of cosmic dust, e.g. toward the Galactic Centre by Kemper et al. (2004) and Min et al. (2007).

Similarly, various crystalline silicate optical constants have been trialled, such as those of crystalline olivine from Mukai & Koike (1990), crystalline $Mg_{1.9}Fe_{0.1}SiO_4$ from Fabian et al. (2001) and crystalline forsterite from Sogawa et al. (2006) and Suto et al. (2006). Those of Mukai & Koike are used for Figures 1, 2 and 3, but our results are qualitatively (though not necessarily quantitatively) similar irrespective of the specific combination of optical constants used (Do Duy et al., in preparation). Models with a volume fraction of crystalline olivine of f=0.01, 0.025, 0.05, 0.075, 0.10, 0.15 and 0.20 are shown in the final panel in Figure 1.

Absorption cross sections C_{abs} are calculated in the Rayleigh approximation, i.e. the grain size is much smaller than the wavelength. This is almost certainly a valid assumption in our case even for grain sizes up to about a micron (Somsikov & Voshchinnikov (1999)) in size, let alone for the 0.1 μm grains typically inferred for the ISM (Mathis et al. (1977)). Given the Rayleigh approximation is valid for the entire grain then of course it is also valid for the EMT inclusions.

Calculations assume a single spheroidal shape, e.g. oblate with a principal axis ratio of 2:1, or a continuous distribution of ellipsoids (CDE, in our case actually spheroids). The latter is used for Figure 1, comprising both oblate and prolate particles, from an axis ratio of 1:1 (i.e. a sphere) up to 5:1, all with equal probability. What is actually plotted in Figure 1 however is not the absorption cross section, but instead the quantity $\exp(-C_{abs})$ which 'mimics' an absorption spectrum.

We have ran tests for different types of CDEs, e.g. with Gaussian weights and different maximum axis ratio, and oriented spheroids as well as randomly oriented ellipsoids (as given in Min et al. (2003)). Results are qualitatively similar (Do Duy, in preparation), but the single shape or oriented spheroids are potentially more realistic. This is because all of the targets presented here (apart from AFGL 2403) show mid-IR polarisation (Smith et al. (2000)). This is a certain sign that at least some of the dust grains along the path to each object are aligned, probably with their short axes along the ambient magnetic field direction (Lazarian (2007)). Obviously this also argues against using any kind of model which assumes spherical dust grains.

3.2 Extracting the 11 μm feature and its optical depth

At least two approaches can be made to extract the 11 μm feature and its optical depth. For instance, the amorphous silicate profile can firstly be extracted by fitting a Planck function B(λ,T) to the 8 and 13 μm points to determine a colour temperature $T_{8/13}$. Subsequently the optical depth τ_λ is calculated from $F_{obs} = B(\lambda, T_{8/13}) \times \exp(-\tau_\lambda)$, where F_{obs} is the observed flux. This is not an entirely physical approach as it assumes that the dust has zero emissivity at 8 and 13 μm. Although these wavelengths are certainly near or even at the edges of the amorphous silicate Si–O stretching band, cosmic dust still retains some emissivity there, as beautifully demonstrated in Figure 10 of Fritz et al. (2011). This shortcoming can be alleviated by scaling the fluxes by a factor equal to an assumed emissivity at these wavelengths, e.g. that of the Trapezium region in Orion. This has historically been used to model in a straightforward way the 8–13 μm spectra of objects within molecular clouds and star forming regions (e.g. Gillett et al. (1975), Hanner et al. (1998), Smith et al. (2000)). Thereafter a new $T_{8/13}$ and amorphous silicate profile can be determined.

However, this does not help with another assumption implicit in this approach, namely that the warm dust emitting behind the absorbing column is optically thick, and thus can be approximated as a black-body. This will be true in many cases (e.g. Smith et al. (2000)) but will not always be true, in which case the underlying emitting dust would have a silicate emission feature and the extracted optical depth under-estimated (although the relative magnitude of the under-estimate will decrease with increasing absorption depth). A powerful demonstration of how different a real continuum can be to a polynomial or even Planck-like contunuum connected between observed fluxes can be seen in Figure 10 of Fritz et al. (2011). They determined the 1–19 μm extinction to the Galactic Centre from hydrogen recombination lines, and subsequently deduced the unextinguished (overlying) spectrum. Nowhere do the unextinguished and observed spectra equal each other.

Even so, this approach has the advantage of simplicity and consistency, and is commonly used (e.g. de Vries et al. (2014) and de Vries et al. (2010), but who instead used a linear interpolation across 8 to 13 μm rather than a black-body fit). After extracting the 9.7 μm feature the 11 μm absorption profile can then be extracted by fitting a low order polynomial from around 10 μm to 12–13 μm, masking out the data in between these wavelengths. Optical depths calculated in this way, and especially the relation between the 9.7 and 11 μm depths for the entire sample, will be presented in Do Duy et al. (in preparation).

In this paper however we use a simpler approach which is less susceptible to the above-mentioned assumptions, but provides no information on the amorphous silicate band. In this approach a polynomial is fit to the observed spectrum between the ranges of about 9.8–10.3 μm and 12.1–13 μm, the precise ranges being dependent on the data quality (e.g. signal-to-noise and/or other instrumental or telluric artefacts). These ranges form a 'local' or 'quasi' continuum and are chosen to be short enough to be as free as possible from potential (strong) cosmic dust spectral features but long enough to adequately constrain the polynomial fit. We

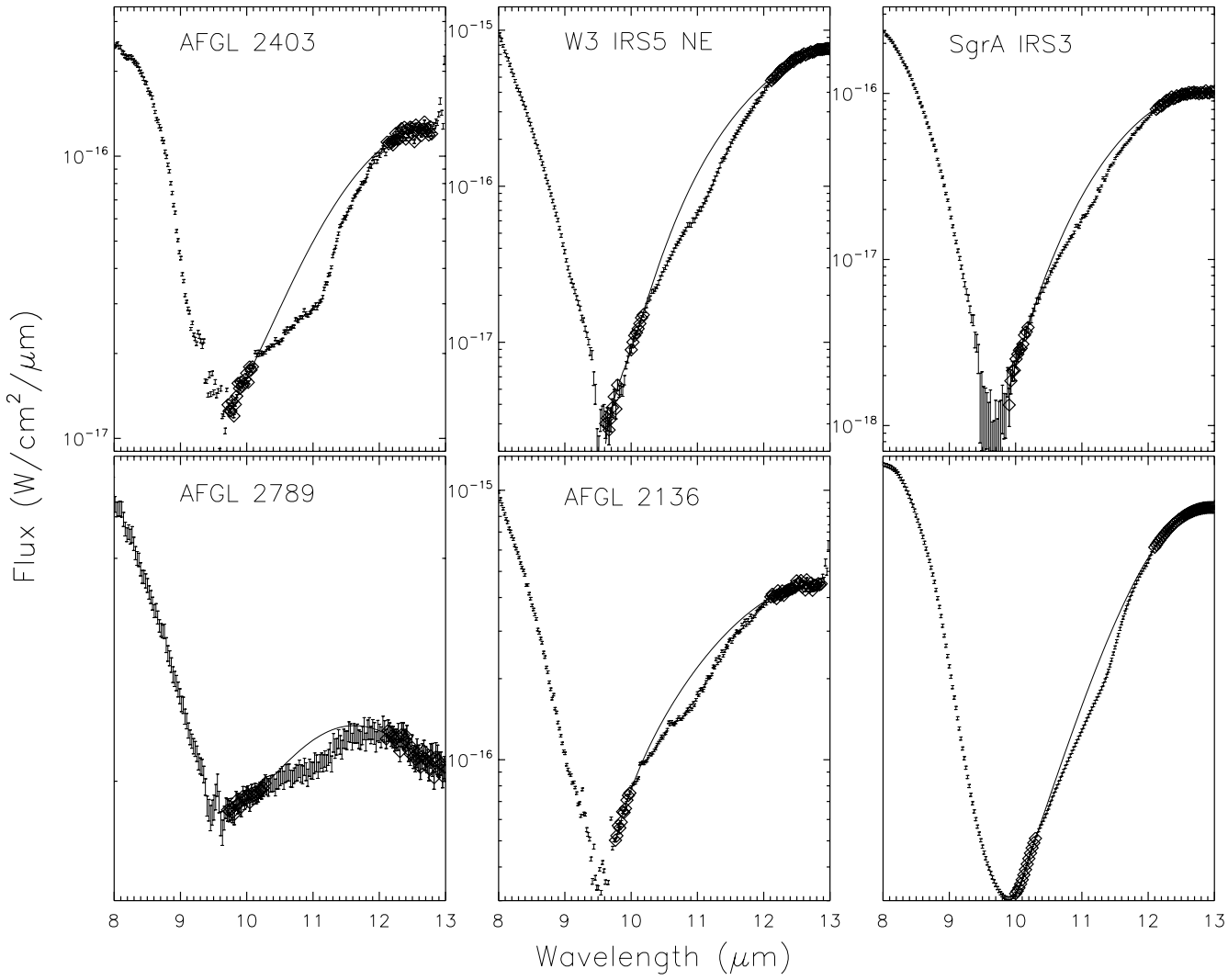

Figure 2. Polynomial fits to 10-13 μm portion of the Gemini spectra in Figure 1, as well as a representative EMT model, in this case oblate 2:1 with a volume fraction of crystalline olivine of 0.05. The W3 IRS5 spectrum is of the slightly brighter NE component of this close double, also called MIR1 in van der Tak et al. (2005).

recognise that real information can be lost (or perhaps even false information injected) with any method of removing a continuum, as cautioned by Jones (2014), which is why we perform the same steps on our model.

Polynomial fits are shown in Figure 2 for the same five targets as in Figure 1. A sample model treated in precisely the same way, in this case for a crystalline olivine volume fraction of 0.05, is shown in the last panel. We note here that broadly equivalent approaches were used by Poteet et al. (2011) and Spoon et al. (2006) to extract their 11 μm absorption features.

The 11 μm feature profile, and its optical depth τ, is subsequently calculated by extrapolating the polynomial across the interval and then deriving τ using a similar equation to that above, in this case $F_{\rm obs} = F_{\rm cont} \times \exp(-\tau_\lambda)$, where $F_{\rm cont}$ is the local continuum given by the polynomial. The left hand panel of Figure 3 shows for the same five sources in Figs. 1 and 2 the 11 μm feature extracted in this way, whilst the right hand panel shows the model treated in precisely the same fashion for volume fractions of crystalline silicate of 0.0, 0.01, 0.025, 0.05 and 0.075. That no 11 μm feature is 'recovered' for the purely amorphous silicate lends credibility to the approach.

4 DISCUSSION

4.1 Central wavelength and profile of the 11 μm feature

The central wavelength of the 11 μm absorption feature is 11.10±0.10 μm for all objects. Whilst that for AFGL 2136 appears to be below 11 μm in Figure 3 this is likely to be an artefact introduced by noise and/or the defringeing process necessary for some T-ReCS spectra. The corresponding feature extracted from its ISO spectrum in Figure 1 is fully consistent with being centred at 11.1 μm. Such a central wavelength was also found for the features discovered by

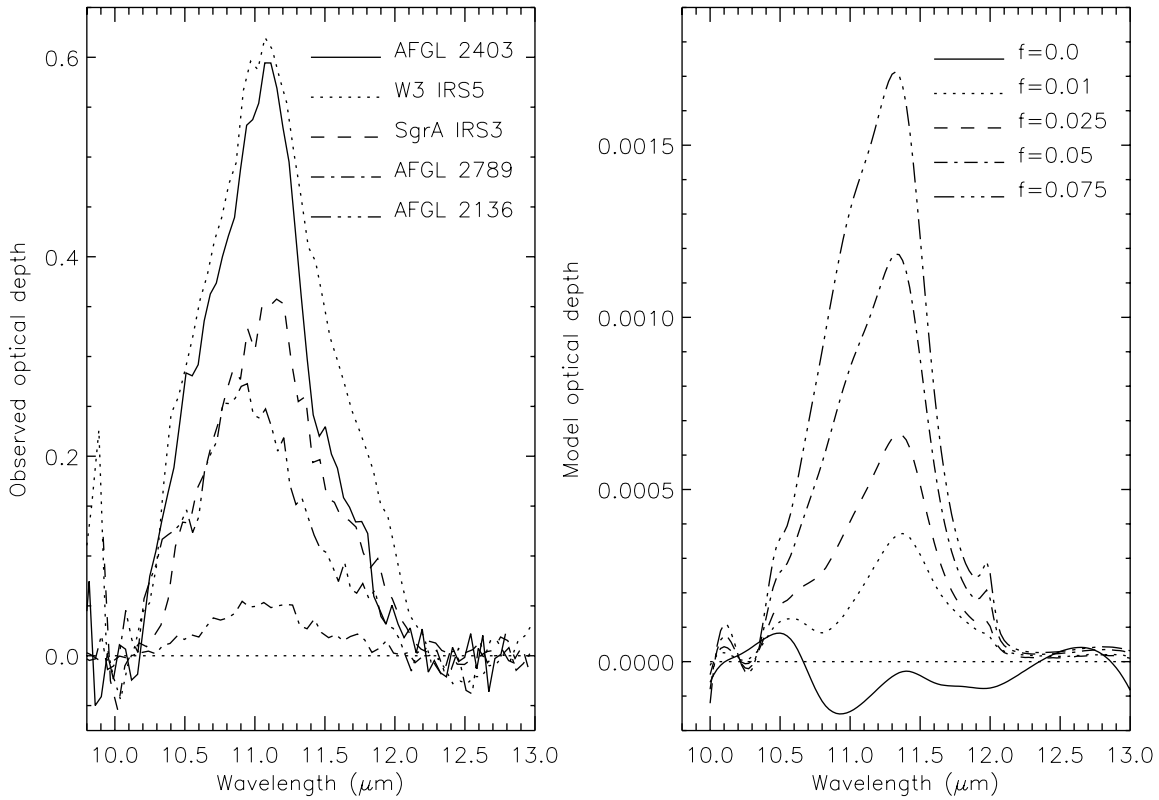

Figure 3. In the left and right hand panels are shown the optical depth profiles around 11 μm extracted from the Gemini observations of Figure 1, and EMT models of oblate 2:1 grains with varying volume fraction of crystalline olivine inclusions. The same technique has been used for both the observations and models. The observations have been averaged in two pixel wide bins for plotting purposes.

Poteet et al. (2011) and Spoon et al. (2006) in a Class 0 YSO and a ULIRG respectively.

Figure 4 displays all the features again, but this time normalised to their respective peaks. Like the central wavelength the profile is also remarkably similar for each source, noting that they represent a range of different environments from a dust factory (AFGL 2403) to the ISM (SgrA IRS3) to dense molecular clouds or even circumstellar envelopes/disks (W3 IRS5, AFGL 2136). The profile is not symmetric about the peak, dropping essentially monotonically on the short wavelength side, whilst on the long wavelength side the drop is much steeper to around 11.5 μm at which point it becomes more gradual.

That the profile is so similar for sources from low (AFGL 2789) to high (W3 IRS5) extinctions strongly suggests that our technique to extract the 11 μm band is not influenced by potential crosstalk of the T-ReCS and Michelle detectors. Indeed, as seen in Figure 2 we have not used the deepest part of the silicate band – where such crosstalk might be expected to be most severe – for the polynomial fit for SgrA IRS3 and AFGL 2136.

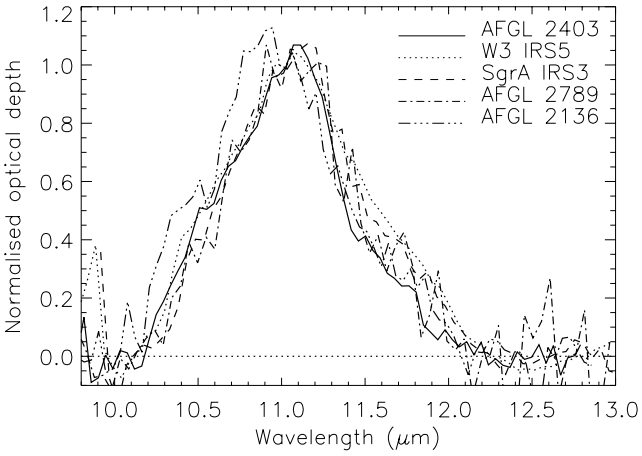

Figure 4. Normalised profiles of the 11.1 μm absorption feature extracted from the Gemini spectra. Each profile has been divided by a peak value given by the mean between 10.9 and 11.2 μm. The observations have been averaged in two pixel wide bins for plotting purposes.

4.2 Possible carriers of the 11.1 μm absorption

Several potential candidates exist for the carrier of the 11.1 μm absorption feature reported here, including hydrocarbons, water ice, silicon carbide (SiC), carbonates and crystalline silicates. All have been identified as components of cosmic dust in one or more types of environments through astronomical spectra and/or as pre-solar inclusions within meteorites or interplanetary dust particles (IDPs), e.g. Boogert et al. (2015), Zinner (2013), Bradley (2010) and Draine (2003a). Considering all of the above candidate species, we present arguments below which we believe

strongly supports a crystalline silicate identification. If nothing else, the data itself, plus modelling and other plausibility arguments, are more consistent with crystalline silicate than any other candidate.

To assist with the discussion below we list in Table 2 for each target the optical depths at various wavelengths for which a discrete spectral feature has been detected. We have included four other sources in the table, namely a second Galactic Centre position plus the deeply embedded YSOs (DEYSO) AFGL 2591, AFGL 4176 and IRAS13481-6124. For convenience we call the Galactic Centre source SgrA IRSX, the 8–13 μm spectrum of which was obtained from the same Gemini-Michelle observation as SgrA IRS3. Its position is several arcsec south of IRS3, within the E-W bar of the SgrA mini-spiral. The three DEYSOs have previously been identified to have an 11 μm absorption band by Aitken et al. (1988), Wright (1994) and Wright et al. (2008) respectively. These objects will be discussed more fully in following subsections (see for instance Figures 10, 13 and 14).

4.2.1 Water ice

Water ice possesses a librational band, the peak wavelength of which varies between about 12 and 13 μm for its crystalline and amorphous phases respectively (e.g. Mastrapa et al. (2009); Maldoni et al. (1998)). Its astronomical identification has historically been extremely difficult, with only a handful of good cases, e.g. the embedded YSO AFGL 961 (Cox (1989); Smith & Wright (2011), though see also Robinson et al. (2012)) and a few low mass YSOs such as HH46 IRS in Boogert et al. (2008). Its detailed study has thus been restricted, due in part to its broadness and overlap with the minimum between the 10 and 20 μm silicate bands.

In centrally heated dust shells it is also susceptible to radiative transfer effects, such that cool dust emission can 'fill-in' and essentially mask the water ice feature, as shown by Robinson (2013) and Robinson & Maldoni (2010). For instance, whilst some of their models did result in a clearly identifiable water ice signature, even resembling the feature we observe (e.g. Fig. 14 in Robinson & Maldoni (2010)), they predict unrealistic levels of absorption within the intrinsically much stronger 3.05 μm water ice band, certainly much higher than seen in our targets (Table 2 and Figure 5). Further, the overall appearance of the $\geq$ 10 μm portion of mid-IR spectra of YSOs with possible librational band absorption in Boogert et al. (2008) is much flatter than we see in our two Gemini-observed and bona-fide embedded YSOs AFGL 2136 and W3 IRS5, as well as AFGL 2591, AFGL 4176 and IRAS13481 to be discussed in a following sub-section. These considerations, plus the difference between the expected and observed central wavelengths, already argues against a water ice explanation.

Even so, water ice absorption is definitely identified in a few of our objects at 3.05 μm (Gibb et al. (2004); Smith et al. (1989)) and 6.0 μm (Keane et al. (2001)). But in neither AFGL 2403 nor AFGL 2789 is it detected (though we note for AFGL 2403 there is little or no continuum below 3 μm in the ISO data which water ice could absorb against). See Figures 5 and 6. Thus, in at least these two sources a water ice carrier for the 11.1 μm absorption can almost certainly be ruled out.

For the Galactic Centre source SgrA IRS3 there is conflicting evidence whether it has 3 μm water ice absorption. Within a broad beam, such as that of ISO, definite absorption is detected (e.g. Chiar et al. (2000) and Figure 5), but several authors, including Chiar et al. (2002), Moultaka et al. (2005) and Moultaka et al. (2004) have shown that the water ice column varies significantly, up to a factor of 5, over relatively small spatial scales of 0.5–2 pc, and certainly within the ISO beam size. This has been attributed by Chiar et al. (2002) to the clumpy nature of the molecular clouds within the Galactic Centre region.

The spectrum of IRS3 in Willner & Pipher (1982) in a 2.5 arcsec beam has a 3.4 μm hydrocarbon absorption feature (see next section) but no strong ice absorption (as stated by the authors). They instead infer that it has probable H_2O gas phase bands from the stellar atmosphere, with peak absorption occurring near 2.9 μm. Indeed, it can be seen in the ISO spectrum in Figure 5 that the 'ice' feature in SgrA occurs at $\sim$ 2.95 μm, significantly shorter than that of the YSOs AFGL 2136 and W3 IRS5.

The spectrum of SgrA IRS3 in Pendleton et al. (1994), obtained in a 2.7 arcsec aperture, has a smoothly rising continuum from 2.9–3.6 μm, apart from 3.4 μm hydrocarbon absorption, unlike the nearby sources IRS7 and IRS6E which have clear absorption around 3 μm. The spectra of IRS3 and IRS7 in Moultaka et al. (2004), taken in a 0.6 arcsec slit, are very similar to those of Pendleton et al. (1994), but that of IRS3 in Chiar et al. (2002), also in a 0.6 arcsec slit, is very different. The work of Moultaka et al. (2005) appears to resolve the discrepancy, showing that IRS3 is coincident with a region of much reduced H_2O absorption. Thus, by analogy with AFGL 2403 and AFGL 2789 it appears highly unlikely that water ice could be responsible for the 11.1 μm absorption seen in SgrA IRS3.

Finally, assuming the same carrier is responsible for all the 11.1 μm features we have detected then the clear lack of a correlation between $\tau_{11.1}$ and $\tau_{3.0}$ or $\tau_{6.0}$ in Table 2 almost certainly rules out water ice as the carrier. Note for instance the discrepancies between $\tau_{3.0}/\tau_{11.1}$ for AFGL 2591 and AFGL 4176 (as well as SgrA IRS3) and the other two YSOs AFGL 2136 and W3 IRS5.

4.2.2 Hydrocarbon

Our observed central wavelength is inconsistent with that expected from isolated (gas-phase) PAHs, for which the typically observed peak wavelength is at 11.22–11.25 μm, at least in the case of emission (e.g. Verstraete et al. (2001); Witteborn et al. (1989)). The central wavelength may change in the case of absorption when the PAH or related hydrocarbon is embedded in or on a host matrix or perhaps as some kind of mantle constituent, e.g. together with water ice. For example, Bernstein et al. (2005) find that in a water ice matrix PAH bands in the 11–13 μm region can shift by $\pm$ 5-10 cm^{-1}. So a gas-phase band at 11.25 μm could feasibly occur in the range of 11.25$\pm$0.13 μm. But Bregman et al. (2000) identify 11.25 μm absorption in the embedded YSO MonR2 IRS3 with a C–H out-of-plane vibrational mode of PAH molecules, a wavelength obviously inconsistent with our data.

As shown by Witteborn et al. (1989) for the four sources they studied, the 11.25 μm PAH band does have an asym-

Table 2. Optical depths, τ_λ

Object	H_2O ice				Hydrocarbons			Unknown	Silicate
	11.1	3.0	6.0	3.4	3.47	6.2	7.25	6.85	9.7
AFGL 2403	0.60/0.55	nd	nd, <0.02	nd, <0.05	nd, <0.05	≤0.04	nd, <0.005	0.045@6.6 μm	2.7-4.4
AFGL 2789	0.05/0.04	nd, <0.05	≤0.02	nd, <0.005	nd ≤0.02@3.53 μm	nd, <0.01	≤0.005	nd 0.035@6.6 μm	**0.7**-2.3
AFGL 2136	0.27/0.28	2.72-3.60	0.23-0.30	≤0.12	0.10-0.14	0.03-0.06	0.04	0.18-0.27	**3.5**-5.1
W3 IRS5	0.60/≥0.45	2.78-3.48	0.26-0.33	nd, <0.03	0.133-0.14	<0.02	0.04	0.22-0.28	**5.6**-7.4
SgrA IRS3	0.35	≤0.3-0.63	–	0.19-0.31	0.12-0.20	0.18	–	0.16	≥7
SgrA IRSX	0.15/0.20	0.50	0.10@6.1 μm	0.20	0.05	0.05	0.03	0.05	3.6
AFGL 2591	0.27	0.69-0.92	0.12	≤0.03	0.045	<0.02	≤0.03	0.04-0.17	**2.8**-4.4
AFGL 4176	0.22/0.20	0.3-0.5	0.03	0.05	0.05	<0.02	≤0.01	0.02@6.7μm	**3.1**-4.8
IRAS13481	0.10	–	–	–	–	–	–	–	≥1

Note 'nd' means 'not detected', but a 1σ upper limit may be given. The two values x/y for $\tau_{11.1}$ refer to those determined from the Gemini and ISO spectra respectively. In the case of W3 IRS5 the ISO value is a lower limit since 11.25 μm PAH emission perturbs the extracted profile.
Optical depths at 9.7 μm are mainly taken from Wright (1994) and Smith et al. (2000), with the two values being appropriate for optically thick (i.e. featureless blackbody-like) and optically thin underlying emission. The value in bold face is the preferred figure based on the χ^2 of the fit. Otherwise, for SgrA $\tau_{9.7}$ is from Roche & Aitken (1985) and for IRAS13481-6124 $\tau_{9.7}$ is from Do Duy et al. (in preparation).
References for optical depths of the other species are:
AFGL 2136: Gibb et al. (2004), Schutte & Khanna (2003), Dartois et al. (2002), Keane et al. (2001), Dartois & d'Hendecourt (2001), Brooke et al. (1999), Schutte et al. (1996), Willner et al. (1982)
W3 IRS5: Gibb et al. (2004), Keane et al. (2001), Brooke et al. (1996), Allamandola et al. (1992), Smith et al. (1989), Willner et al. (1982)
SgrA IRS3: Pott et al. (2008), Moultaka et al. (2004), Chiar et al. (2002), Tielens et al. (1996), Pendleton et al. (1994), Sandford et al. (1991)
SgrA IRSX: Apart from the first figure for $\tau_{11.1}$ from this work, all other values are from ISO spectroscopy, and hence 'averaged' across a field of view containing most or all of the mini-spiral; Gibb et al. (2004)
AFGL 2591: Gibb et al. (2004), Dartois & d'Hendecourt (2001), Brooke et al. (1999), Smith et al. (1989), Willner et al. (1982); the 6–7 μm region is heavily influenced by H_2O gas phase lines (Helmich et al. (1996))
AFGL 4176: Persi et al. (1986) and our own analysis of the ISO–SWS01 spectrum; the 6–7 μm region is heavily influenced by H_2O gas phase lines (van Dishoeck & Helmich (1996))
AFGL 2403 and AFGL 2789: Our own analysis of the ISO–SWS01 spectra

metric shape, with a long wavelength wing, and is thus broadly consistent with our feature in Figure 4. But assuming our quasi-continuum-subtracted profiles in Figure 4 are a true representation of the feature profile then its FWZI is inconsistent with the much narrower PAH emission band, which only extends between about 11.0–11.6 μm in the four targets of Witteborn et al. (1989). Furthermore, such a PAH feature would likely be accompanied by other bands, particularly an in-plane bending mode at 8.6 μm of comparable integrated strength and an even stronger C–C mode at 7.7 μm. No sign of 8.6 μm absorption or emission is seen in our data (Figure 1), whilst that at 7.7 μm in Figure 5 for AFGL 2136 and possibly W3 IRS5 (potentially explaining the apparent 'early' onset of its 9.7 μm silicate absorption band) is almost certainly due to methane (CH_4) ice as described in Gibb et al. (2004).

Other hydrocarbon absorption features include those of aliphatic groups at 3.38, 3.42, 3.47, 6.85 and 7.25 μm, and aromatic groups at 3.3 and 6.2 μm, and have been identified in absorption spectra along several sightlines through the ISM, eg. Chiar et al. (2013) and references therein. This includes the Galactic Centre (e.g. Figure 5 and Figure 6 here, as well as Chiar et al. (2002), Chiar et al. (2000) and Tielens et al. (1996)), but to our knowledge no such feature around 11 μm has been postulated, let alone identified. For the Galactic Centre sightline the 3.38, 3.42 and 3.47 μm features appear as a triplet of comparable strengths, whilst for YSOs only a broad feature centred near 3.47 μm is typically detected (Brooke et al. (1999); though the ISO spectrum of AFGL 2136 does appear to have a discrete but weak 3.4 μm feature in Figure 5, confirmed after extracting an optical depth spectrum from 3.2 to 3.7 μm). The 3.2–3.8 μm long wavelength wing, peaking at around 3.3 μm and which almost ubiquitously accompanies the 3 μm water ice feature in molecular clouds, is also commonly attributed to a 'continuum' of hydrocarbon absorption, e.g. Gibb et al. (2004) and Smith et al. (1989).

Absorption at 7.25 μm is probably also present in the ISO spectra of W3 IRS5 and AFGL 2136, but not toward AFGL 2403 and AFGL 2789 (Figure 5). Since neither the 7.25 nor 7.7 μm features are seen toward these latter two objects, nor features at 3.4, 6.2 and 6.85 μm, then a hydrocarbon carrier for their 11.1 μm absorption can almost certainly be ruled out.

Once again, assuming the same carrier is responsible for all the 11.1 μm features we have detected then (despite the low number statistics) the lack of a correlation between $\tau_{11.1}$ and any of $\tau_{3.4}$, $\tau_{3.47}$, $\tau_{6.2}$, $\tau_{6.85}$ or $\tau_{7.25}$ in Table 2 almost certainly rules out hydrocarbons as the carrier. Note for instance the discrepancies between $\tau_{3.47}/\tau_{11.1}$ for AFGL 2591 and the other two YSOs AFGL 2136 and W3 IRS5. Further, with larger sample sizes Brooke et al. (1999) and Brooke et al. (1996) find that the 3.47 μm hydrocarbon feature does correlate with the 3 μm water ice band, and Thi et al. (2006), Smith et al. (1989) and Willner et al. (1982) find that the 3.2–3.8 μm long wavelength wing also correlates with the ice band. Since there is no obvious correlation between the 11.1 μm and water ice bands (see previous subsection) then it is highly unlikely a correlation could exist between the 11.1 μm feature and these other bands. We note here that many of the objects in the aforementioned works are common to our larger sample, so these correlations will be studied in more detail in Do Duy et al. (in preparation).

4.2.3 Carbonates

Carbonates have been identified in interplanetary dust particles (IDPs) and meteorites, principally via bands at around 6.8 and 11.4 μm (e.g. Bradley et al. (1992); Sandford (1986); Sandford & Walker (1985)). To our knowledge there has

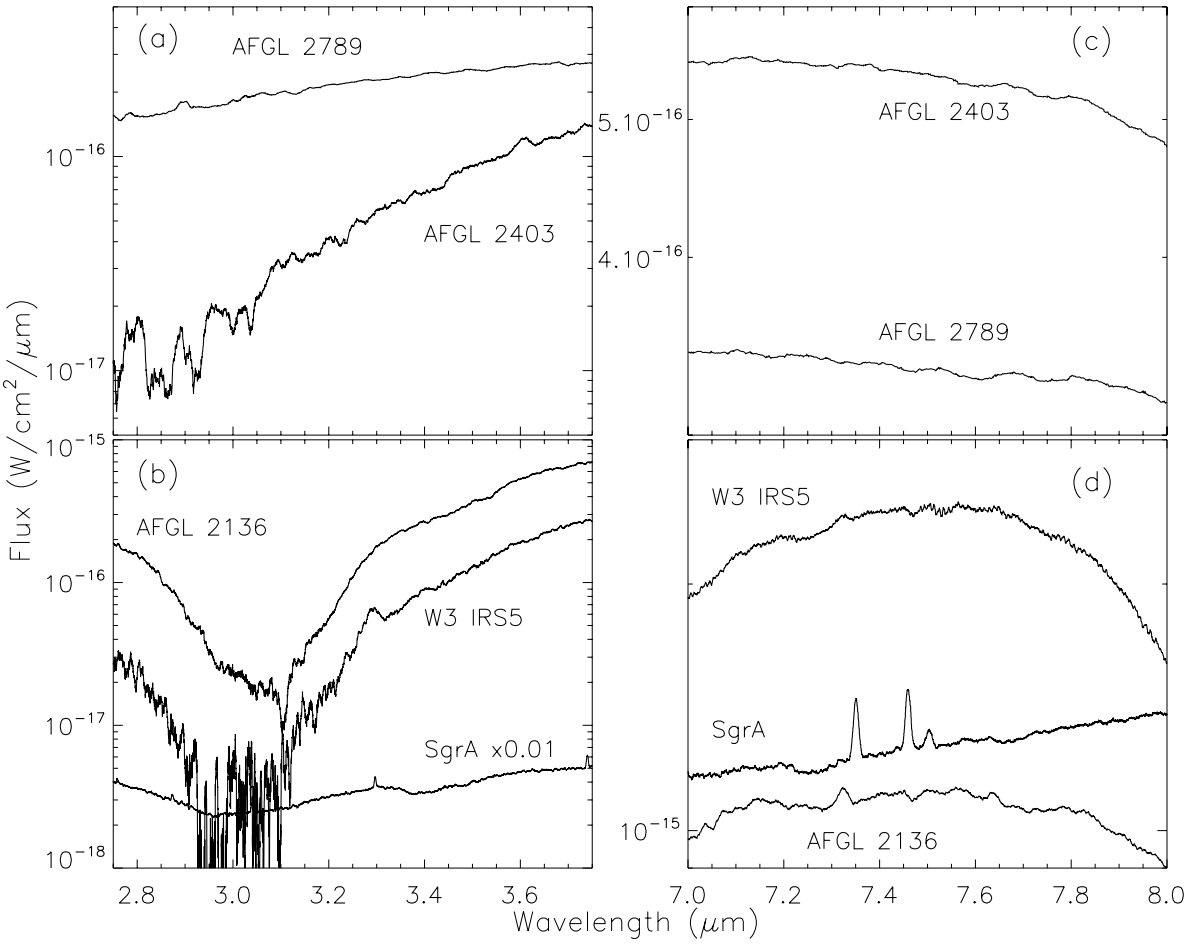

Figure 5. Sigma-clipped and smoothed ISO spectra in the region of a) the 3.05 μm water ice band and b) the 7.25 μm hydrocarbon band. In (a) a hydrocarbon feature at 3.4 μm is seen toward the Galactic Centre, and perhaps also for AFGL 2136. Whilst the 3.4 μm band is certainly detected in small-beam and narrow-slit spectra of SgrA IRS3, the 3 μm absorption is relatively weak or non-existent (see text for details). That there is probably no water ice band in AFGL 2403 is demonstrated by the fact that the signal is flat from 3.1 μm onwards, unlike the cases of W3 IRS5 and AFGL 2136. In (b) there is a known 7.25 μm hydrocarbon feature toward the Galactic Centre, and probably also in the spectra of W3 IRS5 and AFGL 2136, but not toward AFGL 2789 or AFGL 2403. Probable 7.7 μm methane ice absorption is detected in AFGL 2136, and possibly W3 IRS5 and SgrA, but no 7.7 μm feature is seen in AFGL 2789 and AFGL 2403.

been no pre-solar carbonate grain detected, i.e. one with an isotopic anomaly compared to our solar system (e.g. Zinner (2013)). Carbonates have also been tentatively identified in the far-infrared spectra of a few extra-solar-system objects, including calcite ($CaCO_3$, near 93 μm) and dolomite ($CaMg(CO_3)_2$, near 62 μm) in two planetary nebulae by Kemper et al. (2002b) and Kemper et al. (2002a), and calcite in the solar-type protostar NGC1333 IRAS4 by Ceccarelli et al. (2002).

If carbonates were responsible for our 11.1 μm absorption feature then they would have to be Mg-rich (i.e. $MgCO_3$) as it is only for the Mg cation that the band occurs at 11.10 μm. For other abundant and likely cation metals Ca and Fe the feature occurs at 11.33 and 11.42 μm respectively (Lane & Christensen (1997)). Otherwise dolomite at 11.19 μm is just within our 0.1 μm uncertainty band.

The 6.8 μm carbonate band is intrinsically several times stronger than the 11.1–11.4 μm band, providing a potentially critical diagnostic constraint. As seen in Figure 6 three of our targets do have an absorption feature centred around 6.8 μm. In fact, this feature is almost ubiquitous in the spectra of both high and low mass YSOs (Boogert et al. (2008); Gibb et al. (2004)), and is seen in the ISM toward the Galactic Centre (Chiar et al. (2000); Tielens et al. (1996)). At least for the YSOs it is assessed to be made up of two components, differing in their volatility, centred around 6.75 and 6.95 μm (Boogert et al. (2008), Keane et al. (2001)). Whilst several candidates exist for the feature(s), positive identification of either component remains a mystery (Boogert et al. (2015)), and according to Boogert et al. (2008) the carrier cannot be the same for the YSOs and the ISM. We refer to the aforementioned papers for a discussion of the relative merits of each candidate. However, Keane et al. (2001) rule out a carbonate interpretation based on the overall shape of the observed band being poorly fit by carbonates, although they also use the perceived lack of an accompanying 11.4 μm feature to support their case, which we have shown is possibly incorrect for many sources.

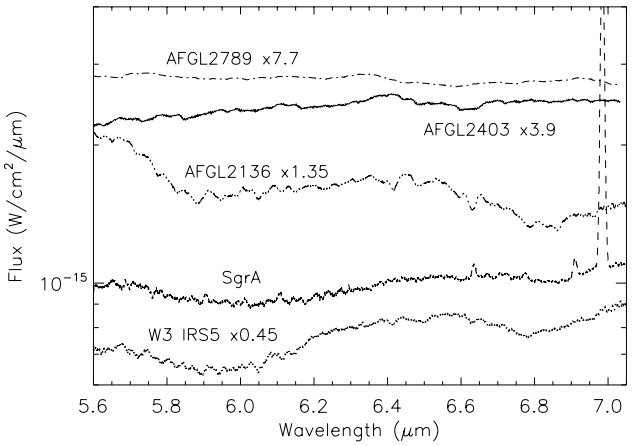

Figure 6. Sigma-clipped and smoothed ISO spectra in the region of the 6.0 and 6.85 μm water ice and 'unidentified' bands respectively. Relatively sharp features in the spectrum of AFGL 2136, e.g. at $\sim$ 6.4 and 6.6 μm, arise from hot gas-phase water (van Dishoeck & Helmich (1996)).

As for the cases of water ice and hydrocarbons, Figure 6 shows that neither AFGL 2789 nor AFGL 2403 have a feature around 6.8 μm, so that a carbonate carrier for their 11.1 μm absorption feature can almost certainly be ruled out. Further, assuming the same carrier is responsible for all the 11.1 μm features we have detected then the lack of a correlation between $\tau_{11.1}$ and $\tau_{6.85}$ in Table 2 almost certainly rules out carbonates as the carrier. Note for instance that the higher quality ISO measurement of $\tau_{6.85}$ for AFGL 2591 – given in Gibb et al. (2004) and compared to the much lower spectral resolution data of Willner et al. (1982) – is up to a factor of $\sim$ 5 lower than that of any other object, yet their $\tau_{11.1}$ are broadly similar.

4.2.4 Silicon carbide (SiC)

Silicon carbide has a lattice mode, the central wavelength of which occurs – on average – at 11.15±0.05 μm in emission (and occasionally in absorption) in astronomical spectra of carbon stars (Clément et al. (2003)). Along with the agreement in central wavelength with our feature, the FWZI's are also reasonably consistent. Thus, SiC could be a candidate for the absorption band we observe in our small sample of Figure 1. Pre-solar SiC has been found in meteorites, suggesting some must survive after being formed in C-star outflows. But it has not so far been unambiguously detected in the ISM (Whittet et al. (1990)), although Min et al. (2007) inferred a fractional abundance of 2.6–4.2%, with 9–12% of the available Si in SiC grains, based on a shoulder around 11 μm in the extinction curve toward the Galactic Centre. Such a shoulder was also detected in the VLTI MIDI study of SgrA IRS3 by Pott et al. (2008), who state it occurs at 11.3 μm and also tentatively assign it to SiC.

To our knowledge only a single detection has been claimed for the presence of SiC in the disk or envelope of a young star, namely SVS13 (Fujiyoshi et al. (2015)). But its spectrum looks markedly different to those we present here, and the SiC identification was based largely on a unique mid-IR polarisation signature (Fujiyoshi et al. (2015); Smith et al. (2000); Wright et al. (1999)). Once again we defer a full discussion of the SiC possibility to a subsequent paper describing the full sample (Do Duy et al. in preparation). For now we instead use polarisation data in the following section to argue against SiC being the carrier.

4.3 A crystalline silicate carrier

Given the similarity of central wavelength and band profile for all five sources in Figures 1 to 4, as well as three other YSOs to be presented in this section – AFGL 2591, AFGL 4176 and IRAS13481-6124 – we believe it is very likely that the same carrier is responsible for their 11.1 μm absorption features. Further, the above discussion highlights that – of the several possible carriers – water ice, hydrocarbons and carbonates can almost certainly be excluded in the cases of AFGL 2789 and AFGL 2403 given the lack of concomitant features in those spectra. Moreover, given the absence of a correlation between the depths of the 11.1 μm feature and 3–8 μm bands of water ice, hydrocarbons and carbonates, a strong argument exists that none of these materials can be the 11.1 μm carrier in any of the objects. Crystalline silicates and perhaps SiC therefore remain the only options. We will show later that SiC in at least three sources is highly unlikely, based on polarisation considerations.

If any trend can be seen in Table 2 it is that $\tau_{11.1}$ increases with increasing $\tau_{9.7}$, e.g. the respective values from AFGL2789 to IRAS13481-6124 to SgrA IRSX to the four other YSOs as well as SgrA IRS3 (excluding AFGL 2403 given its status as a dust factory). Interestingly, Alexander et al. (2003) find a correlation between the depth of a feature at 11.2 μm and the depth of the 9.7 μm silicate band in their sample of ISOCAM spectra of YSOs in the Corona Australis, ρ Ophiuchus, Chamaeleon I and Serpens molecular clouds. Whilst they do not show a correlation plot, they state that the proportionality is negative, which we presume to mean that the 11.2 μm depth decreases as the 9.7 μm depth increases (or vice-versa). This then leads them to identify the 11.2 μm feature as an emissive shoulder on the silicate feature, rather than an independent feature of some other species. This seems highly unlikely to us, as many of their spectra resemble those presented here, e.g. HH100 IR in their Figure 4 and which is part of our larger sample to be presented in Do Duy et al. (in preparation).

The putative $\tau_{9.7}$ – $\tau_{11.1}$ correlation that we find does not necessarily mean that the 11.1 μm feature must originate from a silicate. But it does mean that whatever carrier is responsible always occurs together with silicates. Moreover, given no other known cosmic dust constituent seems able to account for the 11.1 μm feature there is a strong implication that it must itself be a silicate band.

The central wavelength of 11.10±0.10 μm is consistent with crystalline silicate, especially the magnesium-rich olivine end-member forsterite. Admittedly, at first sight the observed central wavelength appears to be different to that typically quoted of $\sim$ 11.3 μm for crystalline forsteritic olivine of Fabian et al. (2001) and others (e.g the models in Figure 3). But as shown by Tamanai et al. (2006) this is likely to be a result of the conditions under which the laboratory data were taken. They showed that for free-flying, aerosol crystalline forsterite the primary bands occur at around 9.85 and 11.1 μm, shifted shortward by

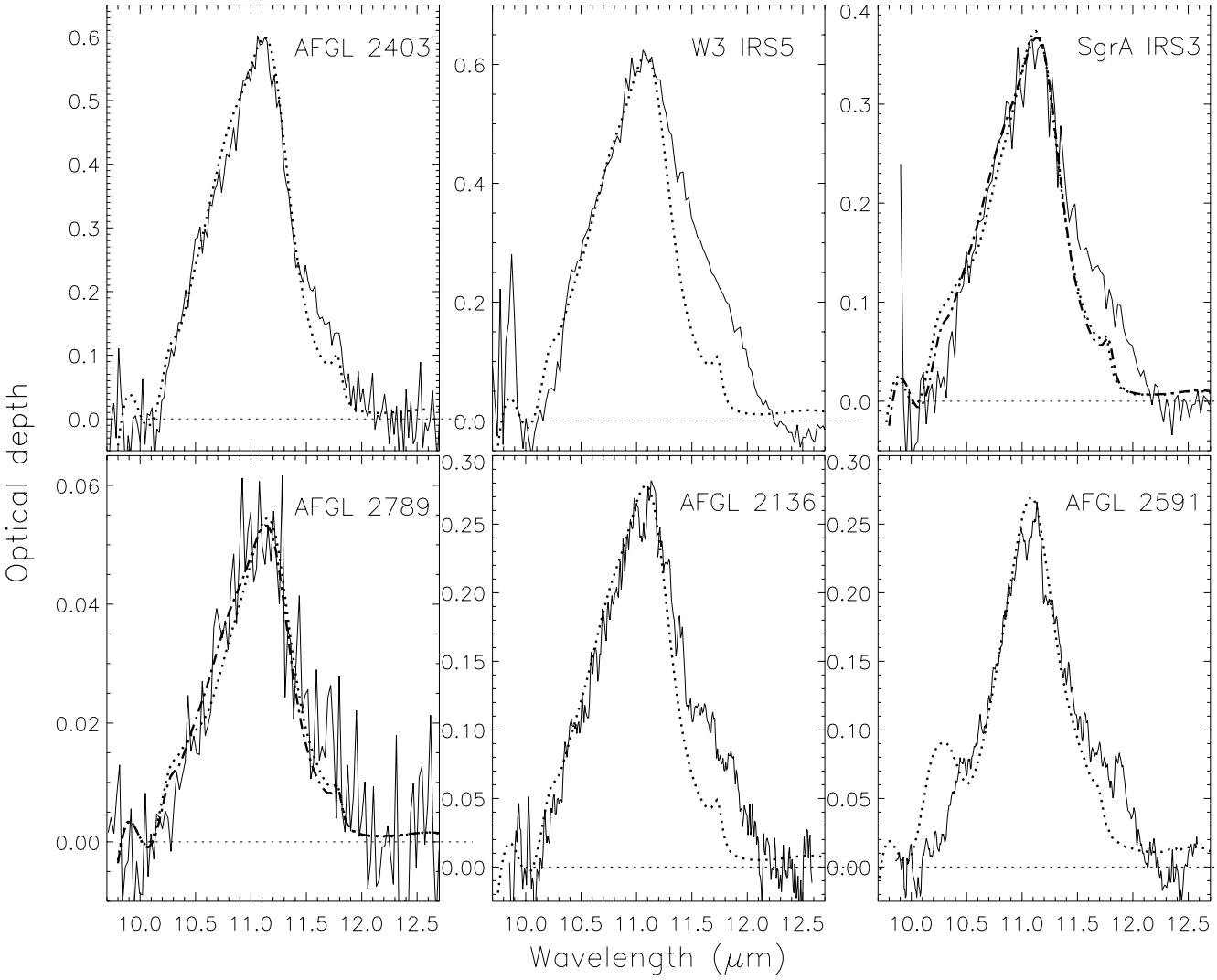

Figure 7. Comparison between observed and model 11.1 μm feaures, the latter extracted using the same polynomial technique as described in the text. The fractions of crystalline olivine in each model are 0.075 for AFGL 2403, 0.05 in W3 IRS5 and AFGL 2136, 0.025-0.05 (dotted/dashed) for SgrA IRS3 and AFGL 2789 and 0.01 for AFGL 2591, using the optical constants of Mukai & Koike (1990) along with those of Dorschner et al. (1995). The model feature has been shifted by -0.2 μm for AFGL 2403, AFGL 2789 and SgrA IRS3, -0.25 for W3 IRS5 and AFGL 2136, and -0.29 μm for AFGL 2591, consistent with the findings of Tamanai et al. (2006). This shift aligns the primary peak but not the secondary peaks at 10.5 and 11.9 μm, which apparently do not shift between aerosol and matrix-embedded particles in the work of Tamanai et al. (2006). The ISO data used for AFGL 2136 and AFGL 2591 have been averaged in 20 pixel wide bins for plotting purposes.

0.20 ± 0.05 μm from the band position when the forsterite is embedded on a KBr pellet. Thus, the wavelength of the astronomical feature we detect and that expected for terrestrial crystalline forsterite are the same. On the other hand, weaker bands at 10.1, 10.4 and 11.9 μm show little or no shift. That the main bands shift and the minor bands do not shift obviously makes comparing complete forsterite profiles of laboratory and observed spectra problematic.

The feature in our 'template' or 'control' target AFGL 2403 almost certainly arises from crystalline forsterite, or at least olivine with a higher Mg than Fe content. This is because accompanying detections of both the 33.6 and 69 μm forsterite bands were made by de Vries et al. (2014). Accepting this to be the case then the similarity of the band profile – central wavelength and overall shape – in the other sources suggests the same carrier.

As seen in Figure 7 the observed and model profiles broadly resemble each other. For the model we have used a single oblate 2:1 shape as it appears to best match the mid-IR polarisation profile of the diffuse interstellar medium dust (Wright & Glasse (2005), Wright et al. (2002) and in preparation; see also Draine & Allaf-Akbari (2006) and Hildebrand & Dragovan (1995)). The model profiles have been shifted shortward by 0.2–0.3 μm, in accordance with the results of Tamanai et al. (2006) and which nicely aligns the peak wavelengths at 11.1 μm. Unfortunately such a bodily shift of the profile also moves the 10.5 and 11.9 μm sub-

bands, which as noted above is not replicated in the results of Tamanai et al. (2006).

Whilst we have not attempted to optimise the comparison between the model and observed profiles in Figure 7, the crystalline olivine volume fraction is around 7.5% in AFGL 2403, and the others vary between 1% and 5%. Assuming the density of the crystalline and amorphous silicates are the same then these figures are also their mass fractions. The value for AFGL 2403 is in reasonable agreement with the abundance (mass fraction) of 11±3% and 8±2% inferred by de Vries et al. (2014) from the 11 μm and 69 μm bands respectively. The value of 2.5–5% for SgrA IRS3 is larger than the best-fit mass fraction of 1.1% for the ISM path to the Galactic Centre of Kemper et al. (2005) or 0.6–1.5% of Min et al. (2007), but our 'minimum' value is in reasonable agreement with the firm upper limit of 2.2% of Kemper et al. (2005). Our range is also in reasonable agreement with the limit of 3–5% postulated by Li et al. (2007).

As a caveat on the above figures we note that they assume the optical properties of specific silicates, i.e. the crystalline olivine of Mukai & Koike (1990) mixed with amorphous olivine $MgFeSiO_4$ of Dorschner et al. (1995). A different set of refractive indices, which may well have used a different technique in their determination, or have a different Mg/Fe ratio, for either one or both of the amorphous and crystalline components, may change these estimates.

As an example, when the crystalline component was changed to the forsteritic olivine $Mg_{1.9}Fe_{0.1}SiO_4$ sample of Fabian et al. (2001) we were not able to obtain as good a match to the extracted optical depths. The model profile remained too narrow compared to the observations even up to a crystalline fraction of 7.5%. A proper model fit to the entire observed spectrum, as opposed to our relatively simplistic approach using a single extracted feature, is probably required in these cases. An example of this is demonstrated in Figure 8 for AFGL 2789. In this case our inferred value for the crystalline olivine fraction of 2.5-5% in Figure 7 – using Mukai & Koike (1990) optical constants – is consistent with the value of about 3% obtained from a preliminary model and which uses Fabian et al. (2001) optical constants. This model will be described in detail in Do Duy et al. (in preparation).

4.3.1 Other signatures of crystalline silicate in the 8–13 μm region?

Our (re-)discovery of the 11.1 μm feature, and its likely association with crystalline silicate (specifically forsterite), motivated us to search for other spectral features which could strengthen this identification. Within the 8–13 μm window discrete features might be present at around 10 and 11.9 μm, with perhaps other shoulders or inflections in between, as suggested by the models in the final panel of Figure 1.

Given its large optical depth and good signal-to-noise our best ground-based spectrum for searching for other features is probably that of W3 IRS5 NE. This is presented again in Figure 9, along with a model with a relatively large crystalline olivine volume fraction in order to emphasise the features. The model is shifted by 0.15 μm shortward, consistent with the work of Tamanai et al. (2006), and is not meant to be a model for W3 IRS5 NE, but merely to guide the eye to possible similarities.

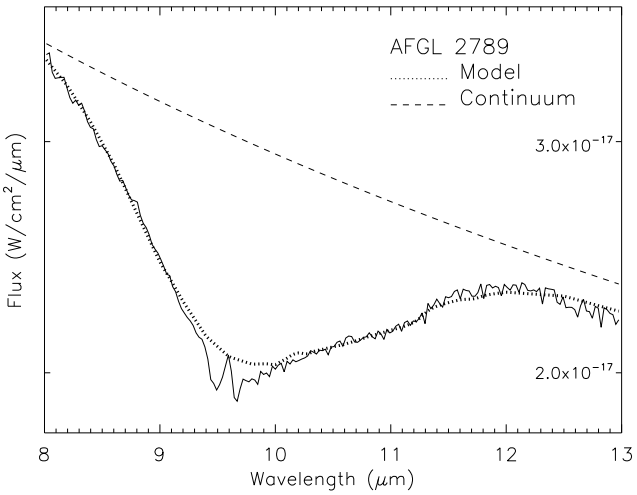

Figure 8. Comparison between observations of AFGL 2789 (solid line) and a representative model (dotted line). The modelling method is adapted from that of Hanner et al. (1998) and Hanner et al. (1995), which finds its roots in Gillett et al. (1975). In this case it includes three separate populations of dust, resulting in mass fractions of 0.1 μm sized grains of amorphous olivine, amorphous pyroxene and crystalline forsterite of 58%, 39% and 3% respectively. Optical constants for olivine and pyroxene are taken from Dorschner et al. (1995) and for forsterite from Fabian et al. (2001). The wavelength range 9.2–10.0 μm has been excluded from the fit due to the imperfect telluric correction around the 9.6 μm ozone band.

The spectrum of W3 IRS5 does – at least qualitatively – display features, or perhaps better described as perturbations, that are tantalisingly similar to those expected from a mixture of amorphous and crystalline olivine. These are marked in Figure 9 with vertical bars. For instance, there appears to be a very weak 11.9 μm feature. Also, in the middle of the broad 11 μm band there is a slope change in the model spectrum which is potentially reflected in the data. Similar such 'features' are also seen between 9.8–10.5 μm in both the model and data.

4.3.2 Crystalline silicate feature at 11.85 μm

Admittedly the existence of features other than at 11.1 μm in our Gemini spectra is not entirely conclusive. But at R $\simeq$ 100 our ground-based spectra barely have the spectral resolution to detect the aforementioned features. Therefore we utilised the ISO–SWS database, for which R is about an order of magnitude higher and which also allows a search for crystalline features at longer wavelengths, e.g. 20–45 μm.

The left hand panel of Figure 10 shows the SWS06 spectra of the massive embedded YSOs AFGL 2136 and AFGL 4176, as well as the SWS01 spectrum of AFGL 2591. For comparison the SWS01 spectra of the OH/IR stars AFGL 2403, OH26.5+0.6 and AFGL 230 (OH127.8+0.0) are shown in the right hand panel. In much the same way that AFGL 2403 is used as a template for the 11.1 μm feature, OH26.5+0.6 and AFGL 230, as known sources of crystalline silicates, also act as templates for other potential features. This includes crystalline enstatite in the case of AFGL 230, and which we discuss in a little more detail in Appendix B.

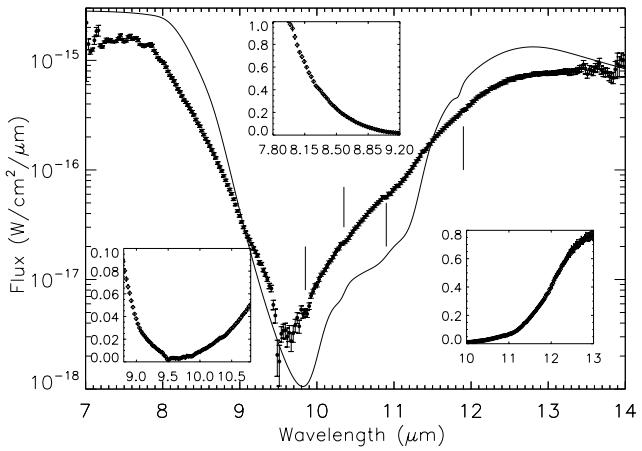

Figure 9. Spectrum of W3 IRS5 NE reproduced from Figure 1, along with a representative model containing a volume fraction of 0.20 of crystalline olivine from Mukai & Koike (1990). Insets show zooms, on a linear flux scale and in units of 10^{-15} W/cm^2/μm, of selected wavelength intervals. The zoom around 8.3 μm is included since both Fujiyoshi et al. (2015) and Poteet et al. (2011) detected a feature at this wavelength in the YSOs SVS13 and HOPS-68 respectively. In Fujiyoshi et al.'s model it came from annealed SiO_2, whilst Poteet et al. did not mention it in their paper. The vertical lines guide the eye to possible correspondences between the observations and model. Note that the model has been bodily shifted by 0.15 μm to shorter wavelengths, in line with the finding of Tamanai et al. (2006) that the main forsterite peaks, but not the minor peaks, shift between free-flying and matrix-embedded measurements. Consequently the 11.9 μm features do not precisely align in the plot.

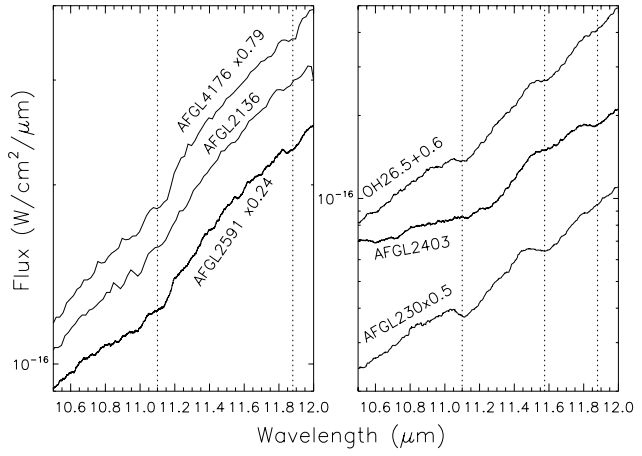

Figure 10. 10.5–12.0 μm ISO–SWS spectra of three YSOs (left hand panel) and three OH/IR stars (right hand panel). In all three YSOs, all of which have a clear 11.1 μm absorption feature, there is also an apparent absorption band centred around 11.85 μm. That both features also exist in the OH/IR stars, known sources of crystalline silicates, suggests a similar interpretation for the YSOs. See also Sylvester et al. (1999) for detailed analysis of the OH26.5 and AFGL 230 ISO 2–200 μm spectra.

All the OH/IR template sources clearly show the 11.1 μm forsterite feature. But in addition they possess a feature around 11.6 μm, most prominent in AFGL 230 and which can be identified with crystalline enstatite. Furthermore, OH26.5 and AFGL 2403 also show a band at $\sim$ 11.85 μm. Similarly, the three YSOs possess such an 11.85 μm feature. Notably, the extracted 11 μm band for AFGL 2591, and probably also for AFGL 2136, in Figure 7 shows this feature, as would be expected. We also find the feature in the SWS spectrum toward the Galactic Centre (Figure A1), but given the special status of this ISM path we reserve its discussion to a later section (also see Appendix A).

Since the relevant band 2C of the SWS is not documented to have a feature in its RSRF at 11.85 μm, unlike the case at 9.35, 10.1 and 11.05 μm, we assess that it is a real spectral feature in these targets. Paradoxically the non-detection of an 11.85 μm feature in the ISO spectrum of W3 IRS5 supports this contention, but which we attribute to the complicated source structure within the large ISO beam (e.g. its binary nature and extended mid-IR emission; van der Tak et al. (2005)).

Finally, although not noted by the respective authors, we point out that a band at this wavelength appears in the crystalline silicate-rich spectra of the ULIRG IRAS08572+3915 in Spoon et al. (2006) (their Figure 2) and the Class 0 protostar HOPS-68 in Poteet et al. (2011) (their Figure 2).

4.3.3 Crystalline silicate features at 20–30 μm

Our identification of probable crystalline silicates in our sample of YSOs (as well as the ISM toward the Galactic Centre, see Appendix A) is further strengthened when consideration is made of the 20–45 μm interval. Figure 11 shows the ISO SWS01 spectra of several of our targets, plus others, in this spectral range. The data was treated in a similar manner to that previously described, but with the following additional considerations.

Firstly, data from band 3E, with the relatively narrow wavelength interval of 27.5–29 μm, was completely neglected. It is notoriously unreliable in its spectral shape, severely affected by fringes, and in most cases can at best only be used to provide a flux (see Leech et al. (2003)). This means that there is a small gap in our spectra, but which is partially filled by the overlapping of band 4 down to around 28 μm.

Secondly, we neglected the band 3D data beyond 27.0 μm because of the well documented blue leak, in which around 10% of the 14 μm flux leaks to the $\geq$ 27 μm region (see Leech et al. (2003)). Thirdly, the band 4 data was corrected for the related effects of delayed responsivity from 40–45 μm and memory effects from 28–33 μm, which for relatively strong sources can cause a large difference in the spectral shape in these regions between the up and down scans. See Appendix C for a brief description. Notably band 3D is immune to such effects, and the up/down scans overlay almost precisely for the objects considered here.

Included in Figure 11 are a variety of sources, comprising six YSOs in (a) and (b), three OH/IR stars in (c), two Herbig Be stars in (d) and one pre-planetary nebula (PPN, HD44179 also known as the Red Rectangle) also in (d).

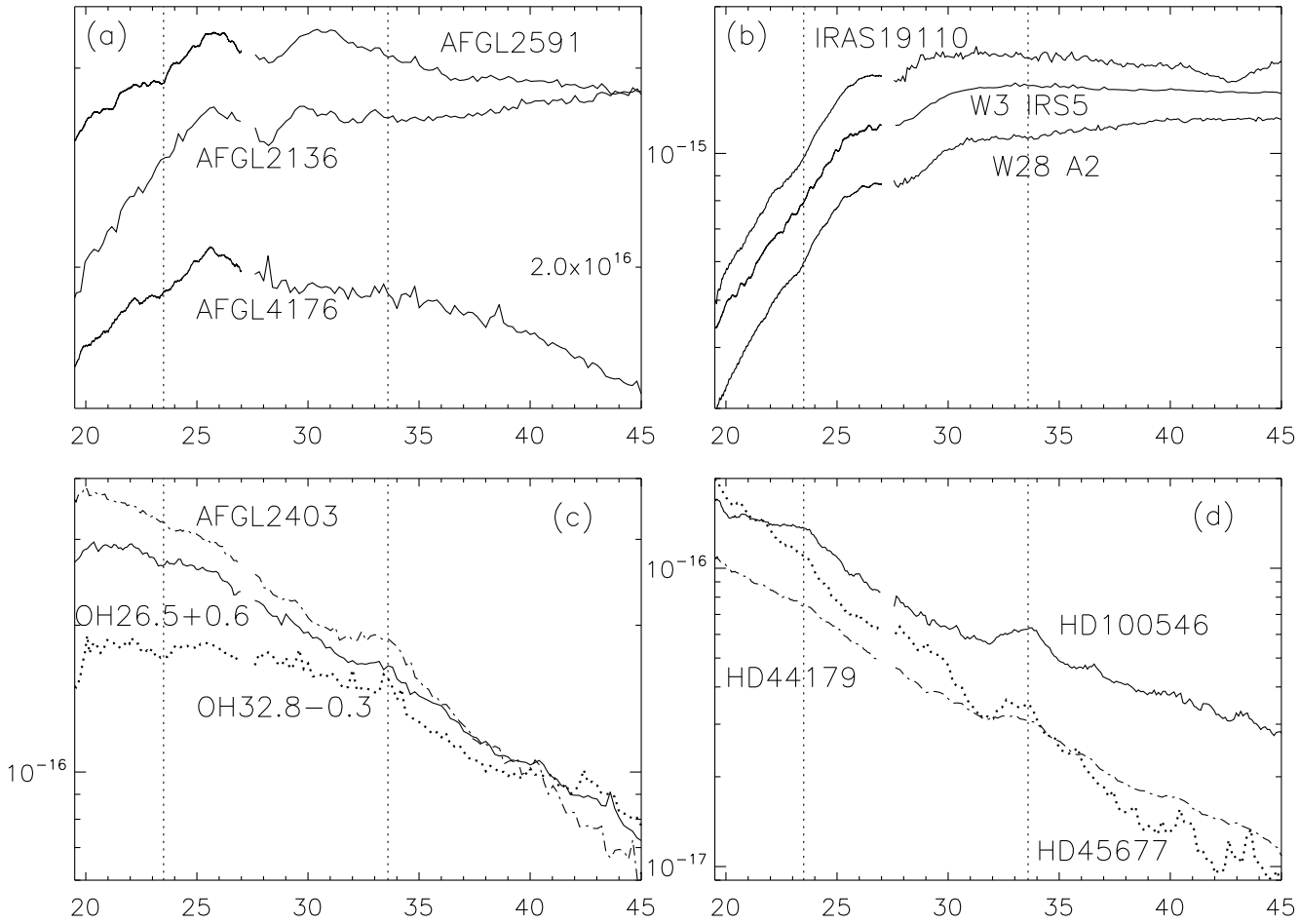

Figure 11. 19.5–45 μm ISO–SWS01 spectra of a selection of targets. The vertical axis is flux measured in units of W/cm^2/μm and the horizontal axis is wavelength in microns. Included in each panel are three embedded YSOs in (a), another three YSOs in (b) but which might have a more complex emission structure within the relatively large ISO beam (e.g. the binary nature of W3 IRS5 and associated extended emission), three OH/IR stars in (c), two Herbig Be stars in (d) and the pre-planetary nebula HD44179 (the Red Rectangle) also in (d). Vertical lines mark the wavelengths of crystalline silicate features at 23.5 and 33.6 μm. The SWS spectrum of HD100546 has previously been studied in detail by Malfait et al. (1998), and those of HD45677 and HD44179 by Molster et al. (2002). Since the ISO–SWS aperture size increased from 14×27 to 20×33 arcsec between bands 3D and 4, and the sources may be marginally extended at these wavelengths, there could be a small flux mismatch such that the band 4 data had to be scaled to match band 3D. Scaling factors applied to each source are the following: AFGL 2136 band 4 - 0.70; AFGL 4176 band 3D - 0.52, band 4 - 0.61; AFGL 2591 band 3D - 0.53, band 4 - 0.42; W3 IRS5 band 4 - 0.77; W28 A2 band 3D - 0.71, band 4 - 0.75; IRAS19110 band 3D - 3.73, band 4 - 3.39; OH26.5 band 3D - 0.95; OH32.8 band 3D - 3.21, band 4 - 2.94; AFGL 2403 band 3D - 3.36, band 4 - 3.21; HD100546 band 4 - 0.85; HD45677 band 3D - 1.52, band 4 - 1.69; HD44179 band 3D - 0.29, band 4 - 0.26.

As previously mentioned the OH/IR stars are established sources of crystalline silicates, and the same is true for the Herbig stars and PPN objects (e.g. Molster et al. (2002)). Thus, they are included here as templates in the study of the YSOs, few of which have previously been inferred to possess crystalline silicates (e.g. Demyk et al. (1999)).

All of the YSOs have at least one, and in several cases two, absorption features in the 20–30 μm interval, one at about 23.5 μm and the other around 28 μm. The 23.5 μm band is visible as a shallow feature in AFGL 2591 and AFGL 4176, or as a shoulder (or inflection) in IRAS19110+1045 (G45.07+0.13) and W28 A2 (G5.89-0.39). These latter two also possess the 11.1 μm absorption feature in their ISO spectra (see Appendix B, where we also speculate on the presence of crystalline enstatite in these two YSOs). Demyk et al. (1999) and Dartois et al. (1998) previously detected the 23.5 μm feature in IRAS19110, as well as another YSO AFGL 7009S, but neither pursued an analysis. Along with W28 A2 we have found it in several other YSOs.

The 23.5 μm band has a corresponding absorption feature in the three OH/IR stars, previously presented in Sylvester et al. (1999) for OH26.5 and OH32.8, and a corresponding emission feature in the two Herbig Be stars and one PPN. It has been detected in many other sources in both ISO and Spitzer spectra of OH/IR and other evolved stars (e.g. Jiang et al. (2013); Molster et al. (2002)), predominantly as an emission feature, as well as in Herbig and/or T Tauri star disks (Juhász et al. (2010); Watson et al. (2009); Sargent et al. (2009); Meeus et al. (2001)).

In all these cases the 23.5 μm feature is universally identified as a crystalline forsteritic band, based on its similarity

to a feature seen in laboratory measurements of magnesium rich crystalline olivines (Pitman et al. (2010); Sogawa et al. (2006); Suto et al. (2006); Koike et al. (2003); Jäger et al. (1998b); Mukai & Koike (1990)). To our knowledge there is no documented problem with the RSRF of the SWS band 3D, and so we favour a crystalline olivine interpretation in the much younger YSOs – still in their embedded phase – as well. A detailed discussion is deferred to a later paper (Do Duy et al., in preparation), but in Appendix B we show the feature extracted in a similar manner to that for the 11.1 μm band, as well as comparison to a representative amorphous+crystalline silicate model.

An absorption feature at around 28 μm is also evident in the YSOs in Figure 11, being most apparent in AFGL 2591 and AFGL 2136. The fact that this feature occurs across two separate bands of the SWS has both good points and bad points. For instance, that both the long and short wavelength sides of bands 3D and 4 respectively dip down provides a level of confidence that they trace a real spectral feature. This is despite the central wavelength being part of the 'missing' band 3E, and that the larger band 4 aperture size may include more extended emission. On the other hand, one must always be wary about features at the band edges given that the RSRF of band 4 does decrease relatively steeply from about 30 μm to 29 μm, and that we are utilising data beyond the nominal 29 μm minimum 'valid' wavelength for band 4 (Leech et al. (2003)).

As 'insurance' against the possibility that the 28 μm feature is an artefact we have examined many tens of other SWS01 spectra covering several different source types, spectral shapes and flux levels. We do not see a pattern that would suggest our 28 μm feature identification is an artefact. A few examples are included in Figure 11-c and -d, where there is no apparent problem with the RSRF. This is in the sense that for the objects in (c) and (d) their spectra continue to monotonically decrease in the 'transition interval' from band 3D to band 4, showing no 'anomalous' structure mimicking the shape of the RSRF in that region. Indeed, in our experience the majority of artefacts introduced by the ISO RSRF have their origin in relatively narrow 'downward' features which in turn mimic 'emission' bands in the target spectrum.

Accepting that the 28 μm feature in our YSO sample in Figure 11-a and -b is real then once again a similar band has previously been detected. This has typically been in emission, in spectra of both dust factories (outflowing winds of evolved stars) and dust repositories (disks around young stars). These respectively include old stars in perhaps all post-main sequence evolutionary phases (Jiang et al. (2013); Gielen et al. (2007)), and cicumstellar disks of Herbig Ae/Be stars (Juhász et al. (2010)) and T Tauri stars (Watson et al. (2009)). Again it is universally attributed to crystalline silicate based on its similarity to a laboratory band.

As already noted there is no 28 μm feature in the other sources of Figure 11, either in emission or absorption (except perhaps for HD45677 in emission). But in the case of the OH/IR stars the crystalline silicate features appear to switch from absorption at 23.5 μm to emission at 33.6 μm. It is thus natural to conclude that the 28 μm feature is likely to be self-absorbed in these sources, due to radiative transfer effects within their circumstellar shells, and is hence difficult or impossible to distinguish against the continuum without extremely good signal-to-noise.

Finally, we note that 23.5 and 28 μm absorption bands have been identified in the crystalline silicate-rich spectra of at least one other embedded YSO, the Class 0 object HOPS-68 by Poteet et al. (2011).

4.3.4 Crystalline silicate and other features at 30–45 μm

This brings our discussion to the conspicuous absence of a 33.6 μm feature in the YSOs of Figure 11, despite the presence of this feature in absorption in HOPS-68 and in emission in all the other sources of Figure 11-c and -d. Our current explanation is that this band is self-absorbed in most YSOs, in a similar fashion to the 28 μm band of some OH/IR stars.

A radiative transfer study, varying parameters such as the central source temperature and luminosity, circumstellar envelope density and temperature structure, and the overall opacity and dust composition, is required to test this hypothesis. Whilst beyond the scope of the present paper we have begun work on this study, but note here that this feature is also not apparent in the ULIRG IRAS08572+3915 of Spoon et al. (2006), despite the crystalline silicate bands at lower wavelengths being clearly detected.

As some indication that spectral bands in the 30–45 μm region can go into emission, absorption or disappear depending on specific parameters of the source, we can look to the case of IRAS19110+1045. Whilst this YSO has a 3.1 μm water ice absorption band, as well as features of other ice species, in the 2–10 μm interval, they are in no way abnormal or atypical compared to the other embedded YSOs measured with ISO. Yet it is the only one with an absorption feature at $\sim$ 43 μm, seen in panel (b) of Figure 11 and discussed in detail by Dartois et al. (1998), who attributed it to a lattice mode of crystalline water ice.

Similarly, in the case of the Orion YSO cluster, bright in the mid-IR and including the BN Object and IRc2, no 43 μm ice band can be discerned, as seen in panel (a) of Figure 12, and consistent with the independent (but higher S/N) SWS06 spectrum presented in van Dishoeck et al. (1998). Yet only an ISO beamsize or so away to the SE and NW along the outflow axis (Allen & Burton (1993)), at the shock positions known as Pk1 and Pk2 respectively (Beckwith et al. (1978)), the band appears prominently in emission.

To potentially further alleviate a concern that the 33.6 μm crystalline silicate feature may be absent in star forming environments we show spectra of several HII regions in panel (b) of Figure 12. In all of them, representing a range of excitation conditions and flux levels, there is a possible feature, or indeed a plateau of emission, extending between about 32 and 37 μm. It bears a remarkable similarity to the complex of crystalline silicate bands seen for instance in the OH/IR stars, Herbig Be stars and PPN in (c) and (d) respectively of Figure 11.

Features similar to these, and interpreted as evidence for Mg-rich crystalline silicates, were first identified in ISO–SWS spectra of star forming regions (HII regions, photodissociation regions or PDRs) by Jones et al. (1999) in M17 and Cesarsky et al. (2000) in Orion. However, a question was raised over their reality by Molster & Kemper (2005),

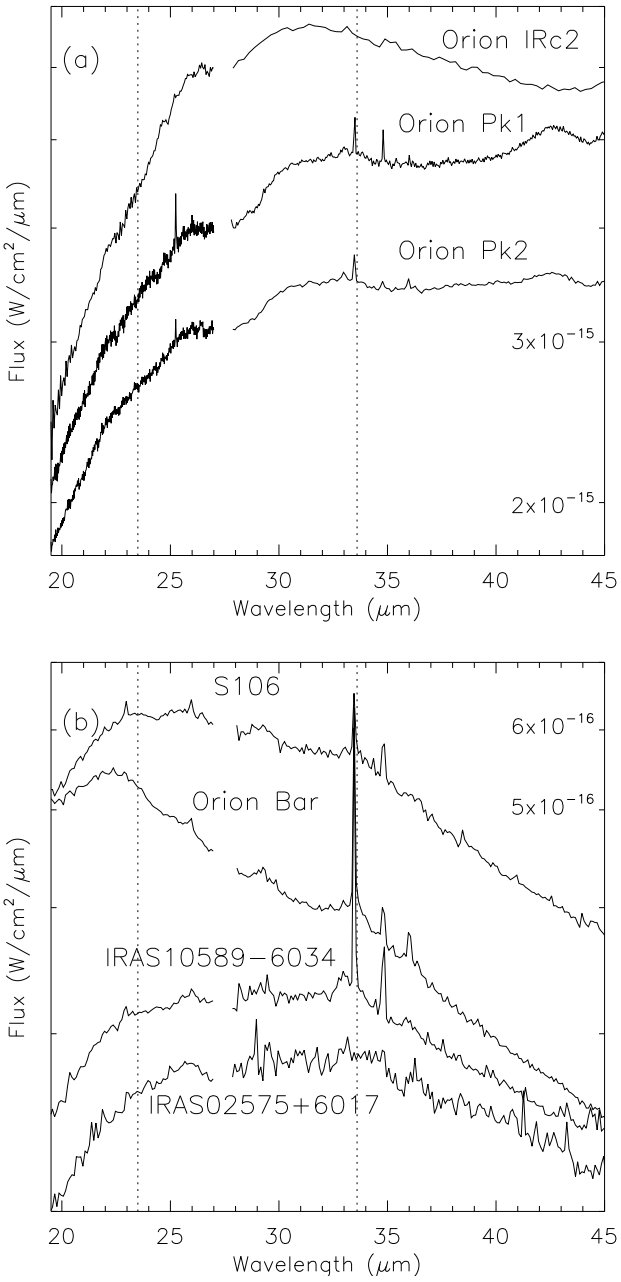

Figure 12. (a) 19.5–45 μm ISO–SWS01 spectra of three positions in Orion, centred on IRc2, Pk1 and Pk2. The IRc2 and Pk1 spectra have previously been presented in Gibb et al. (2004) and Rosenthal et al. (2000), though without discussion of the presence or otherwise of crystalline silicates or the 43 μm water ice feature. (b) 19.5-45 μm ISO–SWS01 spectra of several HII regions. That of S106 has previously been presented by Van den Ancker et al. (2000), the two IRAS sources by Peeters et al. (2002) and the Orion Bar by Cesarsky et al. (2000). Scaling factors applied to each source are the following: Orion Pk2 band 4 - 0.52; Orion Pk1 band 3D - 1.56, band 4 - 0.99; Orion IRc2 band 3D - 0.53, band 4 - 0.42; Orion Bar band 3D - 0.40; S106 band 3D - 1.27, band 4 - 0.58; IRAS02575 band 3D - 4.82, band 4 - 3.86; IRAS10589 band 3D - 2.46, band 4 - 1.77.

who claim them to be artefacts. See also Peeters et al. (2005) who cites a paper in preparation by Kemper et al., but which has not so far been published to our knowledge.

There are certainly good reasons to be careful in interpreting the presence of features in ISO–SWS band 4 spectra, given the aforementioned responsivity and memory effects. That the 'average' dust temperature is such that the Planck-like spectra of most of these targets turns over in the 30–40 μm region (see for example the spectral atlas of Peeters et al. (2002)) also makes feature identification and extraction more complicated.

Further, in this particular range it is feasible that not only a high continuum flux but also the bright emission line intensity (e.g. [S III] at 33.481, [Si II] at 34.815 and [Ne III] at 36.014 μm) could perturb the shape of the spectrum. This would probably depend alot on the speed with which the particular SWS01 observation was conducted, being more likely for speed 1 than speed 4. In the many tens of SWS01's we have looked at – across a broad range of source types, flux levels and speeds – we have not seen an obviously attributable such effect, or at least not one which is sufficiently broad to 'mimic' a several micron wide (FWZI) emission plateau.

Finally, there are features in the RSRF of band 4 at $\sim$ 31, 33 and 36.5 μm which could feasibly conspire to create the observed feature (we note no in-orbit band 4 RSRF was ever derived, and hence it relies on laboratory data; Leech et al. (2003)). But the only one which we know as having been documented to appear in fully reduced spectra is that at 33 μm, seen for instance in the SWS06 data of Orion IRc2 in Wright et al. (2000).

We have looked into all of the above-mentioned band 4 issues, and remain confident in the reality of the solid-state dust features seen in Figure 12. This includes the 43 μm water ice band at the Orion shock positions in Figure 12-a, and the 33.6 and 36 μm features in several HII regions in Figure 12-b.

4.4 A polarisation perspective

Detection of a polarisation signature from the 11.1 μm absorption band could potentially provide a valuable constraint on its carrier. Linear polarisation via dichroism obviously requires grains to be non-spherical with a particular axis mutually aligned along a common direction (e.g. Aitken (1989)). In most alignment mechanisms it is the short axis of spinning grains which becomes aligned along the direction of an ambient magnetic field (see Lazarian (2007)).

Assuming grains to be spheroidal – making the problem more tractable – cross sections for absorption of radiation along the major and minor axes peak at different wavelengths (Draine & Lee (1984)). The polarisation cross section C_{pol} is formed by a subtraction of these cross sections, in a sense magnifying small differences between them, whilst the absorption cross section C_{abs} is formed from a sum (Lee & Draine (1985)). Since the cross sections are also sensitively dependent on the grain dielectric function, a unique identifier of the responsible material, then spectropolarimetry – especially across a resonance – becomes a powerful probe of dust grain mineralogy, more so than conventional spectroscopy alone.

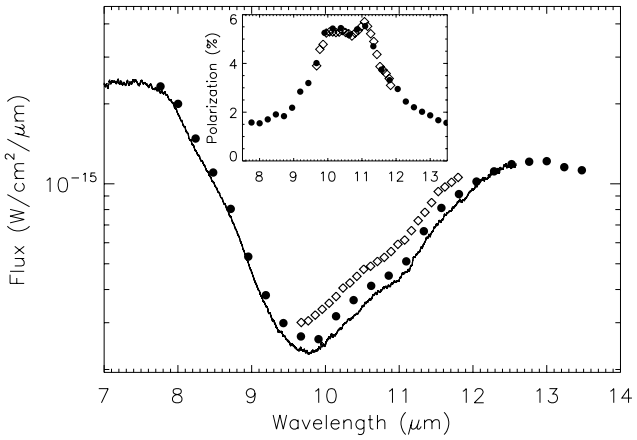

Figure 13. The main plot shows the UCLS low and high resolution spectra of AFGL 2591 (solid circles and open diamonds respectively), whilst the ISO spectrum is shown as a solid line. Note how an inflection around 11 μm at low resolution is resolved into a bona fide absorption band at higher resolution. The inset displays the low (solid circles) and high (open diamonds) resolution polarisation spectrum, containing the sharp polarisation feature around 11.1 μm first discovered by Aitken et al. (1988).

4.4.1 Polarisation-to-absorption ratio considerations

At a spectral resolution R $\simeq$ 40 Aitken et al. (1988) first found a polarisation signature likely to be associated with 11.1 μm absorption in the massive embedded YSO AFGL 2591. They interpreted the feature to be due to a structured – as opposed to amorphous – silicate produced during an annealing episode. This was based principally on the feature having a polarisation-to-absorption ratio, or p/τ, of around 0.05 compared to a value of $\sim$ 0.02 for the amorphous silicate feature, as well as preliminary modelling of the 8–13 μm spectrum using the dielectric function of disordered, radiation damaged olivine.

The quantity p/τ acts as a proxy for the material band strength (opacity or cross section per gram in cm^2/g, or C_{abs}/V in cm^{-1}) as shown by Martin (1975). Obviously the polarisation depends on the degree of alignment of the grains and/or the angle to which the magnetic field is inclined to the plane-of-the-sky, whilst τ depends on neither. In the case of AFGL 2591 the comparison of p/τ for each dust component relies on them being similarly aligned, a safe assumption given the constancy of the observed polarisation position angle presented in Aitken et al. (1988).

Wright et al. (1999) extended the modelling of AFGL 2591 to more realistic optical properties, and found a reasonable match between observed and modelled 8–13 μm spectra using a mixture of amorphous and crystalline silicate, represented by the Draine & Lee (1984) 'astronomical silicate' and crystalline olivine from Mukai & Koike (1990). The volume fraction of crystalline olivine inclusions occupying the amorphous silicate matrix was around 17.5%. But as will be shown later this possibly represents an absolute maximum, and could be a factor of around two lower for a different set of optical constants.

Higher resolution (R $\simeq$ 100) observations of the AFGL 2591 11.1 μm polarisation feature obtained with the UCLS instrument, shown in Wright (1994) and here in Figure 13, confirmed its reality and revealed its profile. Similar resolution observations obtained with Michelle on UKIRT also showed it, presented in Wright & Glasse (2005). These demonstrated that the polarisation maximum was shifted to a longer wavelength, by 0.05–0.10 μm, than the extinction maximum, a direct prediction of polarisation by dichroism.

These higher resolution data sets also established that the true p/τ of the feature is more like about 0.1, twice that inferred by Aitken et al. (1988) and suggesting an even higher band strength and thus more structured material. For instance, if the band strength of the 'astronomical silicate' of Draine & Lee (1984) is 10^4 cm^{-1} then that of the 11.1 μm carrier is of the order of 5×10^4 cm^{-1}, or 3000 and 15000 cm^2/g respectively if expressed as an opacity.

Interestingly, at 11 μm the crystalline forsterite of Fabian et al. (2001) has a band strength of around 20000 cm^2/g along the x and y axes, in good agreement with the observed value. On the other hand, the Mukai & Koike (1990) crystalline olivine band strength is only $\sim$ 5500 cm^2/g. This difference already suggests that the two sets of optical data would require different amounts of the crystalline component to match the data.

For SiC the band strength is instead around 3500 cm^2/g and just over 5000 cm^2/g for the Pégourié (1988) and Laor & Draine (1993) varieties respectively, whilst it ranges between 40000–90000 cm^2/g for the samples of Pitman et al. (2008) and Choyke & Palik in Palik (1985). These SiC values of either several thousand or several tens of thousand cm^2/g are obviously too low and too high respectively compared to the AFGL 2591 data, and make SiC of any variety an unlikely carrier of the 11 μm feature in at least AFGL 2591. Furthermore, the silicate–SiC polarisation models presented in Fujiyoshi et al. (2015) for the YSO SVS13 show that SiC actually broadens the 8–13 μm polarisation profile, as well as shifts the peak to longer wavelengths, with an increasing SiC contribution. It is never able to reproduce the sharp peak of the relatively narrow 11.1 μm polarisation feature seen in AFGL 2591.

Since the discovery of Aitken et al. (1988) it took 20 years until a second positive detection of an 11.1 μm polarisation feature was made by Wright et al. (2008), again in a massive embedded YSO called IRAS 13481-6124. Before that the only other possible case was AFGL 4176, also a DEYSO, presented in Wright (1994). See Figure 14. In these two objects the respective p/τ for the 10 and 11.1 μm bands are $\sim$ 0.01 and 0.05 for AFGL 4176, and $\leq$0.04 and $\sim$ 0.10 for IRAS13481.

A caveat on these p/τ comparisons at 9.7 and 11.1 μm, alluded to earlier, is that p obviously originates only from aligned dust, whilst τ could have contributions from both aligned and unaligned dust. The comparisons above would not change if there was an unpolarised component to the spectrum only so long as the mineralogy of the unaligned and aligned dust was the same. However, if there was an unpolarised component from amorphous silicates, then $(p/\tau)_{9.7}$ would decrease faster than $(p/\tau)_{11.1}$. The latter could then appear to be (unreasonably) much larger than the former, and a direct comparison misleading concerning their relative band strengths. From the modelling presented in the next subsection this could be the case for AFGL 2591, although it does not change our assessment of crystalline silicates. On the other hand, if there was a polarised component

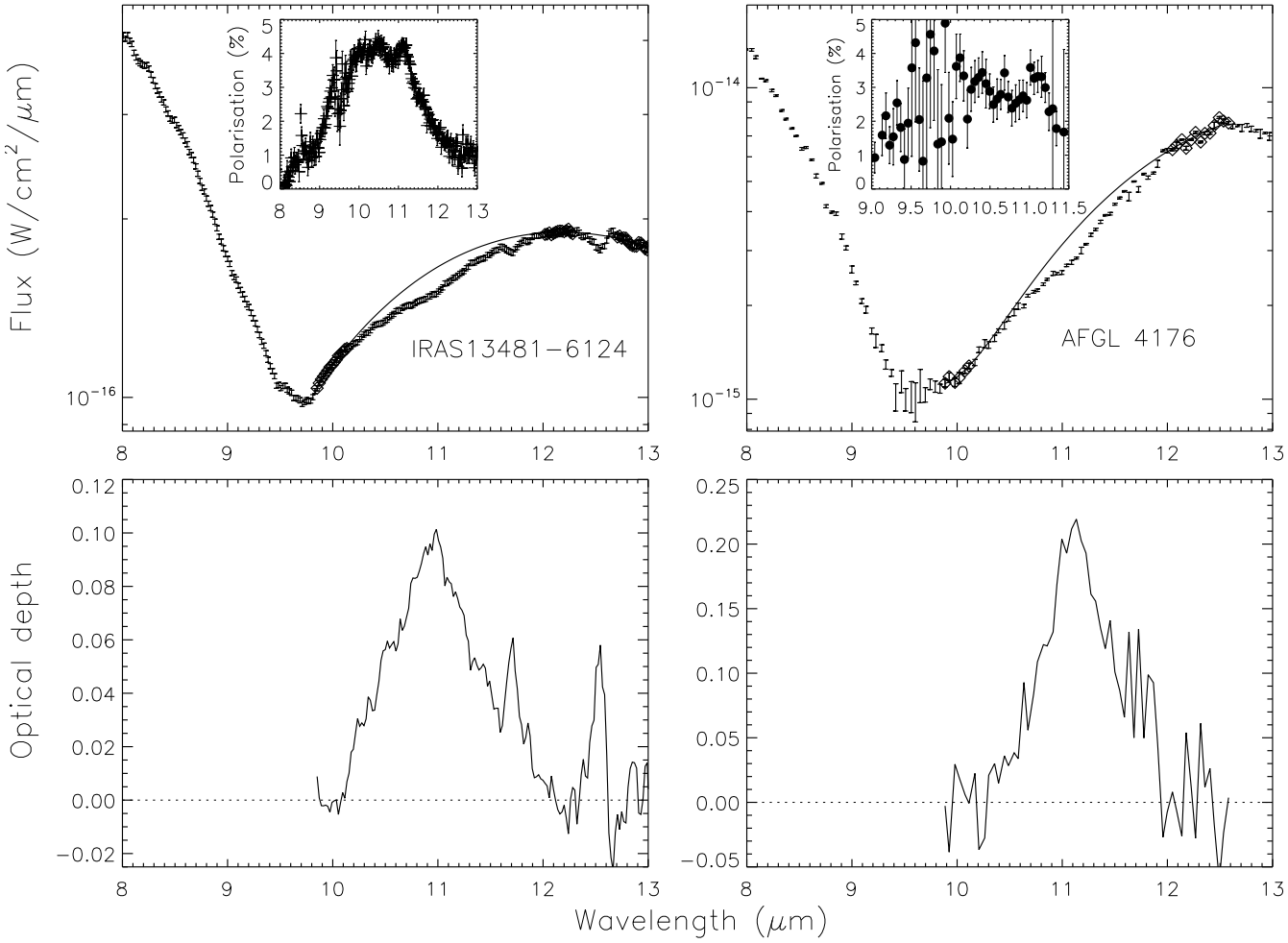

Figure 14. The top panel shows the observed spectra of IRAS13481-6124 (left) and AFGL 4176 (right), previously presented in Wright et al. (2008) and Wright (1994) respectively, along with an extrapolated polynomial across the 11.1 μm feature. The insets show the polarisation data, demonstrating a positive detection of a feature around 11.1 μm in IRAS13481 and a tentative detection in AFGL 4176. The IRAS13481 data was obtained with TIMMI2 in January and June 2006 at the ESO 3.6 m telescope, whilst the conventional spectrum of AFGL 4176 was obtained with the UCLS on the ANU 2.3 m telescope in January 1989 and the polarisation data acquired with the UCLS on the AAT in May 1992. The bottom panel shows the optical depth spectra of the extracted 11.1 μm feature, which is obviously very similar in central wavelength and profile to those in Figure 7. The narrow features around 11.7 and 12.5 μm in IRAS13481 are due to telluric absorption bands.

from amorphous silicates, then $(p/\tau)_{9.7}$ would be unchanged whilst $(p/\tau)_{11.1}$ would decrease. In this case the latter could then appear to be (unreasonably) much lower than it would otherwise be (even as low as zero), and again a direct comparison misleading concerning their relative band strengths. This situation is also considered in the following subsection, potentially explaining why an 11.1 μm polarisation signature is not seen in the majority of sources in the mid-IR polarisation atlas of Smith et al. (2000).

4.4.2 Modelling the polarisation spectrum

The original modelling of the AFGL 2591 polarisation by Aitken et al. (1988) and subsequently Wright et al. (1999) used optical constants for both amorphous and crystalline silicates that are somewhat outdated and/or cannot provide mineralogical information. For example, the crystalline olivine of Mukai & Koike (1990) was not identified with a particular Fe/Mg ratio.

Further, the astronomical silicate of Draine & Lee (1984) was constructed to fit the 10 μm emission spectrum of the Trapezium region of Orion, and its 20-to-10 μm band ratio was defined from an 'average' of the emission of dust shells around oxygen-rich evolved stars. Whilst of significant utility in radiative transfer modelling of spectral energy distributions, due to its broad wavelength coverage and consistency with causality via the Kramers-Kroenig relations, it has not proved as successful in modelling the detailed shape of specific 10 and 20 μm silicate bands. This is especially the case in polarisation, even for the BN Object in the same cloud, Orion, as the Trapezium (Wright & Glasse (2005), Wright et al. (2002); Hildebrand & Dragovan (1995); O'Donnell (1994); Henning & Stognienko (1993); Aitken et al. (1989), Aitken et al. (1988); Lee & Draine (1985),

Draine & Lee (1984); but see also Fujiyoshi et al. (2015) and Wright et al. (1999) where it is mixed with SiC to provide a good match to the Class I YSO SVS13 polarisation).

We have thus calculated new models using laboratory-based refractive indices of silicates with well defined mineralogical properties. For the crystalline component the Fabian et al. (2001) forsteritic olivine with formula $Mg_{1.9}Fe_{0.1}SiO_4$ is used. We have already noted previously the difference in band strength between this and the Mukai & Koike (1990) sample. This may partly stem from the fact that the Mukai & Koike and Fabian et al. optical constants are respectively derived from transmission and polarised reflection measurements. Originating from these different techniques is that the Mukai & Koike data consists of only a single set of optical constants (actually oscillator parameters), whilst those of Fabian et al. comprise three data sets, corresponding to the vibrational directions parallel to the crystallographic axes x, y and z. Sihvola (1994) and Sihvola & Pekonen (1994) present generalised formulae for the effective dielectric function in the case of randomly oriented and spherical biaxial crystallite inclusions – of which forsterite is a member given its orthorhombic structure.

For the amorphous component the olivine with formula $Mg_{0.8}Fe_{1.2}SiO_4$ from Dorschner et al. (1995) was initially used, since it provides a very good match – in terms of both wavelength of peak polarisation ($\lambda_{P,max}$) and FWHM – to the polarisation profile of dust in the diffuse ISM, as shown in Wright et al. (2002) and Wright & Glasse (2005). It was also used by Mathis (1998) in his models of the diffuse ISM silicate features, and their consistency with observed heavy element abundances. The scenario we envisaged was that this would be the form of the bulk of the silicate dust deposited in the molecular cloud from which AFGL 2591 formed, and which would subsequently be processed.

However, whilst this combination could provide a good match to the 10 μm polarisation spectrum of AFGL 2591 it also produced a 20 μm polarisation far in excess (about a factor of 2) of that observed by Aitken et al. (1988). Given that the position angles within the 10 and 20 μm windows are the same, and spectrally constant, then pure dichroic absorption is almost certainly the sole operating mechanism. In other words it is unlikely that a 'crossed polariser' effect is diluting the 20 μm polarisation. Therefore the discrepancy between the observed and model 20 μm polarisation must originate in the optical constants of the amorphous silicate, which indeed has a relatively high 20-to-10 μm band ratio. In addition to this problem, the combination also had an internal inconsistency in the difference between the Fe/Mg ratios of the two components.

Other laboratory-derived optical constants for amorphous olivine exist in the publications of Day (1979), Scott & Duley (1996) and Jäger et al. (2003), specifically including the magnesium end-member forsterite, Mg_2SiO_4. Additionally, Day (1981) provides refractive indices for the iron end member Fe_2SiO_4. Interestingly, these works plus others like Dorschner et al. (1995) show a strong trend whereby the 20-to-10 μm band ratio increases with increasing iron content. This suggests that perhaps the amorphous host (matrix) component $Mg_{0.8}Fe_{1.2}SiO_4$ contains too much iron. On these bases we elected to use the optical constants of a Mg-rich amorphous silicate, specifically those of Day (1979) which gave a FWHM and $\lambda_{P,max}$ more consistent with observations.

Figure 15 shows the observed AFGL 2591 polarisation (a-e) and optical depth τ (f) spectra against calculations of the polarisation and absorption cross sections respectively. The optical depth has been extracted using the method outlined in Section 3.2, also used by Fujiyoshi et al. (2015) for the Class 1 YSO SVS13. The peak optical depth and 8–13 μm colour temperature of around 2.3 and 385 K agree reasonably well with the best-fit optically-thick two-component model in Smith et al. (2000).

With our selection of optical constants a reasonable match to the polarisation could be found using a mildly prolate-shaped grain with a crystalline silicate inclusion volume fraction of 0.10 (Figure 15-a), and in the interests of clarity we show only this model. We do not claim that this is the shape of the grains within the AFGL 2591 envelope, as there is certainly sufficient flexibility in the model's input parameters (i.e. shape, principal axis ratio, optical constants, EMT mixing rule, inclusion volume fraction) to provide an equivalently good match for oblate grains, or even a CDE.

For instance, a finding of prolate grains would need to be tempered by the fact that i) oblate grains better match the ISM 8–13 μm profile (Wright et al., in preparation), as well as the BN Object in the Orion molecular cloud (Hildebrand & Dragovan (1995); Lee & Draine (1985); Draine & Lee (1984), and ii) perfectly aligned prolate grains are only half as efficient polarisers as oblate grains of the same principal axis ratio (Hildebrand & Dragovan (1995), Hildebrand (1988). The latter potentially places a constraint on the grain alignment mechanism.

On the other hand, Greenberg & Li (1996) surmise that prolate grains, of a weakly-constrained though preferred axial ratio of 3:1, better fit the 8–13 μm BN profile, though apparently only by inclusion of an as-yet unproven organic refractory mantle (e.g. see Li et al. (2014); Chiar et al. (2006); Adamson et al. (1999)). They also argue that elongated (prolate-like) rather than flattened (oblate-like) grains are a more realistic end-product of clumping. Also, Siebenmorgen et al. (2014) suggest that prolate silicate grains – with axial ratio around 2:1 – are responsible for the ISM visible polarisation along 4 of the 5 lines-of-sight they studied.

Probably the most robust conclusion we can make about the grain shape is that they do not need to be very highly elongated or flattened. Indeed, both mildly prolate and oblate shapes can adequately match the 'trapezoid-like' shape of the AFGL 2591 polarisation profile, as well as the peak of the 11.1 μm feature, though obviously the model profile in Figure 15-a is too narrow. For a principal axis ratio of 2:1 the prolate grain better matches the ratio of the two main peaks at around 10.1 and 11.1 μm. But this ratio is shape-dependent, and for the same crystalline fraction of 0.10 a 6:1 oblate grain provides an equivalent match. For a 2:1 oblate grain the crystalline fraction must be increased to around 0.15 to adequately match the peak ratio at 10.1 and 11.1 μm.

The narrowness of the amorphous+crystalline silicate model in Figure 15-a has already been mentioned, and no amount of fiddling with the input parameters can broaden it and/or provide the polarisation observed in the 'wings' at $\leq$ 8.5 μm and $\geq$ 13 μm. One or more extra sources of emissivity are required. To identify what these could be

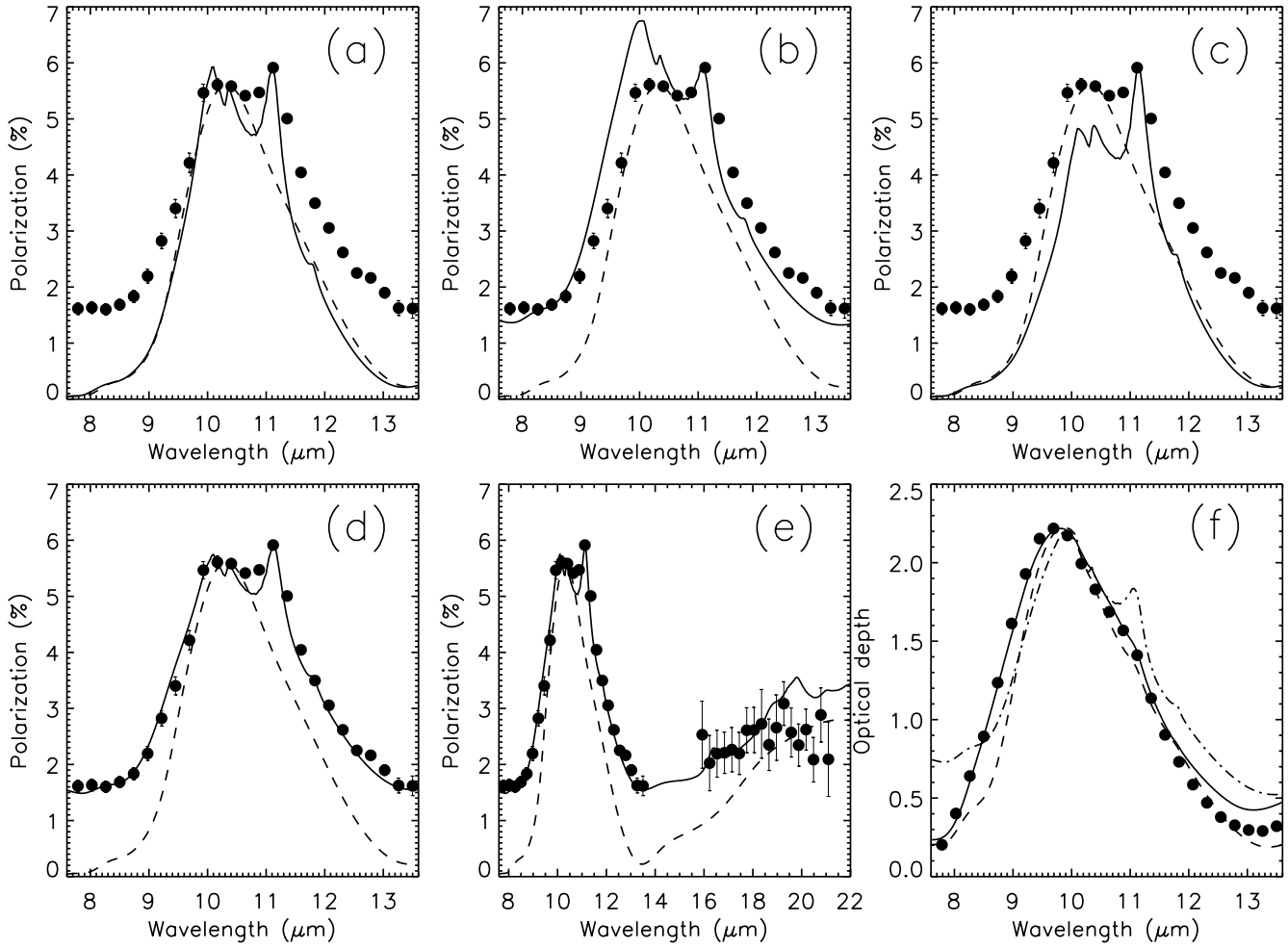

Figure 15. a-e: Models for the polarisation of AFGL 2591, using EMT and a mixture of amorphous and crystalline silicates, and assuming the Rayleigh approximation. The grains are assumed to be prolate with a principal axis ratio of 2:1. (a) amorphous+0.1×(crystalline forsterite), (b) amorphous+0.1×(crystalline forsterite)+0.24×(graphitic carbon), (c) amorphous+0.1×(crystalline forsterite)+0.40×vacuum, (d) amorphous+0.1×(crystalline forsterite)+0.24×(graphitic carbon)+0.40×vacuum, where the numbers refer to the volume fraction of that particular component of the grain. (e) Same as (d) but extended to the 20 μm band. In all cases the dashed line is for the amorphous component only. (f) Models for the optical depth spectrum, where the dot-dashed curve is the absorption cross section for the same model in (d) and (e), whilst the solid curve has an additional but unpolarised amorphous component. Consistent with the work of Tamanai et al. (2006) these partially crystalline models have been shifted by -0.1 μm. See text for further details.

we appeal to the well known and established growth-by-coagulation scenario of dust in molecular clouds (e.g. Bromley et al. (2014); Stognienko et al. (1995)). In one variant of this scheme proposed by Mathis & Whiffen (1989) the most abundant species of solid state matter – i.e. sub-μm silicate and carbon particles – stick together when they collide to form composite particles, upon which mantles of ices and/or hydrocarbons or organics can form. Further collisions continue to grow the particle, the interior of which may then contain many voids. Such a picture of porous (or fluffy) dust has essentially become a standard feature of recent cosmic dust models, capable of explaining many phenomena (e.g. Voshchinnikov et al. (2006)) and perhaps finding direct support in observations of at least some interplanetary dust particles (IDPs; Bradley (2010)).

In any model for the AFGL 2591 polarisation we can effectively rule out the presence of ices since the 3.1 μm water ice band is unpolarised (Holloway et al. (2002); Hough et al. (1989); Dyck & Lonsdale (1980); Kobayashi et al. (1980)). But other major components of the dust to be considered would be carbon, vacuum and possibly metallic iron. None have a spectral feature in the 8–13 μm region, but instead would form a 'continuum'. Since most other models, such as those cited above, use silicate, carbon and vacuum, and to minimise as much as possible the number of free parameters, we also confine our model to these three components. Also, the fact that metallic iron is featureless suggests it would only be a proxy for one or both of the also featureless carbon and vacuum components.

The refractive indices of the carbon component are taken from Jager et al. (1998a) for their sample synthesized by pyrolizing cellulose material at 1000° C, which they de-

scribe as an ordered graphitic substance. Panels (a) to (d) of Figure 15 thus shows the sequence of how such a multicomponent dust model is built up to match the 8–13 μm portion of the AFGL 2591 polarisation spectrum (solid lines), whilst panel (e) includes the 16-21 μm data (Aitken et al. (1988); see also Smith et al. (2000)). Dashed lines are for the case of purely amorphous Mg_2SiO_4 silicate with the same grain shape parameters.

In constructing these models the volume fractions of carbon and vacuum are 0.24 and 0.40 respectively. Such relatively large figures may begin to push the validity of EMT, so we have used the Bruggeman rule for the multi-component grain, due in large part to its inherent symmetry with respect to interchanging the components. This rule was also preferred by Sokolik & Toon (1999) in their modelling of multi-mineral aerosol aggregates. It has been shown by various authors to be more robust for large volume fractions of inclusions and/or a relatively large contrast between the refractive indices of the host and inclusion materials (Ossenkopf et al. (1992); Ossenkopf (1991); Stroud (1975)). It has provided a good approximation to more exact methods like the Discrete Dipole Approximation (DDA) to calculate the optical properties of small particles (Voshchinnikov et al. (2007); Perrin & Lamy (1990)), and even mid-IR experiments on aerosol particles with mineral compositions (e.g. silica, corundum, haematite, anhydrite; Ruan et al. (2011)). In calculating such an EMT we have again used the work of Sihvola (1994), who presents a generalised formula encompassing several of the known mixing rules, including Maxwell-Garnett, Bruggemann (Polder-van Santen) and Coherent Potential. Further, he provides an iterative solution for the effective medium of a multi-component mixture, negating the need to solve a cubic, quartic etc. polynomial for 2, 3, etc. different inclusion materials.

In the context of the relative volume fractions, the figure of 0.40 for vacuum is within the likely range postulated by Mathis (1998) and Mathis (1996) of ≥ 0.25 – based on abundance constraints – and ≤ 0.60 – based on the width of the visible interstellar polarisation curve. For the silicate and carbon components Mathis (1996) states for his model that silicates (or Fe/Mg/Si oxides) comprise 77% of the mass of the composite silicate+carbon+vacuum grains, with the other 23% obviously comprising the various forms of carbon. Since the volume fraction of vacuum is 0.45 in his model, and using densities of respectively 3.3 and 2.0 g cm^{-3} for silicate and carbon, then their inferred volume fractions are ~ 0.20 and 0.35. Thus, the volume fractions of carbon and vacuum in our AFGL 2591 polarisation model are in pretty good agreement with those of ISM dust from Mathis (1996).

The final model in Figure 15-d provides quite a good match to the entire 8–13 μm spectrum, inclusive of its overall trapezoid shape, FWHM, peak ratios at 10.1 and 11.1 μm, and the short and long wavelength 'wings'. This is apart from the region between the two peaks at around 10.5–10.8 μm, likely a result of the laboratory and cosmic crystalline forsterites (unsurprisingly) not being exact analogues.

The model and observed 20-to-10 μm polarisation ratios in Figure 15-e are also in reasonable agreement. As noted by Smith et al. (2000), AFGL 2591 has the lowest such ratio amongst the 4 objects for which the absorptive component is well constrained (from a total of 6 with data in both windows). That it is also unique amongst those objects in having an 11.1 μm polarisation feature suggests a mineralogical relation between the two phenomena, possibly the high Mg/Fe ratio proposed here.

Having said that, the 19–22 μm portion of the spectrum is problematic, especially in the sense of the data not showing a distinct feature at about 19.5 μm. We have not found a model, nor can currently suggest a mineralogical explanation, to produce the sharp 11.1 μm feature but be essentially structureless in the 20 μm band. However, we note the relatively poor S/N at 20 μm compared to 10 μm, which results from the extreme difficulty in conducting spectropolarimetric observations in the 20 μm atmospheric window, with its multitude of telluric water vapour bands. New observations on a 10-m class telescope with a dual-beam instrument, such as CanariCam (Telesco et al. (2003)), would be advantageous.

Our model also predicts quite prominent secondary polarisation peaks at around 10.4 and 11.9 μm. Although we are very confident in our identification, observational confirmation of these would seal the interpretation of crystalline fortsteritic olivine silicate in at least AFGL 2591. This was attempted by Wright & Glasse (2005) using Michelle on UKIRT, but the S/N was inadequate. Again, CanariCam on the Gran Telescopio Canarias would provide the best – currently only – opportunity to detect these features.

4.4.3 Separate grain populations of different mineralogy?

As seen in the dot-dash line in panel (f) of Figure 15 the model which nicely matches the AFGL 2591 polarisation cannot match the optical depth spectrum. This is unlike the case of SVS13 in Fujiyoshi et al. (2015) where the two observational quantities are well represented by the same model. For AFGL 2591 there is clearly a large discrepancy in the amounts of crystalline forsterite required to account for the absorption feature in the conventional spectrum of AFGL 2591 and the associated polarisation signature, i.e. volume fractions of around 1% and 10% respectively. Further, the amorphous forsterite is too narrow to account for the bulk of the AFGL 2591 absorption (dashed line). We hypothesise that these discrepancies are due to an unpolarised and purely amorphous (or much lower crystallinity) component to the absorption. The solid line of Figure 15-f shows such a model for the same grain shape parameters as in a-e, and where the purely amorphous component contributes about twice as much as the partially crystalline one. For this purely amorphous component we used the olivine $Mg_{0.8}Fe_{1.2}SiO_4$ of Dorschner et al. (1995) for reasons already stated above.

If correct this would constitute evidence of distinct populations of grains with different mineralogies, although we cannot say which lies closer to the star, or indeed whether they are mixed within the same region. An argument against the latter scenario is that one population is aligned and the other not, although it is feasible that one might couple to the magnetic field more effectively than the other (e.g. if the partially crystalline and Mg-rich silicate grains have a component of free iron). Whatever the case, for a dual-population scenario the 'apparent' crystallinity as determined from the conventional spectrum is an 'average' over both populations

and/or along the line-of-sight, and is obviously lower than the 'real' crystallinity within a localised region.

This also raises an interesting quandary when AFGL 2591 is compared with the few tens of other polarised YSOs in the atlas of Smith et al. (2000), including W3 IRS5, AFGL 2136 and AFGL 2789 here, as well as SgrA IRS3. The 11.1 μm absorption feature in their conventional flux spectra is very similar to that of AFGL 2591, yet their polarisation shows no evidence of an associated signature. So could it be that the estimated crystalline fractions in these objects are in fact lower limits to what might actually exist? Perhaps a 'pocket' of higher crystallinity dust exists along their lines-of-sight, but which is either not aligned, or has a lower abundance, and thus contributes little or nothing to the polarisation. Or is it instead that the disk and/or envelope of AFGL 2591 (along with IRAS13481-6124 and perhaps AFGL 4176) contains dust that is more highly processed than most other embedded YSOs, perhaps from an annealing episode as postulated by Aitken et al. (1988)?

Given the similarity of the sources in terms of their age, mass and that they drive an outflow, plus the almost ubiquitous presence of the 11.1 μm absorption band (as shown here and in Do Duy et al., in preparation), it is tempting to favour the first scenario. Figure 16 shows such an example, where the same model is used as in Figure 15-f for the optical depth, but now the amorphous component is polarised. The 11.1 μm polarisation feature is almost indistinguishable, and only a minor tweak to the relative contributions of the partially crystalline and amorphous components would make it disappear altogether, consistent with its non-detection in most other targets. See the Figure 16 caption for further details. Whilst a promising explanation, a real answer to the questions posed above must await higher sensitivity and resolution data on more sources, hopefully to be obtained with CanariCam in the near future.

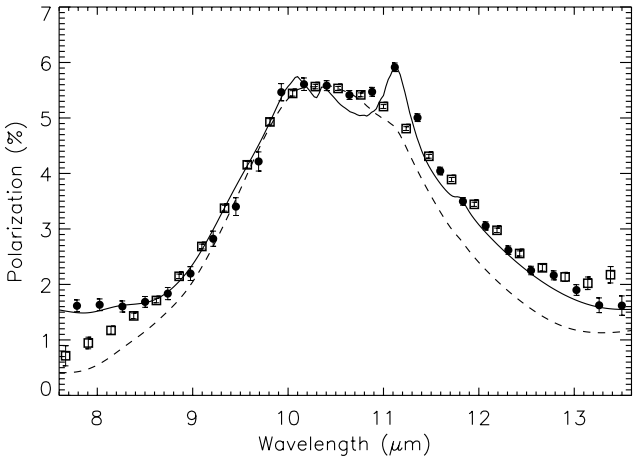

Figure 16. The solid line shows the same model as in Figure 15-d and -e, whilst the dashed line includes a component of polarisation from purely amorphous silicate which contributes about twice as much as the partially crystalline component. The open squares are the data for the BN Object in Orion (e.g. Smith et al. (2000), Aitken et al. (1989)). Curiously, the BN data and the dashed line bear at least a qualitative similarity to each other in the vicinity of 11 μm, namely a steepening of the profile, which may hint at a previously unknown crystalline fraction in BN. Indeed, its conventional spectrum in the mid-IR interferometric study of Boley et al. (2013) shows an 11 μm feature on some baselines, and our own larger data set shows it too (Do Duy et al., in preparation).

4.5 Speculating on implications for the cosmic dust life-cycle

We have presented a strong case for the widespread existence of crystalline silicates – comprising up to a few or even several percent of the total silicate content – in various cold astrophysical environments. Thus we can begin to speculate on the implications this might have for cosmic dust evolution. This is particularly so for the interstellar medium, represented here by SgrA IRS3.

4.5.1 YSO envelopes or disks

The detection of the 11.1 μm absorption band in all of our Class 1 YSOs, along with one or more other bands at 11.85, 23.5 and 28 μm, suggests that the hitherto couple of reported cases of the Class 0 YSO HOPS-68 by Poteet et al. (2011) and Class I YSO SVS13 of Fujiyoshi et al. (2015) are not unique or in any way peculiar. Hence the silicate crystallisation phase must either i) begin much earlier than generally accepted during YSO evolution, i.e. if not before then during the embedded Class 0–I rather than the protoplanetary Class II–III phase, or ii) the dust originally deposited in the parent molecular cloud from the surrounding ISM was already partially crystalline.

If the former case is true then there are some interesting questions which could be posed. For instance, is a crystallisation process still 'required' to occur in the disks of T Tauri and Herbig stars, as reviewed by Henning (2010)? If not, then is a radial mixing or some other transport process still needed to explain the existence of crystalline silicates in comets, which are thought to have formed in the cold, outer regions of our own protoplanetary disk? Or if a crystallisation process is still 'required', will it be more efficient, and/or act over a shorter time, if the starting point already contains crystalline seeds, from which the process may propagate?

On the other hand, if the latter case is true does this then raise a question over the efficiency of the amorphisation and/or destruction processes proposed in the ISM? Or if not, then how do ISM grains, i.e. those formed in situ in the ISM, condense and/or accrete as partially crystalline?

Answers to these questions, if indeed they become necessary, will only be possible once we have a firmer basis on which to conclude that ISM silicate dust does indeed contain a crystalline component. In the following subsections we examine the evidence for partially crystalline grains along the path to the Galactic Centre, and discuss some implications.

4.5.2 Path to the Galactic Centre

Along the extended path toward the Galactic Centre, passing though spiral arms of the Galaxy, there are multiple molecular and diffuse clouds. Of the approximately 30 magnitudes of visual extinction typically quoted as an 'average' toward the Galactic Centre, Whittet et al. (1997) suggest that about 10 magnitudes occurs in molecular clouds and

the remainder in diffuse clouds, where grains would probably be with and without ice mantles respectively.

Before beginning specific speculation a caveat is in order, namely that we do not know with precision how the silicate extinction – let alone that within the 11.1 μm absorption band – is distributed along the line-of-sight to SgrA IRS3. Indeed, it is not even known with certainty where IRS3 is located with respect to the dynamical centre of our Galaxy (Goto et al. (2008)).

We discuss IRS3's location in Appendix A, but for now assert that at least half of the total silicate absorption, including that of the 11.1 μm band, occurs in the ISM and is not merely local to IRS3. This is supported by the presence of the band in the 8–13 μm spectra of IRS1, IRS7 and IRS10 obtained with Subaru/COMICS and shown in Okada et al. (2003), although they did not discuss it. It is also supported by our own mid-IR spectroscopy of the Galactic Centre Quintuplet cluster (Do Duy et al. in preparation), as well as ISO observations of several other positions toward SgrA. As previously noted some of the latter data has already been presented by various authors, but here and in Appendix A we show additional data as well as provide a new analysis of the previously published results. Details can be found in Appendix A but here we simply quote the important findings.

The 11.1 μm feature can be seen in the spectrum of a position several arcseconds south of IRS3, within the E-W bar of the SgrA mini-spiral and which we call IRSX, obtained from the same Gemini Michelle observation as SgrA IRS3 (Figure A1-a and -c). This is similar to the position at which the "diffuse bar" spectrum was obtained by Okada et al. (2003). Whilst the 11.1 μm optical depth of IRSX is about half that of IRS3, the IRSX amorphous silicate optical depth is also roughly half that for IRS3. So the relative strengths of the 11.1 μm band are similar. Further, despite the assertion of Kemper et al. (2004) the 11.1 μm feature can indeed be seen in both ISO spectra centred near SgrA*, again with a similar $\tau_{11.1}/\tau_{9.7}$ as for IRS3 and IRSX. Even more telling for a crystalline silicate identification is that in the same ISO spectra an 11.85 μm feature is also detected (see Figure A1-b and -d).

Similar to the case of the embedded YSOs, a 23.5 μm feature is seen in the SgrA* spectrum, as well as in spectra taken at positions offset approximately 41 and 45 arcseconds to the SSW and NNE respectively, within the so-called circumnuclear disk or ring (CND/R). The same holds for a 28 μm band. See Figure A2-a and -b. The two features are even more prominent in the spectrum of the so-called Pistol star in Figure A2-c.

All of the above leaves us in little doubt that crystalline silicates are present in one or more clouds in the ISM along the line-of-sight toward the Galactic Centre. Averaged along the line-of-sight the crystalline component comprises up to a few percent of the total silicate content, as judged from the crude model for the 11.1 μm band of SgrA IRS3 in Figure 7.

However, the precise abundance is not very well constrained, due mostly to uncertainties in the dust properties. These stem from both the morphology of the grains, e.g. bare versus mantled silicate, as well as the optical properties of the silicate (especially the crystalline component) and the mantle constituent(s). For instance, Li et al. (2007) note that the original crystalline upper limit of 2.2% reported by Kemper et al. (2005) must be raised to around 5% if a water ice mantle coats the grains (assuming a mantle-to-core volume ration of ~ 0.55).

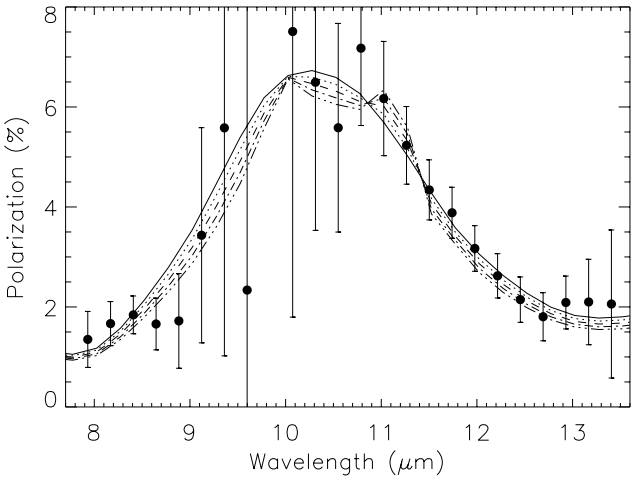

Figure 17. Mid-IR polarisation spectrum of SgrA IRS3, along with representative models. Note how between about 10.5 and 11.5 μm the model polarisation is firstly quite flat and then steepens. Neither property is seen in the data that can be reasonably trusted to accurately represent the true polarisation profile, i.e. from about 10.8 μm onwards.

In addition to our rough estimate of the crystalline silicate fraction toward SgrA IRS3 we can try to obtain an independent estimate from its mid-IR polarisation spectrum presented in Aitken et al. (1986) and Smith et al. (2000). Unlike AFGL 2591 and IRAS13481-6124, but like most other YSOs, an 11.1 μm polarisation signature has not been detected despite the very clear absorption band in Figure 1. It is interesting to see if an upper limit from the polarisation agrees with the estimate from the conventional spectrum.

Figure 17 shows the 8–13 μm polarisation spectrum of SgrA IRS3, similar to that shown in Smith et al. (2000), along with several models. Given the poor S/N in the middle of the band the models have been normalised to the average polarisation within the 10.7–12.0 μm interval. The basis of the models is the olivine silicate $Mg_{0.8}Fe_{1.2}SiO_4$ from Dorschner et al. (1995). However, this was too narrow compared to the data, not being able to fit the short and long wavelength 'wings' of the band, let alone produce the level of polarisation observed from 1.4–4.2 μm along the very nearby IRS7 sightline by Adamson et al. (1999) and Nagata et al. (1994). Therefore, similar to the case of AFGL 2591, and consistent with the interstellar dust life-cycle suggested by Jones et al. (2013), inclusions of graphitic carbon (optical constants from Jager et al. (1998a)) and vacuum were added using EMT, with volume fractions of 0.125 and 0.20 respectively. This model is shown as the solid line, which assumes oblate 2:1 grains (though the grain shape is unconstrained given the wavelength of peak polarisation is not constrained by the data). Having also been binned to match the approximate resolution (or sampling) of the data of about 0.25 μm, this model provides an acceptable match to the spectrum.

The dashed line and three subsequent others are for models with crystalline silicate inclusions with volume fractions of 0.025, 0.05, 0.075 and 0.10, using the optical con-

stant of Fabian et al. (2001). Within the error bars we can not rule out any crystalline silicate fraction in this range. However, despite the poor S/N, given the monotonic decrease of the polarisation from about 10.8 μm onwards we believe that if a crystalline silicate fraction of more than about 5% were present then it would have been detected. Whilst noting that this refers only to the aligned dust population, whereas the conventional spectrum samples all dust, at least the two estimates of the crystalline silicate fraction are consistent. Having said that, the quality of the polarisation data is inadequate, and it is hoped that CanariCam on the GTC can produce a more stringent constraint.

In the interests of completeness we also examined the effect SiC has on the polarisation, since Min et al. (2007) infers that between 2.6 and 4.2% of the dust grain mass is SiC. If this is implemented into our model then the volume fraction would be between about 2 and 3%. Using SiC optical constants from Laor & Draine (1993), preferred by Min et al. (2007), or those of Pégourié (1988), then such a volume fraction could still be consistent with the observations. On the other hand, if the optical constants of Pitman et al. (2008) or Palik (1985) are assumed then a volume fraction of 2–3% significantly perturbs the polarisation spectrum, and would probably have been detected.

4.5.3 Crystalline silicates in the ISM

It is widely believed that silicates in the ISM are either completely amorphous or have such a low crystalline fraction as to be undetectable (Henning (2010)), to the point where this has essentially become a basic tenet of the cosmic dust life cycle (e.g. Jones et al. (2013)). One version of this cycle asserts that the silicate dust ejected into the ISM by AGB stars is destroyed through processes like collisional fragmentation and sputtering on a timescale shorter than the ISM residence time. This residence time, defined as the period between when a grain is injected into the ISM from its parent evolved star outflow to when it is consumed in a new star, is generally agreed to be a few Gyr (Slavin et al. (2015); Jones & Nuth (2011); Draine (2009)). On the other hand, the destruction time scale is typically thought to be around a factor of 10 lower (Draine (2009), Mouri & Taniguchi (2000)), so that something like $\sim$ 95% of the silicate dust observed in the ISM was formed in the ISM.

Precisely how silicates form in the ISM is not well understood (Jones & Nuth (2011)), but may involve accretion of condensible atoms onto the surface of pre-existing particles (Draine (2009)). Voshchinnikov & Henning (2010) claim to have found evidence for such accretion. Such ISM silicate grains are expected to be completely amorphous. More recent estimates of the silicate destruction timescale have increased it by a factor of several, e.g. Slavin et al. (2015), alleviating somewhat the requirement to form silicates in the ISM but not completely eliminating it.

Whatever the case, accepting that only 5% of silicate dust in the ISM is stardust, and that at most 15% of such stardust is crystalline (Henning (2010)), then we may expect to observe a crystalline fraction of $\leq$ 0.75%. However, this does not take account of the relatively rapid amorphisation processes which would probably act on the dust. As reviewed by Henning (2010), the approximately 15% crystalline mass fraction of silicate dust ejected into the ISM by AGB stars is likely to be amorphised through energetic particle collisions on timescales of tens of Myr, much shorter than both the destruction and residence timescales (Bringa et al. (2007); Jäger et al. (2003)).

Thus we would expect any surviving silicate stardust in the ISM to be completely amorphous, and any silicate dust grown in the ISM to also be completely amourphous. Obviously this is consistent with the previous upper limits of a few to several percent for the path to the Galactic Centre (Li et al. (2007); Min et al. (2007); Kemper et al. (2005)). But it is inconsistent with the detection of ISM crystalline silicate reported here of up to a few percent for essentially the same path, i.e. to SgrA IRS3. So detection of crystalline silicates toward SgrA IRS3 and other Galactic Centre positions has a potentially very significant bearing on one or more of: i) the lifetime of stellar-produced silicate grains in the ISM, ii) amorphisation of stellar-produced silicates in the ISM, and/or iii) the growth process of silicate grains in the ISM.

Of course a caveat here is that, despite multiple sightlines toward the GC containing crystalline silicates, this could still be regarded as a special case. They are all along a somewhat confined path within our Galaxy that intersects many of the same clouds, as judged for instance by the similar velocities of absorption components of several molecular tracers (e.g. see discussion in Appendix A for references). A sensitive survey of other sightlines is clearly required, which we have begun and a few examples of which will be presented in our paper describing the whole sample (Do Duy et al., in preparation).

Notably however, even if the GC ISM path is unique and/or the crystalline silicates occur within a particular cloud (e.g. within a few hundred parsecs of the GC itself), our results still have important implications for the cosmic dust life cycle. Any amount of crystallinity in these environments would be unexpected.

5 CONCLUSIONS

The major observational result of this paper is that an absorption feature at 11.1 μm exists in the spectra of eight embedded Class 1 YSOs – AFGL 2136, W3 IRS5, AFGL 2789, AFGL 2591, AFGL 4176, IRAS13481-6124, W28 A2 and IRAS19110+1045 – and the path through the ISM to the Galactic Centre sources SgrA IRS3 and a position we call (for convenience) SgrA IRSX. Curiously, this feature has escaped widespread attention. This is despite it being hinted at in previous observations of multiple YSOs and the ISM at lower spectral and/or spatial resolution, and actually resolved in a Class 0 YSO by Poteet et al. (2011). It even appears in the mid-IR interferometric study of many DEYSOs of Boley et al. (2013), including three studied here – AFGL 2136, AFGL 4176 and IRAS13481-6124 – where in some cases it also shows a possible spatial (baseline) dependence. To date the feature has not been studied in the detail provided here.

The wavelength of this feature, and its spectral profile, is similar to that observed toward the OH/IR stars and dust factories AFGL 2403, OH26.5+0.6 and AFGL 230, known to be sources of crystalline silicates. Also, other potential carriers for the feature in AFGL 2789 – such as water ice,

hydrocarbons and carbonates – can be excluded to varying degrees of confidence (high, medium and high respectively) based on the lack of expected accompanying features at shorter wavelengths. A model of separate populations of sub-micron amorphous olivine and crystalline forsterite grains match very well the observed AFGL 2789 spectrum. Further, models of magnesium-rich (forsteritic) crystalline olivine mixed with amorphous olivine – to represent a partially crystalline grain structure as an 'effective medium' – match very well the central wavelength and spectral profile. However, this is only the case if the work of Tamanai et al. (2006) is utilised, which shows an ~ 0.2 μm shift of the primary features to shorter wavelengths.

Detection of a polarisation signature in the sources AFGL 2591 and IRAS13481-6124, and possibly AFGL 4176, suggests a carrier with a relatively high band strength, and this too is consistent with a crystalline silicate interpretation. The implied volume fraction from an EMT model to the AFGL 2591 polarisation is around 10%, larger than the few percent that would be inferred based solely on the absorption feature in the conventional spectrum of this as well as the other YSO and Galactic centre targets. This suggests that 'pockets' of relatively high crystallinity material could be hidden in at least some of the other sources, only revealed if the dust is aligned.

Using the ISO Data Archive we also examined the 20-45 μm spectra of these and other sources. Doing so allowed us to identify features that support our contention that the 11.1 μm feature is carried by crystalline silicate. For instance, we find evidence for features at 11.85, 23.5 and 28 μm in absorption toward several of our YSO targets, as well as toward multiple positions within the Galactic Centre. A 33.6 μm absorption band is however conspicuously absent in all these spectra. But such a feature is detected in emission, in conjunction with another at 36 μm, in the spectra of several HII regions. This provides further confidence in our assessment that crystalline silicates are commonly, if not ubiquitously, present in the very early stages of star formation.

The seemingly common existence of crystalline silicates at any abundance level in the ISM, and envelopes or disks of embedded YSOs, presents a challenge to models which attempt to explain the cosmic dust life cycle. These models use as a foundation that silicate dust is completely amorphous in the ISM and molecular clouds. There are certainly good physics-based reasons to believe this would be the case, given the multitude of grain destruction and amorphisation processes proposed in the literature. But observationally this appears to be no longer the situation. Of course, more observations are required, especially of truly diffuse ISM paths and ideally coupled with spectropolarimetry.

Finally, we have shown that ground-based mid-IR slit spectroscopy, at a moderate spectral resolution, and even of bright sources on 10 m-class telescopes, still has a part to play in the study of cosmic dust. We have a much larger sample of sources, most of which also show the 11.1 μm absorption band, e.g. well known YSOs like S140 IRS1, S255 IRS1 and NGC7538 IRS1, and ISM sightlines to the Galactic Centre Quintuplet members. The entire sample is currently under study, is producing some interesting and surprising results, and will be presented and discussed in a forthcoming paper (Do Duy et al., in preparation).

ACKNOWLEDGEMENTS

Based on observations obtained at the Gemini Observatory, which is operated by the Association of Universities for Research in Astronomy, Inc., under a cooperative agreement with the NSF on behalf of the Gemini partnership: the National Science Foundation (United States), the National Research Council (Canada), CONICYT (Chile), the Australian Research Council (Australia), Ministério da Ciência, Tecnologia e Inovação (Brazil) and Ministerio de Ciencia, Tecnología e Innovación Productiva (Argentina). Based on observations with ISO, an ESA project with instruments funded by ESA Member States (especially the PI countries: France, Germany, the Netherlands and the United Kingdom) and with the participation of ISAS and NASA. The version of the ISO data presented in this paper correspond to the Highly Processed Data Product (HPDP) set called "'High resolution processed and defringed SWS01s"' by W. Frieswijk et al. CMW acknowledges financial support from an Australian Research Council Future Fellowship FT100100495 and previously DP0345227. Tho Do Duy acknowledges financial support from a UNSW Canberra Research Training Scholarship and a UNSW Canberra Tuition Fee Scholarship. We thank David Aitken, Craig Smith and Patrick Roche for obtaining much of the UCLS data used to complement the work here, and the reviewers for well considered and thorough reviews of both this work and an earlier version.

REFERENCES

Adamson A. J., Whittet D. C. B., Chrysostomou A., Hough J. H., Aitken D. K., Wright G. S., Roche P. F., 1999, ApJ, 512, 224
Aitken D. K., 1989, in Böhm-Vitense E., ed., ESA Special Publication Vol. 290, Infrared Spectroscopy in Astronomy. pp 99–107
Aitken D. K., Roche P. F., Bailey J. A., Briggs G. P., Hough J. H., et al., 1986, MNRAS, 218, 363
Aitken D. K., Roche P. F., Smith C. H., James S. D., Hough J. H., 1988, MNRAS, 230, 629
Aitken D. K., Smith C. H., Roche P. F., 1989, MNRAS, 236, 919
Aitken D. K., Moore T. J. T., Roche P. F., Smith C. H., Wright C. M., 1993, MNRAS, 265, L41
Alexander R. D., Casali M. M., André P., Persi P., Eiroa C., 2003, A&A, 401, 613
Allamandola L. J., Sandford S. A., Tielens A. G. G. M., Herbst T. M., 1992, ApJ, 399, 134
Allen D. A., Burton M. G., 1993, Nature, 363, 54
Becklin E. E., Matthews K., Neugebauer G., Willner S. P., 1978, ApJ, 219, 121
Beckwith S., Persson S. E., Neugebauer G., Becklin E. E., 1978, ApJ, 223, 464
Bernstein M. P., Sandford S. A., Allamandola L. J., 2005, ApJSupplement Series, 161, 53
Bohren C. F., Huffman D. R., 1983, Light Scattering and Absorption by Small Particles
Boley P. A., et al., 2013, A&A, 558, A24
Boogert A. C. A., et al., 2004, ApJSupplement Series, 154, 359
Boogert A. C. A., et al., 2008, ApJ, 678, 985
Boogert A. C. A., Gerakines P., Whittet D., 2015, ARA&A, 53, 541
Bowey J. E., Adamson A. J., Yates J. A., 2003, MNRAS, 340, 1173
Bradley J. P., 2010, in Henning T., ed., Lecture Notes in Physics, Berlin Springer Verlag Vol. 815, Lecture Notes in Physics,

Berlin Springer Verlag. pp 259–276, doi:10.1007/978-3-642-13259-9_6
Bradley J. P., Humecki H. J., Germani M. S., 1992, ApJ, 394, 643
Bregman J. D., Witteborn F. C., Allamandola L. J., Campins H., Wooden D. H., Rank D. M., Cohen M., Tielens A. G. G. M., 1987, A&A, 187, 616
Bregman J. D., Hayward T. L., Sloan G. C., 2000, ApJLetters, 544, L75
Bringa E. M., et al., 2007, ApJ, 662, 372
Bromley S. T., Goumans T. P. M., Herbst E., Jones A. P., Slater B., 2014, Physical Chemistry Chemical Physics, 16, 18623
Brooke T. Y., Sellgren K., Smith R. G., 1996, ApJ, 459, 209
Brooke T. Y., Sellgren K., Geballe T. R., 1999, ApJ, 517, 883
Calvet N., Magris G. C., Patino A., D'Alessio P., 1992, Rev. Mex. Astron. Astrofis., 24, 27
Campins H., Ryan E. V., 1989, ApJ, 341, 1059
Ceccarelli C., Caux E., Tielens A. G. G. M., Kemper F., Waters L. B. F. M., Phillips T., 2002, A&A, 395, L29
Cesarsky D., Jones A. P., Lequeux J., Verstraete L., 2000, A&A, 358, 708
Chiang E. I., Goldreich P., 1997, ApJ, 490, 368
Chiar J. E., Tielens A. G. G. M., Whittet D. C. B., Schutte W. A., Boogert A. C. A., Lutz D., Van Dishoeck E. F., Bernstein M. P., 2000, ApJ, 537, 749
Chiar J. E., Adamson A. J., Pendleton Y. J., Whittet D. C. B., Caldwell D. A., Gibb E. L., 2002, ApJ, 570, 198
Chiar J. E., et al., 2006, ApJ, 651, 268
Chiar J. E., Tielens A. G. G. M., Adamson A. J., Ricca A., 2013, ApJ, 770, 78
Clément D., Mutschke H., Klein R., Henning T., 2003, ApJ, 594, 642
Cox P., 1989, A&A, 225, L1
Dartois E., d'Hendecourt L., 2001, A&A, 365, 144
Dartois E., et al., 1998, A&A, 338, L21
Dartois E., d'Hendecourt L., Thi W., Pontoppidan K. M., Van Dishoeck E. F., 2002, A&A, 394, 1057
Day K. L., 1979, ApJ, 234, 158
Day K. L., 1981, ApJ, 246, 110
Demyk K., Jones A. P., Dartois E., Cox P., d'Hendecourt L., 1999, A&A, 349, 267
Demyk K., Dartois E., Wiesemeyer H., Jones A. P., d'Hendecourt L., 2000, A&A, 364, 170
Dorschner J., Begemann B., Henning T., Jaeger C., Mutschke H., 1995, A&A, 300, 503
Draine B. T., 2003a, ARA&A, 41, 241
Draine B. T., 2003b, ApJ, 598, 1026
Draine B. T., 2009
Draine B. T., Allaf-Akbari K., 2006, ApJ, 652, 1318
Draine B. T., Lee H. M., 1984, ApJ, 285, 89
Dyck H. M., Lonsdale C. J., 1980, The Astronomical Journal, 85, 1077
Fabian D., Henning T., Jäger C., Mutschke H., Dorschner J., Wehrhan O., 2001, A&A, 378, 228
Fritz T. K., et al., 2011, ApJ, 737, 73
Fujiyoshi T., Wright C. M., Moore T. J. T., 2015, MNRAS, 451, 3371
Geballe T. R., Oka T., 1989, ApJ, 342, 855
Gibb E. L., et al., 2000, ApJ, 536, 347
Gibb E. L., Whittet D. C. B., Chiar J. E., 2001, ApJ, 558, 702
Gibb E. L., Whittet D. C. B., Boogert A. C. A., Tielens A. G. G. M., 2004, ApJSupplement Series, 151, 35
Gielen C., Van Winckel H., Waters L. B. F. M., Min M., Dominik C., 2007, A&A, 475, 629
Gillett F. C., Forrest W. J., Merrill K. M., Soifer B. T., Capps R. W., 1975, ApJ, 200, 609
Glass I. S., Matsumoto S., Carter B. S., Sekiguchi K., 2001, MNRAS, 321, 77
Glasse A. C., Atad-Ettedgui E. I., Harris J. W., 1997, in Ardeberg A. L., ed., Society of Photo-Optical Instrumentation Engineers (SPIE) Conference Series Vol. 2871, Optical Telescopes of Today and Tomorrow. pp 1197–1203
Goto M., McCall B. J., Geballe T. R., Usuda T., Kobayashi N., Terada H., Oka T., 2002, Publications of the Astronomical Society of Japan, 54, 951
Goto M., et al., 2008, ApJ, 688, 306
Goto M., Geballe T. R., Indriolo N., Yusef-Zadeh F., Usuda T., Henning T., Oka T., 2014, ApJ, 786, 96
Greenberg J. M., Li A., 1996, A&A, 309, 258
Hanner M. S., Brooke T. Y., Tokunaga A. T., 1995, ApJ, 438, 250
Hanner M. S., Brooke T. Y., Tokunaga A. T., 1998, ApJ, 502, 871
Helmich F. P., et al., 1996, A&A, 315, L173
Henning T., 2010, ARA&A, 48, 21
Henning T., Stognienko R., 1993, A&A, 280, 609
Herman J., Habing H. J., 1985, Phys. Rep., 124, 257
Hildebrand R. H., 1988, QJRAS, 29, 327
Hildebrand R. H., Dragovan M., 1995, ApJ, 450, 663
Holloway R. P., Chrysostomou A., Aitken D. K., Hough J. H., McCall A., 2002, MNRAS, 336, 425
Hough J. H., Whittet D. C. B., Sato S., Yamashita T., Tamura M., Nagata T., Aitken D. K., Roche P. F., 1989, MNRAS, 241, 71
Jager C., Mutschke H., Henning T., 1998a, A&A, 332, 291
Jäger C., Molster F. J., Dorschner J., Henning T., Mutschke H., Waters L. B. F. M., 1998b, A&A, 339, 904
Jäger C., Dorschner J., Mutschke H., Posch T., Henning T., 2003, A&A, 408, 193
Jiang B. W., Zhang K., Li A., Lisse C. M., 2013, ApJ, 765, 72
Jiménez-Esteban F. M., García-Lario P., Engels D., Perea Calderón J. V., 2006, A&A, 446, 773
Jones A. P., 2014, arXiv preprint arXiv:1411.6666
Jones A. P., Nuth J. A., 2011, A&A, 530, A44
Jones A. P., Frey V., Verstraete L., Cox P., Demyk K., 1999, in Cox P., Kessler M., eds, ESA Special Publication Vol. 427, The Universe as Seen by ISO. p. 679
Jones A. P., Fanciullo L., Köhler M., Verstraete L., Guillet V., Bocchio M., Ysard N., 2013, A&A, 558, A62
Juhász A., et al., 2010, ApJ, 721, 431
Keane J. V., Tielens A. G. G. M., Boogert A. C. A., Schutte W. A., Whittet D. C. B., 2001, A&A, 376, 254
Kemper F., Molster F. J., Jäger C., Waters L. B. F. M., 2002a, A&A, 394, 679
Kemper F., Jäger C., Waters L. B. F. M., Henning T., Molster F. J., Barlow M. J., Lim T., De Koter A., 2002b, Nature, 415, 295
Kemper F., Vriend W. J., Tielens A. G. G. M., 2004, ApJ, 609, 826
Kemper F., Vriend W. J., Tielens A. G. G. M., 2005, ApJ, 633, 534
Kessler-Silacci J. E., Hillenbrand L. A., Blake G. A., Meyer M. R., 2005, ApJ, 622, 404
Knacke R. F., Fajardo-Acosta S. B., Telesco C. M., Hackwell J. A., Lynch D. K., Russell R. W., 1993, ApJ, 418, 440
Kobayashi Y., Kawara K., Sato S., Okuda H., 1980, Publications of the Astronomical Society of Japan, 32, 295
Koike C., Chihara H., Tsuchiyama A., Suto H., Sogawa H., Okuda H., 2003, A&A, 399, 1101
Lacy J. H., Faraji H., Sandford S. A., Allamandola L. J., 1998, ApJ, 501, L105
Lane M. D., Christensen P. R., 1997, J. Geophys. Res., 102, 25581
Laor A., Draine B. T., 1993, ApJ, 402, 441
Lazarian A., 2007, J. Quant. Spectrosc. Radiative Transfer, 106, 225
Lee H. M., Draine B. T., 1985, ApJ, 290, 211

Leech K., et al., 2003, The ISO Handbook, Volume V - SWS - The Short Wavelength Spectrometer
Li M. P., Zhao G., Li A., 2007, MNRAS, 382, L26
Li Q., Liang S. L., Li A., 2014, MNRAS, 440, L56
Lutz D., et al., 1996, A&A, 315, L269
Maldoni M. M., Smith R. G., Robinson G., Rookyard V. L., 1998, MNRAS, 298, 251
Maldoni M. M., Egan M. P., Smith R. G., Robinson G., Wright C. M., 2003, MNRAS, 345, 912
Maldoni M. M., Egan M. P., Robinson G., Smith R. G., Wright C. M., 2004, MNRAS, 349, 665
Maldoni M. M., Ireland T. R., Smith R. G., Robinson G., 2005, MNRAS, 362, 872
Malfait K., Waelkens C., Waters L. B. F. M., Vandenbussche B., Huygen E., De Graauw M. S., 1998, Astronomy and astrophysics, 332, L25
Martin P. G., 1975, ApJ, 202, 393
Mastrapa R. M., Sandford S. A., Roush T. L., Cruikshank D. P., Dalle Ore C. M., 2009, ApJ, 701, 1347
Mathis J. S., 1996, ApJ, 472, 643
Mathis J. S., 1998, ApJ, 497, 824
Mathis J. S., Whiffen G., 1989, ApJ, 341, 808
Mathis J. S., Rumpl W., Nordsieck K. H., 1977, ApJ, 217, 425
Meeus G., Waters L. B. F. M., Bouwman J., Van Den Ancker M. E., Waelkens C., Malfait K., 2001, A&A, 365, 476
Min M., Hovenier J. W., de Koter A., 2003, A&A, 404, 35
Min M., Waters L. B. F. M., De Koter A., Hovenier J. W., Keller L. P., Markwick-Kemper F., 2007, A&A, 462, 667
Molster F. J., Kemper C., 2005, Space Sci. Rev., 119, 3
Molster F. J., Waters L. B. F. M., Tielens A. G. G. M., Barlow M. J., 2002, A&A, 382, 184
Molster F. J., Waters L. B. F. M., Kemper F., 2010, in , Astromineralogy. Springer, pp 143–201
Monnier J. D., Tuthill P. G., Ireland M., Cohen R., Tannirkulam A., Perrin M. D., 2009, ApJ, 700, 491
Moultaka J., Eckart A., Viehmann T., Mouawad N., Straubmeier C., Ott T., Schödel R., 2004, A&A, 425, 529
Moultaka J., Eckart A., Schödel R., Viehmann T., Najarro F., 2005, A&A, 443, 163
Mouri H., Taniguchi Y., 2000, ApJ, 534, L63
Mukai T., Koike C., 1990, Icarus, 87, 180
Nagata T., Kobayashi N., Sato S., 1994, ApJ, 423, L113
O'Donnell J. E., 1994, ApJ, 437, 262
Oka T., Geballe T. R., Goto M., Usuda T., McCall B. J., 2005, ApJ, 632, 882
Okada Y., et al., 2003, Astronomische Nachrichten Supplement, 324, 567
Ossenkopf V., 1991, A&A, 251, 210
Ossenkopf V., Henning T., Mathis J. S., 1992, A&A, 261, 567
Palik E. D., 1985, Handbook of optical constants of solids
Peeters E., et al., 2002, A&A, 381, 571
Peeters E., Martín-Hernández N. L., Rodríguez-Fernández N. J., Tielens X., 2005, Space Sci. Rev., 119, 273
Pégourié B., 1988, A&A, 194, 335
Pendleton Y. J., Sandford S. A., Allamandola L. J., Tielens A. G. G. M., Sellgren K., 1994, ApJ, 437, 683
Perrin J.-M., Lamy P. L., 1990, ApJ, 364, 146
Persi P., Ferrari-Toniolo M., Spinoglio L., 1986, A&A, 157, 29
Pitman K. M., Hofmeister A. M., Corman A. B., Speck A. K., 2008, A&A, 483, 661
Pitman K. M., Dijkstra C., Hofmeister A. M., Speck A. K., 2010, MNRAS, 406, 460
Poteet C. A., et al., 2011, ApJ, 733, L32
Pott J.-U., Eckart A., Glindemann A., Schödel R., Viehmann T., Robberto M., 2008, A&A, 480, 115
Riaz B., Martín E. L., Bouy H., Tata R., 2009, ApJ, 700, 1541
Robinson G., 2013, MNRAS, p. stt2115
Robinson G., Maldoni M. M., 2010, MNRAS, 408, 1956
Robinson G., Smith R. G., Maldoni M. M., 2012, MNRAS, 424, 1530
Roche P. F., Aitken D. K., 1984a, MNRAS, 208, 481
Roche P. F., Aitken D. K., 1984b, MNRAS, 209, 33P
Roche P. F., Aitken D. K., 1985, MNRAS, 215, 425
Roche P. F., Packham C., Telesco C. M., Radomski J. T., Alonso-Herrero A., Aitken D. K., Colina L., Perlman E., 2006, MNRAS, 367, 1689
Roche P. F., Alonso-Herrero A., Gonzalez-Martin O., 2015, MNRAS, 449, 2598
Rosenthal D., Bertoldi F., Drapatz S., 2000, A&A, 356, 705
Ruan L. M., Wang X. Y., Qi H., Wang S. G., 2011, Journal of aerosol science, 42, 759
Sako S., et al., 2003, PASP, 115, 1407
Sandford S. A., 1986, Science, 231, 1540
Sandford S. A., Walker R. M., 1985, ApJ, 291, 838
Sandford S. A., Allamandola L. J., Tielens A. G. G. M., Sellgren K., Tapia M., Pendleton Y., 1991, ApJ, 371, 607
Sargent B. A., et al., 2009, ApJSupplement Series, 182, 477
Schödel R., Najarro F., Muzic K., Eckart A., 2010, A&A, 511, A18
Schutte W. A., Khanna R. K., 2003, A&A, 398, 1049
Schutte W. A., Gerakines P. A., Geballe T. R., van Dishoeck E. F., Greenberg J. M., 1996, A&A, 309, 633
Scott A., Duley W. W., 1996, ApJS, 105, 401
Scoville N. Z., Stolovy S. R., Rieke M., Christopher M., Yusef-Zadeh F., 2003, ApJ, 594, 294
Serabyn E., Lacy J. H., Achtermann J. M., 1991, ApJ, 378, 557
Siebenmorgen R., Voshchinnikov N. V., Bagnulo S., 2014, A&A, 561, A82
Sihvola A. H., 1994, Journal of electromagnetic waves and applications, 8, 115
Sihvola A. H., Pekonen O. P. M., 1994, Journal of electromagnetic waves and applications, 8, 1605
Skinner C. J., Tielens A. G. G. M., Barlow M. J., Justtanont K., 1992, ApJ, 399, L79
Slavin J. D., Dwek E., Jones A. P., 2015, ApJ, 803, 7
Smith B. J., 2003, AJ, 126, 935
Smith R. G., Herman J., 1990, A&A, 227, 147
Smith R. G., Wright C. M., 2011, MNRAS, 414, 3764
Smith R. G., Sellgren K., Tokunaga A. T., 1989, ApJ, 344, 413
Smith C. H., Wright C. M., Aitken D. K., Roche P. F., Hough J. H., 2000, MNRAS, 312, 327
Sogawa H., Koike C., Chihara H., Suto H., Tachibana S., Tsuchiyama A., Kozasa T., 2006, A&A, 451, 357
Soifer B. T., Willner S. P., Rudy R. J., Capps R. W., 1981, ApJ, 250, 631
Sokolik I. N., Toon O. B., 1999, J. Geophys. Res., 104, 9423
Somsikov V. V., Voshchinnikov N. V., 1999, A&A, 345, 315
Spoon H. W. W., et al., 2006, ApJ, 638, 759
Stognienko R., Henning T., Ossenkopf V., 1995, A&A, 296, 797
Stroud D., 1975, Physical Review B, 12, 3368
Suto H., et al., 2006, MNRAS, 370, 1599
Sutton E. C., Danchi W. C., Jaminet P. A., Masson C. R., 1990, ApJ, 348, 503
Sylvester R. J., Kemper F., Barlow M. J., de Jong T., Waters L. B. F. M., Tielens A. G. G. M., Omont A., 1999, A&A, 352, 587
Tamanai A., Mutschke H., Blum J., Meeus G., 2006, ApJLetters, 648, L147
Telesco C. M., Pina R. K., Hanna K. T., Julian J. A., Hon D. B., Kisko T. M., 1998, in Fowler A. M., ed., Society of Photo-Optical Instrumentation Engineers (SPIE) Conference Series Vol. 3354, Infrared Astronomical Instrumentation. pp 534–544
Telesco C. M., et al., 2003, in Iye M., Moorwood A. F. M., eds, Society of Photo-Optical Instrumentation Engineers (SPIE) Conference Series Vol. 4841, Instrument Design and Perfor-

mance for Optical/Infrared Ground-based Telescopes. pp 913–922, doi:10.1117/12.458979
Thi W.-F., van Dishoeck E. F., Dartois E., Pontoppidan K. M., Schutte W. A., Ehrenfreund P., d'Hendecourt L., Fraser H. J., 2006, A&A, 449, 251
Tielens A. G. G. M., Wooden D. H., Allamandola L. J., Bregman J., Witteborn F. C., 1996, ApJ, 461, 210
Van den Ancker M. E., Tielens A. G. G. M., Wesselius P. R., 2000, A&A, 358, 1035
Verstraete L., et al., 2001, A&A, 372, 981
Viehmann T., Eckart A., Schödel R., Moultaka J., Straubmeier C., Pott J.-U., 2005, A&A, 433, 117
Viehmann T., Eckart A., Schödel R., Pott J.-U., Moultaka J., 2006, ApJ, 642, 861
Voshchinnikov N. V., Henning T., 2010, A&A, 517, A45
Voshchinnikov N. V., Il'in V. B., Henning T., Dubkova D. N., 2006, A&A, 445, 167
Voshchinnikov N. V., Videen G., Henning T., 2007, Appl. Opt., 46, 4065
Watson D. M., et al., 2009, ApJS, 180, 84
Whittet D. C. B., Duley W. W., Martin P. G., 1990, MNRAS, 244, 427
Whittet D. C. B., et al., 1997, ApJ, 490, 729
Willner S. P., Pipher J. L., 1982, in Riegler G. R., Blandford R. D., eds, American Institute of Physics Conference Series Vol. 83, The Galactic Center. pp 77–81, doi:10.1063/1.33505
Willner S. P., et al., 1982, ApJ, 253, 174
Witteborn F. C., Sandford S. A., Bregman J. D., Allamandola L. J., Cohen M., Wooden D. H., Graps A. L., 1989, ApJ, 341, 270
Wright C. M., 1994, PhD thesis, University of New South Wales
Wright C. M., Glasse A. C. H., 2005, in Adamson A., Aspin C., Davis C., Fujiyoshi T., eds, Astronomical Society of the Pacific Conference Series Vol. 343, Astronomical Polarimetry: Current Status and Future Directions. p. 316
Wright C. M., Aitken D. K., Smith C. H., Roche P. F., 1999, in Greenberg J. M., Li A., eds, NATO Advanced Science Institutes (ASI) Series C Vol. 523, NATO Advanced Science Institutes (ASI) Series C. pp 77–83
Wright C. M., van Dishoeck E. F., Black J. H., Feuchtgruber H., Cernicharo J., González-Alfonso E., de Graauw T., 2000, A&A, 358, 689
Wright C. M., Aitken D. K., Smith C. H., Roche P. F., Laureijs R. J., 2002, in Alves J. F., McCaughrean M. J., eds, The Origin of Stars and Planets: The VLT View. p. 85, doi:10.1007/10856518_10
Wright C. M., Siebenmorgen R., Stecklum B., Sterzik M., Käufl H.-U., 2008, in Society of Photo-Optical Instrumentation Engineers (SPIE) Conference Series. p. 29, doi:10.1117/12.787899
Yusef-Zadeh F., Melia F., 1992, ApJ, 385, L41
Yusef-Zadeh F., Morris M., 1991, ApJ, 371, L59
Zinner E., 2013, Analytical Chemistry, 85, 1264
de Muizon M., D'Hendecourt L. B., Perrier C., 1986, in Israel F. P., ed., Astrophysics and Space Science Library Vol. 124, Light on Dark Matter. pp 221–224
de Vries B. L., Min M., Waters L. B. F. M., Blommaert J. A. D. L., Kemper F., 2010, A&A, 516, A86
de Vries B. L., Blommaert J. A. D. L., Waters L. B. F. M., Waelkens C., Min M., Lombaert R., Van Winckel H., 2014, A&A, 561, A75
van Boekel R. J. H. M., et al., 2004, Nature, 432, 479
van Dishoeck E. F., Helmich F. P., 1996, A&A, 315, L177
van Dishoeck E. F., Wright C. M., Cernicharo J., González-Alfonso E., de Graauw T., Helmich F. P., Vandenbussche B., 1998, ApJ, 502, L173
van der Tak F. F. S., Tuthill P. G., Danchi W. C., 2005, A&A, 431, 993

APPENDIX A: LOCATING SGRA IRS3

The fact that – projected onto the plane-of-the-sky – IRS3 lies only about 5 arcsec (0.2 pc) NW of the dynamical centre of the Galaxy, Sgr A*, makes it likely that the two are also close in 3-dimensional space. But its lack of association with the ionised gas and warm dust of the Galactic Centre (GC) mini-spiral which orbits Sgr A*, evidenced for instance by the non-detection of a 12.8 μm [Ne II] emission line in Figure 1 – unlike the case for IRSX in FigureA1-a – could be used to argue against a physical association. Or instead it could be that IRS3 lies within the innermost region of the cavity encompassed by the $\sim$ 1 pc radius cicumnuclear disk or ring (CND) around Sgr A*.

This latter option finds some support in the M-band imaging of Viehmann et al. (2005). They find extended emission with a bow-shock-like shape around IRS3, which they interpret to be due to strong winds from the nuclear star cluster within about half an arcsecond ($\leq$ 0.02 pc) of Sgr A*. The 8.6 μm images in Pott et al. (2008) show a similar morphology. On the other hand, if such a wind was influencing IRS3 then it might be expected to produce similar phenomena to that observed for IRS7 (only an arcsecond or so away), where a cometary-like tail at least 5 arcsec in length is observed in both radio continuum (Yusef-Zadeh & Melia (1992), Yusef-Zadeh & Morris (1991)) and [Ne II] (Serabyn et al. (1991)).

IRS3 must be further distant than about 4-5 kpc since absorption line spectroscopy of several molecules show narrow features at LSR velocities of -3, -31 and -53 km s^{-1}. Examples include infrared lines of H_3^+ and CO in Goto et al. (2014), Goto et al. (2008), Oka et al. (2005), Goto et al. (2002) and Geballe & Oka (1989). These are also seen in mm-wave rotational transitions, such as CO 3–2 in Sutton et al. (1990). The -3, -31 and -53 km s^{-1} components respectively arise from molecular clouds local to the solar neighborhood, the 3 kpc arm and the 4.5 kpc arm.

Further, a discrete feature at -140 km s^{-1} and a 'trough' of absorption over a velocity extent of minus a few hundred to a few tens of km s^{-1} in the IR H_3^+ and CO transitions toward IRS3 has been identified with clouds of the so-called central molecular zone (CMZ). The CMZ is a region of radius about 200 pc around the Galactic Centre (Oka et al. (2005)). Another component in the IRS3 spectrum at +60 km s^{-1} has recently been identified by Goto et al. (2014) with a compact cloud within the CND, although a previous analysis by Goto et al. (2008) associated it with the well known 50 km s^{-1} cloud on the far side of SgrA. The location of clouds at -72 and +45 km s^{-1} in the IRS3 spectrum remain undetermined (Goto et al. (2014)).

From these considerations IRS3 must lie behind at least the front side of the CMZ as well as the CND, and probably also behind the dynamical centre. But how far behind remains an open question.

A1 Enhanced silicate absorption toward SgrA IRS3

Perhaps consistent with IRS3 lying on the far side of the GC there is additional silicate absorption toward IRS3 compared to other sources within the GC. This was first noted by Becklin et al. (1978), and then by Roche & Aitken (1985),

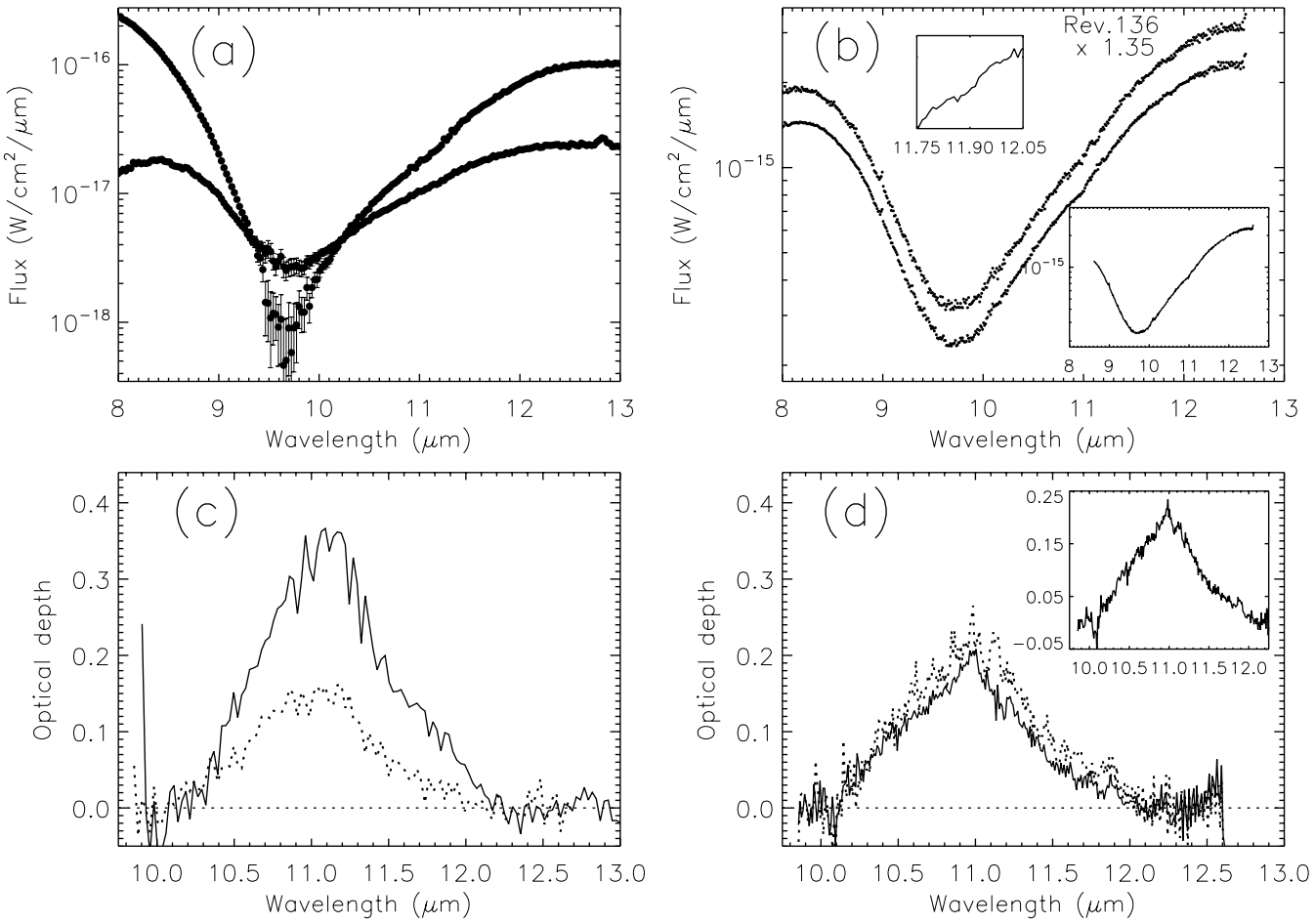

Figure A1. Comparison between spectra of SgrA IRS3 and IRSX obtained simultaneously with Michelle (a), as well as with the two ISO spectra (b). Panels (c) and (d) show their extracted optical depths for the 11.1 μm feature. The emission line at 12.8 μm in SgrA IRSX is from [Ne II], which is clearly absent in SgrA IRS3. An 11.85 μm feature can be seen in both ISO data sets, but is most obvious in the combined spectrum and its extracted optical depth (insets in (b) and (d) respectively). It affirms the identification of crystalline silicates in the ISM path to the Galactic Centre.

based on observations of multiple points within the N-S arm and E-W bar of the SgrA mini-spiral. It can also be seen in Figure A1-a where the IRS3 spectrum is compared with that of a region about 5 arcsec south (we call it IRSX, just east of IRS2). This was obtained from the same Gemini–Michelle observation, thus is immune to possible artefacts from the standard star division, such as the telluric 9.6 μm ozone band mimicking deeper silicate absorption. Clearly the depths of the respective silicate bands toward IRS3 and IRSX are very different.

Whilst IRSX almost certainly has underlying silicate emission, even accounting for this the silicate optical depth $\tau_{9.7}$ was found by Roche & Aitken (1985) to be confined to a narrow range of 3.6±0.3 for almost all of the compact mid-IR sources within the mini-spiral. A value about 0.8–1.3 higher was found for IRS3 by Roche & Aitken (1985) and Becklin et al. (1978) respectively. On the other hand, the almost 3 orders of magnitude extinction at 9.7 μm for IRS3 evident in our spectrum suggests $\tau_{9.7}$ is around 7, double that for the mini-spiral. This is in very good agreement with the figure of 7.0±0.5 inferred by Pott et al. (2008) from their spectrum obtained with mid-IR interferometry.

An enhanced silicate optical depth toward IRS3 holds true even when more recent data on the extinction to the GC is considered. For instance, it is higher than the value of around 4.7 to the ionised gas and warm dust of the mini-spiral, inferred from the data of Fritz et al. (2011) in their Figure 11. They used ISO and other hydrogen recombination line data to determine the extinction from 1 to 19 μm and subsequently 'reconstructed' the underlying continuum emission.

The origin of the extra silicate absorption toward IRS3 was suggested by Roche & Aitken (1985) and Becklin et al. (1978) to lie in a dust shell intrinsic (or local) to IRS3 itself, possibly a result of mass loss assuming IRS3 to be an O-rich star. However, the recent mid-IR observations of Pott et al. (2008) have cast a question over this model. They find that IRS3 consists of up to three components. The largest is a diffuse emission region found from direct 8.6 μm imaging and extending over a few arcseconds (and also seen in the L- and M-bands by Viehmann et al. (2005)). Embedded within this

is a compact component, unresolved in the direct images but resolved by interferometry into two additional components, the most compact of which has a wavelength-independent FWHM of 18±1 mas (144 AU at 8 kpc) surrounded by another component whose FWHM increases with wavelength from $\leq$ 40 mas to $\geq$ 50 mas (320–400 AU) between 8 and 13 μm.

Interestingly, the additional silicate absorption toward IRS3 cannot occur at spatial scales less than several hundred AU since the mid-IR visibilities of Pott et al. (2008) are spectrally featureless for all baselines. Combined with radiative transfer modelling this leads Pott et al. to conclude that IRS3 is in fact a cool ($\sim$ 3000 K) C-rich star with a carbonaceous circumstellar dust shell. The additional silicate absorption therefore probably occurs at radii of tens of thousands of AU from IRS3, presumably exterior even to the few arcsec extended dust region which is still hot enough to be emitting at L, M and 8–13 μm (Viehmann et al. (2006) and Viehmann et al. (2005)). Whether this is physically associated with IRS3 is an open question, but if so then it would likely be a detached dust shell which resulted from a previous (O-rich) phase of IRS3's evolution.

Whatever the origin of the dust producing the enhanced silicate absorption toward IRS3, we believe that the bulk of the 11.1 μm absorption band, and thus the putative crystalline silicates, occur in the ISM. This is evident in Figure A1 where we show our spectrum of IRSX against both ISO SWS01 spectra, as well as the extracted optical depths which are essentially equal. Even though $\tau_{11.1}$ for IRS3 is roughly twice that for IRSX and the two ISO-observed positions, when $\tau_{9.7}$ is considered then the relative strengths of the amorphous and putative crystalline silicate bands in all four spectra are essentially equivalent.

A2 $\tau_{9.7}$ vs A_V

Another issue on which the SgrA IRS3 spectrum may feasibly bear, pointed out by Pott et al. (2008), is the long-accepted ratio of visual extinction to the 9.7 μm optical depth, i.e. $A_V/\tau_{9.7}$. For the local ISM this is thought to be around 18 (Roche & Aitken (1984a)) but toward the GC it is more like around 9 (Roche & Aitken (1985)).

From their mid-IR interferometric spectrum of IRS3 Pott et al. (2008) suggested that $A_V/\tau_{9.7}$ could be as low as 4. This was based on an assumption that A_V was only around 25, an often quoted 'average' toward the GC. But other work (e.g. Schödel et al. (2010); Scoville et al. (2003)) has shown that the visual and near-IR extinction varies on relatively small spatial scales – an arcsecond or less – across SgrA. We believe it is more likely that A_V of IRS3 is higher than the 'average' GC value.

Obviously a direct measure of A_V for IRS3 – or indeed any of A_J, A_H or A_K – would be required to decide whether $A_V/\tau_{9.7}$ toward IRS3 is abnormally low. This however is a very difficult task given IRS3 is optically invisible and its spectral type remains uncertain. So at this stage we do not believe the data is sufficient to say with any confidence that $A_V/\tau_{9.7}$ of IRS3 is lower than the commonly-accepted value of around 9 toward the GC.

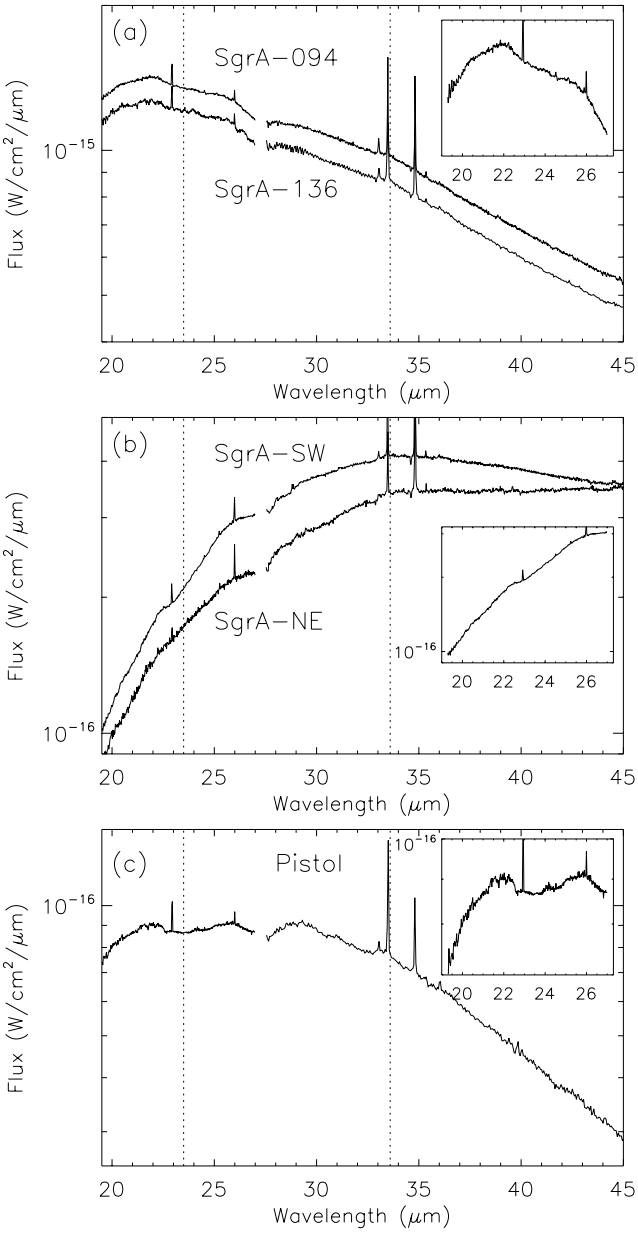

Figure A2. ISO–SWS Galactic Centre data in the 20 to 45 μm interval. (a) two spectra centred on the mini-spiral, with the revolution 94 and 136 band 4 data scaled by factors of 0.52 and 0.43; (b) two spectra at approximately 40–45 arcsec to the SSW and NNE, with the band 4 SSW data scaled by 0.58, band 3D NNE by 1.48 and band 4 NNE by 0.70; (c) a spectrum toward the Pistol star, with the band 4 data scaled by 0.42. Insets are zooms of the band 3D data, showing the clear presence of a feature around 23.5 μm, further strengthening the identification of crystalline silicates in the ISM toward the Galactic Centre.

APPENDIX B: 11 μM BAND IN W28 A2 AND IRAS19110+1045, AND SPECULATION ON CRYSTALLINE ENSTATITE

Since we used the YSOs W28 A2 and IRAS19110+1045 in Figure 11 to demonstrate the existence of a 23.5 μm crystalline silicate band we show here that they also possess an 11.1 μm feature. Figure B1 shows the sigma-clipped and

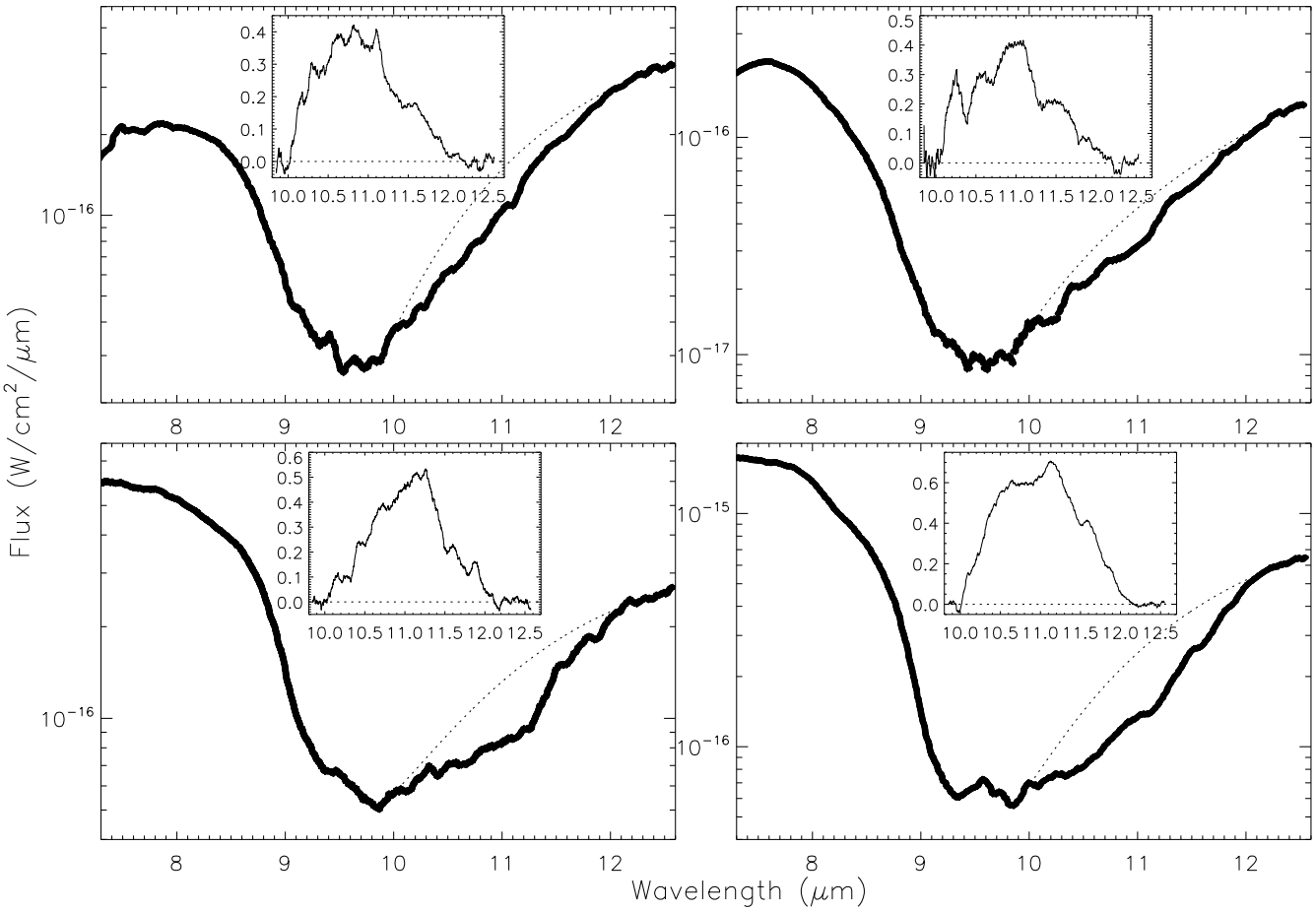

Figure B1. ISO–SWS01 7–13 μm spectra (main), and extracted optical depth (insets), of the YSOs W28 A2 (G5.89-0.39, left) and IRAS19110+1045 (G45.07+0.13, right) on the top row, and the OH/IR stars AFGL 2403 (left) and OH26.5+0.6 (right) on the bottom row. The spectra have been sigma clipped and smoothed. The dotted line in the main plots is the polynomial fit between about 10 μm and 12.1–12.7 μm used to extract the optical depth spectra in the insets. The reader is reminded that narrow features (FWHM $\sim$ 0.1–0.3 μm) may be present at $\sim$ 9.35, 10.1 and 11.05 μm due to structure in the RSRF of the SWS band 2C (Leech et al. (2003)), and which can perturb the shape of the spectrum given their overlap with crystalline enstatite and/or forsterite bands. Also, the OH/IR star spectra, and thus the overall shape of their extracted optical depth spectra and/or relative strengths of features, will likely be more influenced by radiative transfer effects (Maldoni et al. (2005), Maldoni et al. (2004), Maldoni et al. (2003)). Nevertheless, the similarity of the YSO and OH/IR spectra here are strongly suggestive of similar dust mineralogies, specifically the presence of both crystalline forsterite and enstatite.

smoothed ISO SWS01 spectra from 7.3 to 12.6 μm, along with the extracted 11 μm optical depths (insets), of W28 A2 (left) and IRAS19110 (right) in the top row, and for comparison the OH/IR stars AFGL 2403 (left) and OH26.5+0.6 (right) in the bottom row.

Generally speaking the extracted feature of the two YSOs is consistent with that of the other objects presented here. However, in both cases there appears to be another shallow feature, centred around 11.5–11.6 μm, more clearly seen in the optical depth (τ) insets. Looking back at Figure 7, possible corresponding features can be seen in the YSOs W3 IRS5 and AFGL 2136, as well as the ISM path toward SgrA IRS3, in the sense that the extracted optical depths lie significantly above the crystalline forsterite model.

For the IR sources W28 A2 and IRAS19110, being close to or coincident with ultracompact HII regions, it might be thought that extended 11.25 μm PAH emission within the large ISO beam could mimic the dip in τ between the 11.1 and 11.6 μm features. However, these two sources are dominated by solid-state absorption bands, of both silicates and ices, with only very faint 3.3 and possibly 6.2 μm PAH emission bands in W28 A2, and barely detectable 3.3 μm emission in IRAS19110. In neither case are the intrinsically stronger 7.7 and 8.6 μm PAH bands discernible. This is unlike the case for other embedded YSOs which we have looked at in the ISO archive (e.g. W3 IRS5, NGC7538 IRS1, MonR2 IRS3), which, due to their proximity to HII regions, have obvious PAH features. Also, the extracted 11 μm feature, obtained in precisely the same way, is markedly different between YSOs with and without 11.25 μm PAH emission.

Furthermore, as well as a probable 11.85 μm crystalline forsterite band in both IRAS19110+1045 and W28 A2, there appears to be another feature around 10.5–10.6 μm, and/or a distinct broadening of the extracted optical depth spectrum on the short wavelength side of the peak, compared to the

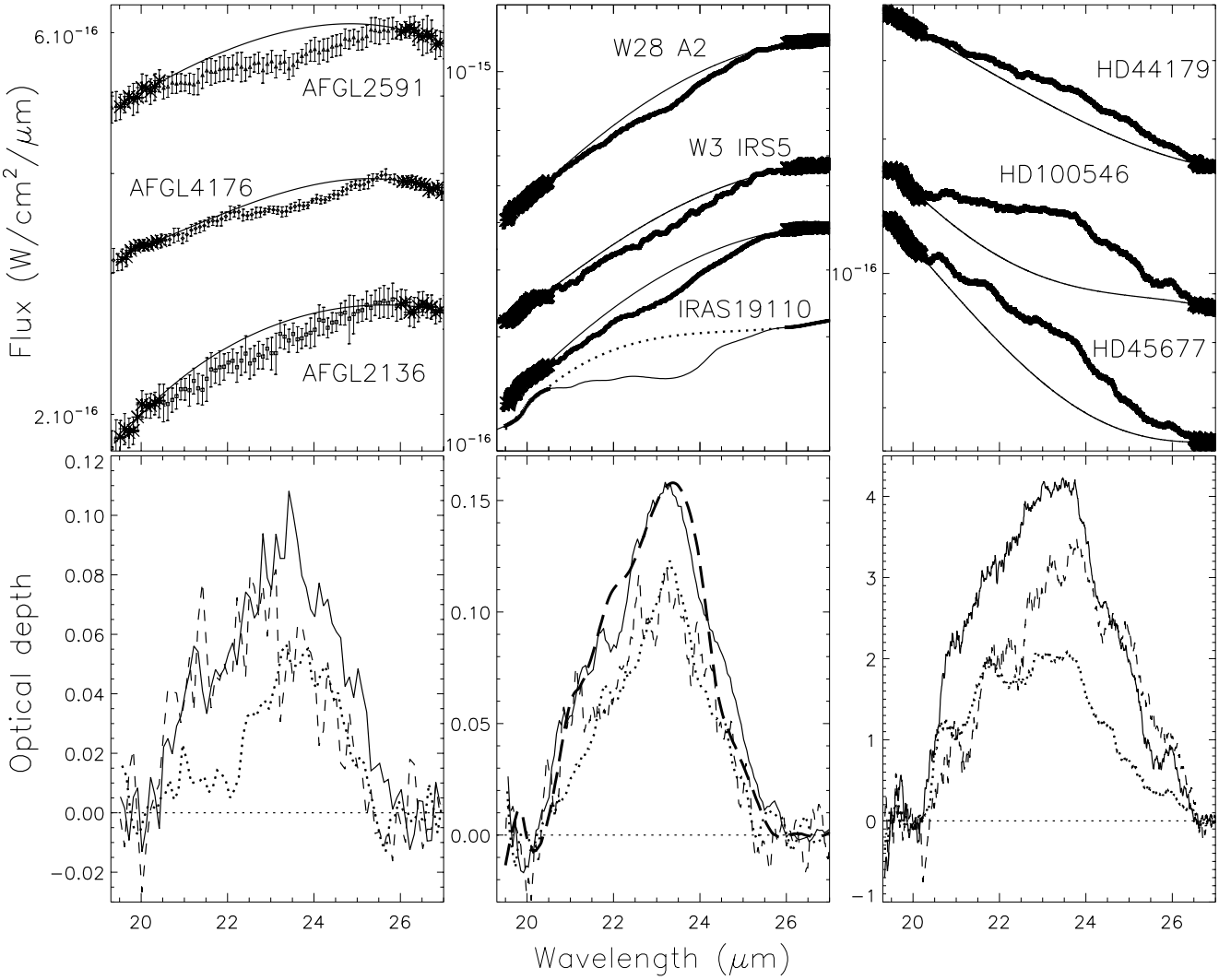

Figure B2. ISO–SWS01 19–28 μm spectra of most of the targets previously presented in Figure 11, aiming to demonstrate both the reality of the 23.5 μm features in the YSOs and its identification with crystalline silicate. Solid lines in the top panels show polynomial fits across the observed feature (dotted line for the model feature in the lowermost spectrum of the middle top panel). The bottom panels show the extracted feature for each source, being optical depths for the absorption cases and continuum subtracted excesses – in units of 10^{-17} W/cm^2/μm – for the emission cases. In the bottom left panel the solid, dotted and dashed spectra are for AFGL 2591, AFGL 4176 and AFGL 2136 respectively. In the bottom middle panel the solid, dotted and light short dashed spectra are for IRAS19110+1045, W28 A2 and W3 IRS5 respectively, and have been averaged in 10 pixel wide bins for plotting purposes. The heavy long dashed line is the model, scaled to match the peak optical depth of IRAS19110+1045. The model uses optical constants of amorphous olivine $MgFeSiO_4$ and crystalline forsterite respectively from Dorschner et al. (1995) and Fabian et al. (2001). Effective medium theory has been used, with a crystalline volume fraction of 0.1 and Maxwell-Garnett mixing rule. In the bottom right panel the solid, dotted and dashed spectra are for HD100546, HD45677 and HD44179 respectively, and have been averaged in 10 pixel wide bins for plotting purposes.

YSOs in Figure 7 and Figure 14. This apparent difference is particularly noticeable for AFGL 2136 and AFGL 2591, also measured with ISO and processed in precisely the same way, thus minimising any doubt over its reality. Once again there is a manifest similarity to the OH/IR spectra.

Overall, the correspondence between the τ spectral shapes of W28 A2 and IRAS19110 and those of the OH/IR stars, which certainly have no PAH emission, is striking and strongly suggests that absorption bands are responsible for the YSO features. Finally, as one more indication of this we point out the likely existence of a feature at $\sim$ 9.3 μm in W28 A2, also seen in the two OH/IR stars. As noted throughout this paper, we caution that a known band 2C RSRF artefact potentially exists at 9.35 μm. But the fact that neither of the other two known band 2C RSRF features (prominently) appear provides confidence that the W28 A2 spectrum contains a real astronomical feature at 9.3 μm.

We speculate that these features can be identified with a crystalline pyroxene, as has been reported for OH/IR stars (Sylvester et al. (1999)). We further speculate that it would be a magnesium rich variant, i.e. enstatite-like, as the wavelengths are in pretty good agreement with the laboratory values for the $MgSiO_3$ aerosol sample of Tamanai et al. (2006). To our knowledge there is little precedent for the presence of cold crystalline pyroxene in the near environs of embedded YSOs, as opposed to its fairly common presence

in emission from the disks of older, though still pre-main sequence, stars (e.g. Juhász et al. (2010)). This is apart from the example of SVS13, recently reported by Fujiyoshi et al. (2015).

B1 The 23.5 μm feature in DEYSOs

Finally, in Figure B2 we show zooms of the 19–28 μm portion of most of the spectra previously presented in Figure 11. This includes the six YSOs with 23.5 μm absorption bands (e.g. W28 A2 and IRAS19110+1045), plus for comparison the objects with 23.5 μm emission, being the two Herbig Be stars HD100546 and HD45677 and the pre-planetary nebula HD44179. Their 23.5 μm bands have been extracted in a manner completely analogous to that used previously for the 11.1 μm feature, as has a representative model (the lowermost spectrum in the top middle panel and heavy dashed line in the bottom middle panel).

As even a cursory examination of the laboratory data for crystalline silicates (both olivine and pyroxene) shows, it is difficult if not impossible to find any wavelength interval in the 20-30 μm region free of a discrete feature (Pitman et al. (2010); Sogawa et al. (2006); Suto et al. (2006); Koike et al. (2003); Jäger et al. (1998b); Mukai & Koike (1990)). However, the 23.5 μm band is intrinsically the strongest and so our choice of 'continuum' in Figure B2 should have only a minor influence on the extracted optical depths or excesses.

There is a clear correspondence between the absorption and emission cases, and the model. This is inclusive of the central wavelength (no shift has been applied) and the overall feature shape, e.g. the shallow and steep slopes on the short and long wavelength sides of the peak. For the emission cases at least some of the short wavelength 'wing' probably arises from crystalline enstatite.

At these wavelengths, and with a dust temperature around 100 K, the competition between emission and absorption is likely to be more important than at 11 μm, and thus a more sophisticated modelling approach is called for. Even so, our confidence in the detection of crystalline forsterite in deeply embedded YSOs, and that it is (perhaps unexpectedly) common, is increased by consideration of the data and preliminary model presented in Figure B2.

APPENDIX C: CORRECTING ISO–SWS BAND 4 RESPONSIVITY/MEMORY EFFECTS OF THE UP/DOWN SCANS

Briefly described here is the technique we used to correct the ISO band 4 (28–45 μm) data for memory/responsivity effects in the spectra presented in Figure 11, Figure 12 and Figure A2.

The SWS01 mode observed the full spectral range 2.4–45.2 μm of the ISO–SWS in two directions, denoted the 'up' and 'down' scans. These refer to grating steps, such that an 'up' scan actually goes from longer to shorter wavelengths, and vice-versa for the 'down' scan. For band 4 the scan starts at 45.2 μm, where for many of the sources considered here – i.e. massive YSOs, HII regions, Orion, Galactic Centre – the flux is hundreds or even many thousands of Jansky. The band 4 detectors take a finite time to respond to such a sudden signal increase, and so there can be a notable 'droop' in the shape of the spectrum from 40–45 μm. This can be seen in Figure C1, which shows the uncorrected up and down scans for the AFGL 2591 SWS01 (speed 3) observation of revolution 357. Conversely, when the down scan begins the detectors 'remember' the illumination history and again take time to respond to the new signal level. The resultant spectral shape is not as predictable as the 'droop' of the up scan, but could potentially mimic a spectral feature. Given the possible existence of a 28 μm crystalline silicate band it is important to account for these effects.

We thus assume that the up (down) scan most accurately represents the true spectral shape in the 28–33 μm (40–45 μm) interval. These wavelength intervals are selected based on experience, depending somewhat on the speed of the SWS01. From Figure C1 it can be seen that between 33 and 40 μm the up/down scans overlay quite well for this speed 3 SWS01. This is also the case for most speed 2's, whilst for speed 4 (slowest) the two scan directions overlay quite well from about 30–43 μm.

With this assumption we then fit a low-order polynomial to the two spectral regions, 28–33 μm of the up scan and 40–45 μm of the down scan, and force the other scan to take on that shape. The correction is done at the detector level, i.e. before sigma clipping and averaging, although the same correction is applied to all 12 detectors. Figure C2 shows the result of this procedure for the same data set as in Figure C1. The up and down scans now overlay well throughout the entire band 4 spectral range.

This paper has been typeset from a TEX/LATEX file prepared by the author.

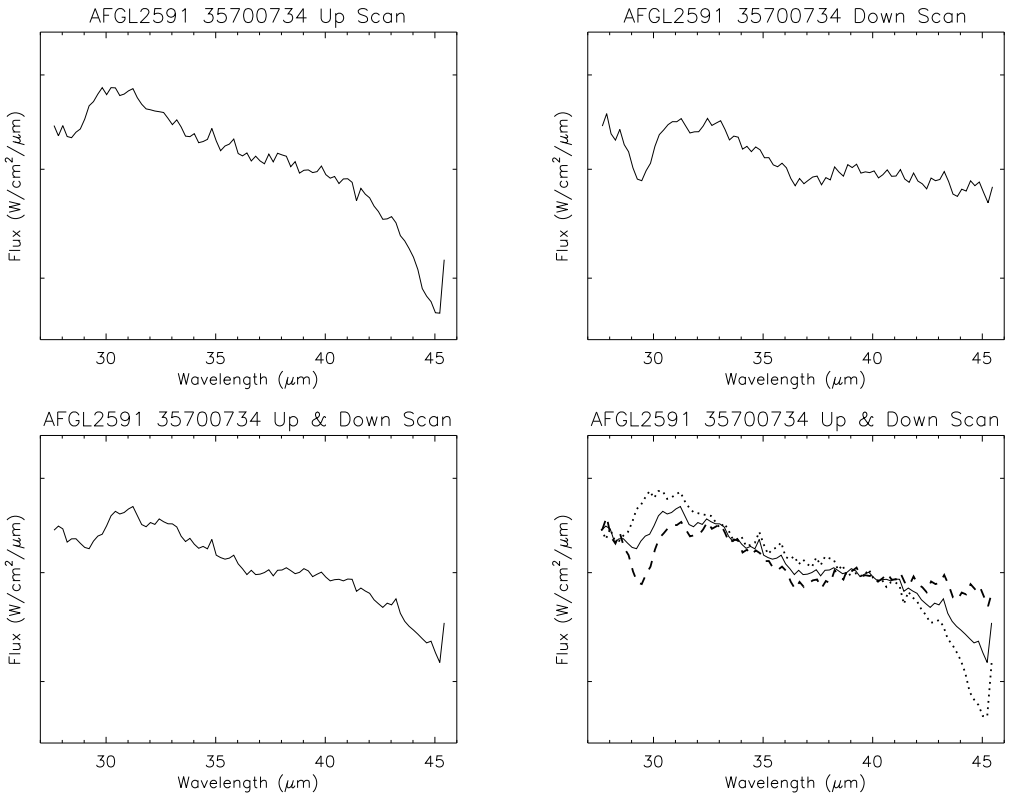

Figure C1. Sigma-clipped and binned uncorrected up and down scans for the band 4 ISO observation of AFGL2591 (tdt=35700734).

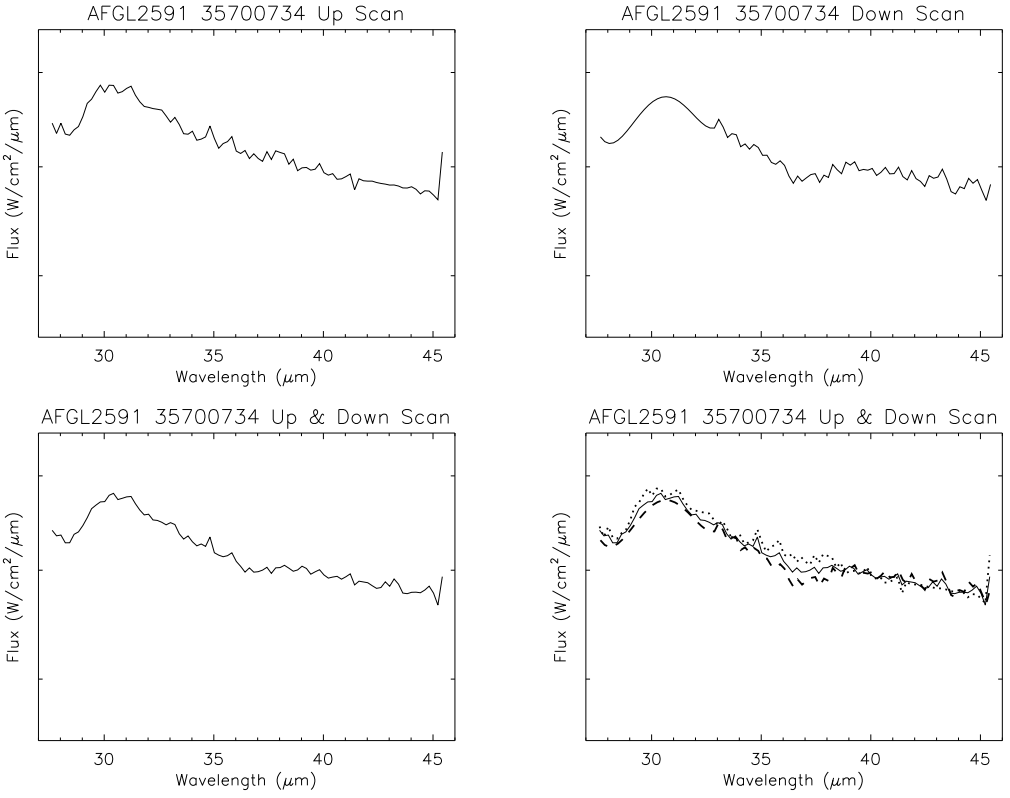

Figure C2. Sigma-clipped and binned corrected up and down scans for the band 4 ISO observation of AFGL2591 (tdt=35700734).